Evaporative Heat and Mass Transfer with Solubility Driven Solidification of Aqueous Droplet Flows

By

Payam Bahadorani

A Thesis Submitted in Partial Fulfillment
of the Requirements for the Degree of

Master of Applied Science in Mechanical Engineering

Faculty of Engineering and Applied Science
University of Ontario Institute of Technology
March 2009

Abstract

Nuclear-based hydrogen production via thermochemical water decomposition using a copper-chlorine cycle consists of a series of chemical reactions that split water into hydrogen and oxygen. This is accomplished through reactions involving intermediate copper and chlorine compounds, which act as catalysts that are recycled in the process. In this thesis, analytical and numerical solutions are developed to predict the behaviour of aqueous cupric chloride droplets in a solution undergoing spray-drying in the Cu-Cl cycle. The aqueous $CuCl_2$ is present as a slurry within the cycle, which will later generate oxygen and hydrogen as a net result. The efficiency of the cycle can be increased by utilizing low-grade waste heat from any industrial source or nuclear power plant to assist in the drying process. There are many different methods employed in industry for drying of solutions. Each method has its own advantages and disadvantages, depending on the application and conditions. In this thesis, analytical correlations of heat and mass transfer are developed for the aqueous solution, subject to various drying conditions. The analysis is performed for moist air in contact with a sprayed aqueous solution of $CuCl_2(2H_2O)$. Validation of the model is performed by comparisons with experimental results obtained from a Niro-spray dryer for $CuCl_2$ and previous experimental and theoretical data for different fluids, on the basis of non-dimensional analysis.

Acknowledgements

There are several people I would like to acknowledge for the help they have given to me during the preparation of this thesis. I would not have been able to do it without them. First and foremost, I would like to express my most sincere gratitude and appreciation to my co-advisors, Professor G.F. Naterer and Professor K. Gabriel for providing me with the unique opportunity to work in this research area, for their expert guidance and mentorship, and for their encouragement and support at all levels.

To our project team manager and post-doctoral researchers that have helped along the way, I am very grateful. Most notably, Dr. R. Gravelsins, and Dr. Z. Wang - their wealth of knowledge has been a valuable source from which I have collected my ideas.

Also, support of this research from Atomic Energy of Canada Ltd. and the Ontario Research Excellence Fund is gratefully acknowledged.

And last but not least, I would like to express my eternal gratitude to my parents, Lila and Ghobad. Much honour in this degree belongs to them for their everlasting love and support. Thank you for giving me a chance to prove and improve myself through all walks of my life. Also, I would like to thank my brothers, Babak, Pejman, Peyman, and special thanks to my younger brother Sepehr, and my girlfriend Leila Karami for the support, help, and encouragement.

This Thesis is dedicated

to my parents.

Table of Contents

List of Figures

List of Tables

Nomenclature

A	area $[m^2]$
A_V	dimensionless surface area per unit volume for heat and mass transfer
a_M	dimensionless surface area per unit volume for mass transfer
a_H	dimensionless surface area per unit volume for heat transfer
Bi	Biot number
C_s	heat capacity of vapour gas mixture $[kJ/kg\ ^oC]$
C_p	specific heat at constant pressure of moist air $[kJ/kg\ ^oC]$
C_w	specific heat of water $[kJ/kg\ ^oC]$
D_v	diffusivity $[m^2/s]$
d	droplet diameter $[m]$
h	enthalpy $[kJ/kg]$
$\bar{h}$	specific enthalpy $[kJ/kmol]$
h_c	heat transfer coefficient $[W/m^2K]$
h_M	mass transfer coefficient $[m/s]$
k	thermal conductivity $[W/mK]$
l	length of chamber $[m]$

L_c	characteristic length scale $[m]$
Le	dimensionless Lewis number, $[\alpha/D_v]$
M	molecular weight $[kg/kmol]$
$\dot{m}$	mass flow rate $[kg/h]$
Nu	Nusselt number $[q_w L/k\Delta T]$
p	partial pressure $[Pa]$
Pe	Peclet number $[RePr]$
p_t	total pressure $[Pa]$
Pr	Prandtl number $[\mu C_p/k]$
q	heat flux $[kg/s^3]$
$\dot{Q}_{conv}$	convection heat rate $[W]$
$\dot{Q}_{evap}$	evaporation heat rate $[W]$
Q	heat absorption $[W]$
$\bar{R}$	molal gas constant $[kJ/kmolK]$
Re	Reynolds number $[\rho VL/\mu]$
Sc	Schmidt number $[\vartheta/D]$
Sh	Sherwood number $[hL/k]$

T	temperature [^oC]
u	internal energy [J/kg]
V	velocity [m/s]
$\bar{V}$	average velocity [m/s]
$\bar{v}$	specific molar volume [$m^2/kg.mol$]
V'	molecular volume [$cm^3/gmol$]
Vol	Volume [m^3]
w	humidity ratio [$kg\ of\ moist\ air\ /\ kg\ of\ dry\ air$]
x	the molal fraction

Greek Letters and Special Symbols

α	thermal diffusivity [J/m^3K]
Δ	difference
∇	gradient operator [$i\frac{d}{dx} + j\frac{d}{dy} + k\frac{d}{dz}$]
μ	dynamic viscosity [$Pa\ s$]
v_H	humidity volume [kg/m^3]
ϑ	kinematic viscosity [m^2/s]

ρ	density $[kg/m^3]$
τ	shear stress $[Pa]$
$\partial(u, v, w)$	velocity of fluid in direction of x, y, z, respectively

Subscripts

1,2,..	state 1, 2, ...
A	substance A
a	air
ave	average value
B	substance B
c	critical
d	solid particles (temperature)
db	dry bulb (temperature)
dp	due point (temperature)
f	saturated liquid
fg	latent heat of moist air evaluated at moist air temperature
fg,w	latent heat of moist air evaluated at water temperature

g	saturated gas
s	surface area
s,w	saturated substance evaluated at water temperature
sat	saturation phase
sc	cross sectional area
w	water
x, y, z	axial direction

Superscripts

′	molal unit
0	evaluated at reference temperature

Chapter 1

Introduction

1.1 Background

Energy is the most important factor in wealth generation, economic and social development. Energy Security and Global Warming are analysed as 21st century sustainability threats and the two major energy challenges for the world are replacing crude oil and reducing greenhouse gas emissions [1].

Many industrialized countries started intensive research programs in the early 1970s to develop renewable energy resources and replace crude oil. The technologies targeted were active and passive solar energy installations for residential and commercial buildings; photovoltaic, wind, and ocean systems for the generation of electricity; water splitting for hydrogen fuel production; and biomass, which consists of all energy-containing waste and virgin forms of non-fossil carbon, for conversion to heat, steam, and electricity, and solid, liquid, and gaseous fuels. Successful commercialization of these indigenous, non-fossil energy resources is expected to reduce non-renewable fossil fuel usage, to gradually eliminate adverse climate changes attributed to fossil fuel consumption, to help achieve national energy security, and to reduce a substantial portion of the increasing trade deficits of some nations caused by the necessity to import oil. Renewable energy utilization would seem to address many of the security, environmental, and energy independence problems encountered since the Fossil Fuel Era began near the end of the 19^{th} century [2].

Hydrogen attracts international interest because of its future potential as a clean energy carrier. But, at present commercial hydrogen is produced from hydrocarbons, and emits carbon dioxide that causes global warming. To prevent these greenhouse gas emissions, hydrogen production from water with nuclear energy is very attractive. As one of the nuclear hydrogen production methods, the thermochemical Copper-Chlorine cycle, is a promising method because it is a more environmental friendly system and the products are only oxygen and hydrogen.

1.2 Motivation and Objectives of Thesis

Hydrogen is a promising reference fuel for future transportation and industrial needs. This issue is particularly due to increasing energy demands all around the world, significantly in emerging economies, which will increase the cost of energy. Hydrogen can be an environmentally cleaner carrier of energy to end-users, particularly in transportation applications, without any release of pollutants (such as particulate matter) or greenhouse gases at the point of end use. Economics, environmental issues, and public acceptance of sustainable development goals are likely as important as the engineering issues of efficiency and reliability in this transformation.

Currently, almost all of the hydrogen production is derived from fossil fuels. This does not address the issue of greenhouse gases, and therefore cannot be considered a sustainable pathway [3]. It is not sustainable to use fossil fuels with high CO_2 emissions and high production cost. Thermochemical processes can be environmentally benign methods to produce hydrogen. A hydrogen economy is unsustainable if fossil fuels are used to generate the hydrogen, so society needs a method that does not use fossil fuels. Currently, hydrogen from electrolysis is too costly because it has to compete against other fuels [4]. Thermochemical cycles split water through a

series of reactions in which water is thermally decomposed. In the thermochemical Cu-Cl cycle, water and heat are the only inputs to the cycle and the net products of the cycle are hydrogen and oxygen. This is accomplished through reactions involving intermediate copper and chlorine compounds, which are recycled. The reference environment is taken to be a temperature of 25°C and atmospheric pressure of 1 atm.

In this thesis, an analytical and numerical solution is used to predict the behaviour of cupric chloride droplets in a solution undergoing spray-drying in the Cu-Cl cycle. The validation of the models involves comparisons with experimental results obtained from a Niro-spray dryer for cupric chloride, as well as previous experimental and theoretical data for different fluids on the basis of non-dimensional analysis. Cupric chloride is an aqueous solution that leaves the electrochemical cell, enters a spray dryer in aqueous form, and later moves into the hydrolysis reactor as a solid. The presence of cupric chloride in the Cu-Cl cycle occurs from electrolytic separation of CuCl into solid copper and aqueous $CuCl_2(2H_2O)$, subsequent drying and then recycling of the particulate. A spray-drying process is used to remove water from the aqueous solution. This thesis presents analytical solutions for drying of the cupric chloride solution. Sensitivity studies are then performed to examine the effects of different solution concentrations and temperatures on the drying process in the spray dryer, as well as cooling tower to use waste energy for evaporation purpose.

Chapter 2

Promising Fuel of the Future

2.1 Literature Review

Hydrogen is a promising clean fuel for future transportation and industrial sectors. It has the highest energy content per unit mass, 120 MJ/kg, among any of the commonly known fuels. Hydrogen is considered a clean fuel that is widely believed to be the world's next generation fuel. Water vapour is the only bi-product produced from hydrogen combustion. This attribute has attracted greater attention in recent years, because of its capabilities as well as the growing environmental concerns regarding fossil fuel dependence [5, 6]. Fossil fuels account for about 80% of the world's annual energy demands; renewable energy contributes 14%, while nuclear energy covers around 6% of the world's energy demand [7]. Recently, sustainable clean energy sources have become significantly more important to the world economy and environment, due to climate change and increasingly limited of fossil-fuel sources. while fossil fuels are being depleted at a higher rate than it takes for their generation process to occur naturally over millions of years.

Since the start of the Industrial Revolution, atmospheric greenhouse gases have increased by about 25%. Concentrations of carbon dioxide in the atmosphere are naturally regulated by numerous processes known as the "carbon cycle". This cycle involves the movement and exchange of carbon from various reserves. The major reservoirs of carbon are interconnected by

pathways of the atmosphere, ocean and land, which are predominantly regulated by the natural process of photosynthesis. Although these natural processes absorb a net sum of 6.2 billion metric tons of CO_2 produced annually, 4 billion metric tons remain present in the atmosphere. This positive imbalance between greenhouse gas emissions and absorption is due to humankind's use of fossil fuel, resulting in the continuing increase of greenhouse gases (GHG), concentration in the atmosphere [8].

In 2006, the energy sector in Canada contributed about 81% (or 583 Mt), [9] of Canada's total GHG emissions. The energy sector accounts for GHG (CO_2, CH_4, and N_2O) emissions from stationary and transport fuel combustion activities, as well as fugitive emissions from the fossil fuel industry. Fugitive emissions associated with the fossil fuel industry are the intentional or unintentional (e.g., leaks, accidents) releases of GHGs that may result from production, processing, transmission, and storage activities. An estimate shows that approximately 516 Mt (or 72%) of Canada's GHG emissions occurred only from direct combustion of fossil fuels which is an overall increase of 21% in GHG emissions since 1990 [9]. Alternatively, renewable energy sources, such as nuclear power, wind power, and other sources for generating electricity by sustainable energies, are predicted to have a more significant impact on emission reductions.

In comparing fossil fuel to hydrogen fuel, hydrogen has a higher efficiency for internal combustion engines, with approximately 20% more efficiency than gasoline combustion engines [10]. In addition, if the energy used to split the water was obtained from renewable power sources and not from burning carbon-based fossil fuels, a hydrogen economy would greatly reduce the emission of carbon dioxide, and therefore have a major role in tackling global warming. Countries without oil reserves, but with renewable energy resources, could use a

combination of renewable energy and hydrogen instead of fuels derived from petroleum (which are becoming scarcer) to achieve energy independence.

The hydrogen economy is a promising vision of the future where the available renewable or nuclear energy sources will be used to generate hydrogen and electricity as energy carriers, capable of satisfying all the energy needs of human civilization. In the context of a hydrogen economy, hydrogen is an energy carrier, not a primary energy source. Some controversy over the feasibility of a hydrogen economy has been raised due to current methods that rely on fossil fuels to produce hydrogen, thus contradicting its original goal of reducing GHGs.

Many ongoing studies involve hydrogen production, namely electrochemical, thermal and biological processes. In all processes, there are a series of reactions involved in order to convert the energy form, for instance, electricity and nuclear heat from power plants are used to break the chemical molecules of water into hydrogen and oxygen. A recent estimate indicates that approximately 96% of the world's hydrogen is produced from non-renewable energy sources (fossil fuel), which does not address the issue of greenhouse gases and climate change [3]. In all methods, an external source of energy such as heat and electricity is required to convert the energy form. Each method also has its own advantages and disadvantages. With a renewable electrical energy supply, such as hydropower, wind turbines, or photovoltaic cells, electrolysis of water allows hydrogen to be made from water without pollution. But it is a costly and relatively efficient method. For this reason, electrolysis has not been widely used in the past.

Thermochemical cycles are one of the most attractive methods of water splitting. Approximately 12 of these cycles are presently under research and testing phases to produce hydrogen and oxygen from water and heat [11]. Thermochemical cycles using renewable energy sources do not generate carbon monoxide as an impurity at any level. They can contribute to

large-scale hydrogen production. Since all the input energy for such processes is heat, they can be more efficient than other methods such as high-temperature electrolysis, because the efficiency of electricity production is inherently limited. Also, the efficiency of electrolysis (electricity to hydrogen) is currently about 80% under ideal conditions. Electricity generation efficiency would have to exceed 65%, thermal to electrical, for the combined efficiency to exceed 52%, thermal to hydrogen, calculated for a thermochemical cycle [11]. Discovery and development of less expensive methods of bulk production of hydrogen and storage will accelerate the establishment of a hydrogen economy.

Unlike hydrocarbons, which are stored extensively at the point of use, such as gasoline tanks of automobiles or propane tanks hung on the side of barbecue grills, hydrogen is quite difficult to store or transport with current technology. Hydrogen gas has good energy density by weight, but poor energy density by volume versus hydrocarbons, hence it requires a larger tank to store. Alternatively, higher volumetric energy density liquid hydrogen or slush hydrogen may be used. Liquid hydrogen requires cryogenic storage and boils around –252.9°C. Its liquefaction imposes on energy loss as energy is needed to cool it down to that temperature. Hydrogen production must therefore be accompanied by efforts to develop a more efficient hydrogen storage system since the smallest leak in a storage tank can cause it to easily escape [6].

For the past 35 years, thermochemical water-splitting cycles have been studied extensively, particularly in the late 70s and early 80s. Unfortunately, during the past decade, thermochemical water-splitting has received less attention. In the past three decades, about 250 thermochemical water splitting cycles have been proposed. Substantial research has been executed on about 12 of these cycles [11].

2.2 Pathway to Future Hydrogen Economy

2.2.1 Thermochemical Cycles

Hydrogen can be produced from different processes, i.e., extraction from hydrocarbon fossil fuels via a chemical path, extraction from water via biological production, using electricity via electrolysis, thermochemical processes via chemical reactions, and by direct heat to split water molecules. Direct thermal dissociation of water requires temperatures higher than 2,000^{o}C, which is neither suitable nor practical for bulk generation due to high energy consumption, and materials issues [12].

To replace fossil fuels with green fuels, there is a rising interest in thermochemical cycles for producing hydrogen by splitting water molecules. Many reactions in series are involved in thermochemical cycles. Currently, there are about 250 thermochemical cycles known in literature. In most cases, thermochemical cycles have been proposed based on chemical reaction processes. Most of them are not economically viable [13]. In thermochemical cycles, the water is thermally decomposed and the products are hydrogen and oxygen, hence the remaining chemicals are recycled within the cycle. Extensive research has been performed on thermochemical cycles and many nuclear and other companies are interested in this method. But most thermochemical cycles for hydrogen production are operated at very high temperatures, around 800^{o}C to 900^{o}C, which currently requires additional heat from other sources besides heat from a nuclear power plant. The new generation of CANDU-SCWR reactors can produce a maximum heat at 625^{o}C, which is still below 900^{o}C. In most cases, the additional heat required is needed from burning natural gas or other fossil fuels, which will then release GHG emission

into the atmosphere. At present, the large-scale production of hydrogen is dominated by steam-methane reforming, SMR, of natural gas [14]. For producing tow hydrogen molecules by steam reforming of methane, more than one molecule of CO2 is emitted, and the annual production of H_2 is about 0.1 Gton, 98% coming from the reforming of the fossil fuels [15, 16]. Due to climate change and cost, those processes are not environmentally and economically sustainable. Many organizations such as Atomic Energy of Canada Limited (AECL), and the U.S. Department of Energy are investing significantly to develop thermochemical technology.

Steam-methane reforming, SMR, unlike nuclear-based hydrogen production, emits greenhouse gases [17]. The Sulfur-Iodine (S-I) cycle, Calcium Bromine-Iron (UT-3) cycle, and Copper-Chlorine cycle are examples of thermochemical cycles. SMR releases a significant amount of carbon dioxide emissions into the atmosphere. This is not a sustainable process for large-scale hydrogen production, due to climate change. The S-I cycle and UT-3 cycle are being investigated by General Atomics and the Japanese Atomic Energy Research Institute. However, those are operated at very high temperature and may suffer from high maintenance costs and corrosion. The S-I cycle, first described in the mid-70s, has had difficulties when separating hydrogen iodine and sulphuric acid. The high operation temperature, approximately 900^{o}C, and corrosive acid are two challenges of this process, increasing the maintenance cost of the process and raising the capital cost. Moreover, most of the nuclear power plants operate at a temperature much lower than 900^{o}C. For instance, CANDU reactors such as CANDU 6, and CANDU-SCWR (Supercritical-Water Cooled Reactor) operate at 320^{o}C and 625^{o}C, respectively. An overview of thermochemical hydrogen production for the above-mentioned cycles is presented in Figure 1 [11, 18, 19].

Alternatively, there are other nuclear-reactor technology candidates, which may be used for hydrogen production at high temperatures. The modular helium reactor (MHR), which can be used both for hydrogen and electricity production, can operate at high temperatures of approximately 850^{o}C. An Advanced High-Temperature Reactor (AHTR) has been proposed to address the requirements specific to high temperature hydrogen production. An AHTR has not yet been built. Another alternative solution is a Secure Transportable Autonomous Reactor (STAR), which is a fast neutron spectrum modular-sized reactor. STAR is based on Russian submarine-reactor technology demonstrated at approximately 500^{o}C. The reactor coolant is liquid lead with a reactor core outlet temperature of 800^{o}C [18].

In comparison with the thermochemical cycles, the Cu-Cl cycle is one of the most promising methods due to its much lower temperature operation. But less research has been performed in this area. Cupric chloride is present in the process in both forms of liquid and solid, i.e., solid, solution and slurry. This makes the process more complicated. The presence of $CuCl_2$ solution in the cycle is due to the electrolytic separation of CuCl into solid copper and aqueous $CuCl_2$. The drying of cupric chloride solution is essential for the process, in order to recycle the cupric-chloride powder.

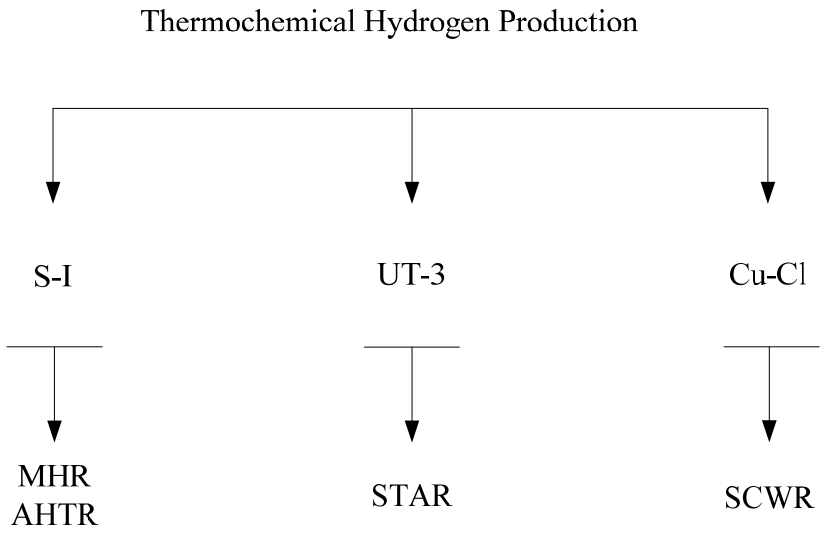

Figure 1. Thermochemical cycles with associated nuclear reactors

2.2.2 Copper-Chlorine Cycle

The Copper-Chlorine cycle has been identified by AECL as the most promising cycle for thermochemical hydrogen production with SCWR. It has advantages of lower operation temperatures and potentially lower cost materials, compared to other methods such as the S-I cycle which is currently pursued by countries such as Japan, US, and France [20]. AECL and the Argonne National Laboratory have been collaborating in the development of the Cu-Cl cycle for hydrogen production using nuclear energy and nuclear waste heat [21]. Since the Cu-Cl cycle requires input temperatures below 550^{o}C, it is feasible for integration with the SCWR. The copper-chlorine cycle is a closed hybrid cycle that consists of thermochemical and electrochemical processes, as shown in Table 1. In the table, Q is the thermal energy and E is the

electrical energy [14, 21]. Water, heat and electricity are the net inputs of the cycle, and copper and chlorine compounds are recycled at the end of the reactions. Figure 2 represents the conceptual layout of a Cu-Cl Cycle. The inputs of the system are water and heat, resulting in net products of oxygen and hydrogen, where Q is denoted as thermal energy and E is the electrical energy. As shown in Table 1 and Figure 2, the solid Cu reacts with HCl gas, producing hydrogen as an output and molten CuCl. The solid Cu required for Step 1 is achieved from Step 2 by using molten CuCl from Steps 1 and 5 through an electrochemical process.

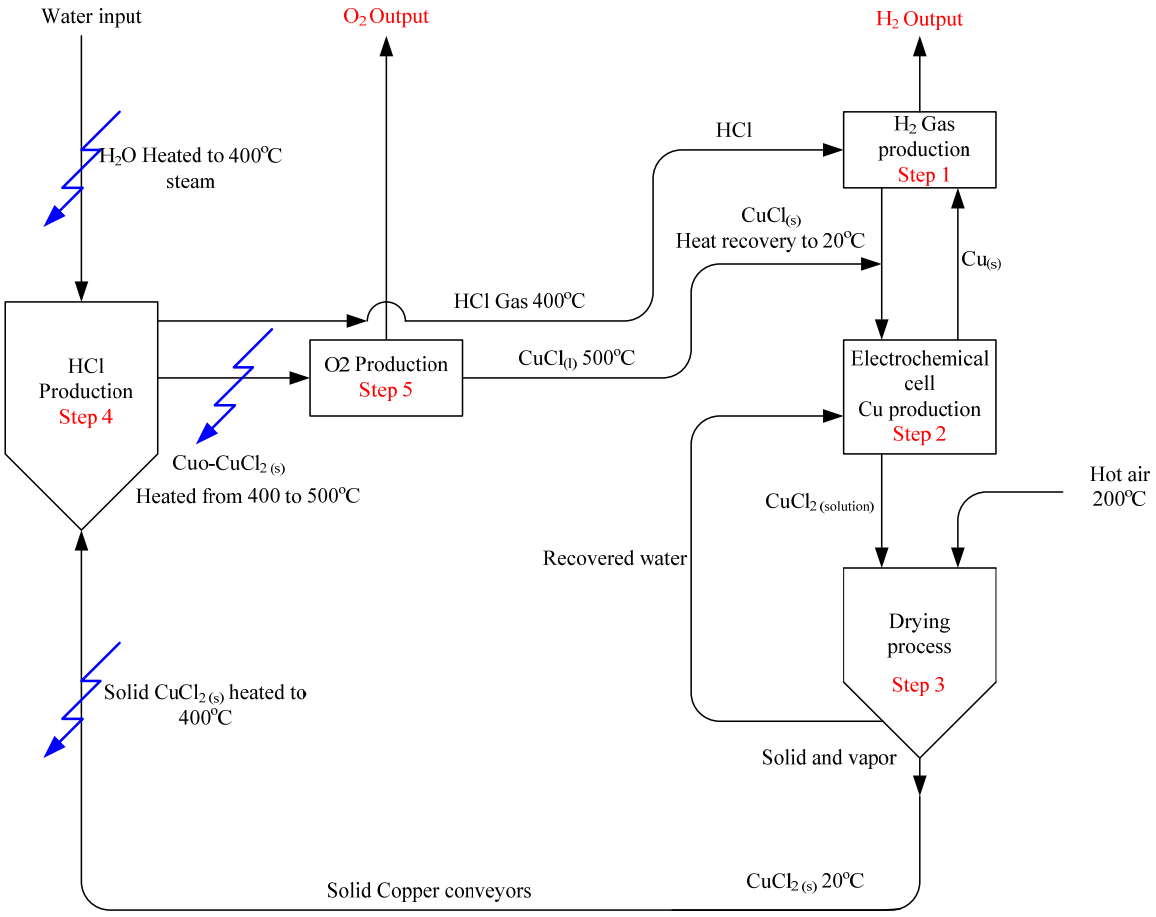

Figure 2. Conceptual schematic of Copper-Chlorine Cycle.

The HCl gas in Step 1 is achieved from Step 4 by using solid cupric chloride and steam. In the last step, $CuO.CuCl_2$ is decomposed into oxygen as an output and CuCl. Hence, the outputs of the system are oxygen and hydrogen, while the other chemical compounds are recycled within the closed system.

Table 1. Reaction steps in Cu-Cl cycle.

Step	Reaction	Temp. Range °C	Feed/Output	
1	$2Cu(s) + 2HCl(g) \rightarrow 2CuCl(l) + H_2(g)$	430 – 475	Feed	Electrolytic Cu + dry Hcl +Q
			Output	H_2 + CuCl(l) salt
2	$4CuCl(s) \rightarrow 4CuCl(aq) = 2CuCl_2(aq) + 2Cu(s)$	30 – 70	Feed	Powder/granular CuCl and HCl + E
			Output	Electolytic Cu and water slutty containing HCl and $CuCl_2$
3	$2CuCl_2(aq) \rightarrow 2CuCl_2(s)$	> 100	Feed	Water slurry containing HCl & $H_2O(g)$+Q
			Output	Powder/granular $CuCl_2$+H_2O/HCl vapours
4	$2CuCl_2(s) + H_2O(g) \rightarrow CuO.CuCl_2(s) + 2HCl(g)$	400	Feed	Powder/granular $CuCl_2$ + $H_2O(g)$ + Q
			Output	Powder/granular $CuO.CuCl_2$+2HCl(g)
5	$CuO.CuCl_2(s) \rightarrow 2CuCl(l) + 0.5O_2(g)$	500	Feed	Powder/granular $CuO.CuCl_2(s)$ + Q
			Output	Molten CuCl salt + O_2

2.2.3 Drying Process

There are many industrial processes to obtain solid particles from slurries and solutions. The spray-drying process is one of the best known drying methods, particularly in the area of particle gas flow since it is one-step drying. Co-current spray-drying is a commonly used method of drying liquid feed by a hot gas. Typically, the hot gas is air, but sensitive materials such as

pharmaceuticals, and solvents like ethanol, require oxygen-free drying, so nitrogen gas can be used instead. The liquid feed varies depending on the material being dried, and it may be a solution, colloid or suspension.

This process of drying is a one-step rapid process which eliminates additional processing. In other drying processes, such as slow drying (utilizing a drum dryer or cooling tower), more steps are required for drying processes. With a co-current spray dryer, the liquid feed is pumped at the ambient temperature through an atomizer device, producing fine droplets in the main drying chamber. Atomizers vary with rotary, single fluid, two-fluid and ultrasonic nozzle designs. These different types have different advantages and disadvantages, depending on the application of the spray-drying process. In some instances, a spray nozzle is used in place of an atomizer for a different dispersion rate [22]. In a co-current spray-drying process, Li et al. [23] presented a sensitivity study with Computational Fluid Dynamics (CFD) modeling. Initial parameters of discrete and continuous phases were determined experimentally and used in the model. The theoretical results were compared with experimental data, then sensitivity of the simulation results to the selected parameters was determined. The authors used a gas turbulence model to analyze the drying kinetics, effects of atomizing air, and turbulent particle dispersion, which are crucial parameters affecting the accuracy of the CFD modeling.

One of the key issues in the spray-drying process is determination of the drying kinetics and degradation kinetics for heat sensitive products. An experimental test was performed for drying kinetics in spray-drying by Zbicinski et al. [24]. In this experimental analysis, various measuring techniques were developed to determine the spray structure and gas temperature (microseparator). A phase Doppler anemometry technique was used to determine initial spray atomization parameters, the structure of the spray during drying, particle size distribution,

velocity of the particles, and mass concentration of the liquid phase. The analysis of the results showed that the particle size distribution became uniform, due to spray dispersion during drying. No aerodynamic segregation of particles was found. The analysis of initial velocity of the particles showed it was not only a function of diameter, but also a function of the distance from the axis of the spray.

Lin and Chen [25] used a reaction engineering approach to predict the drying behaviour of skim and whole milk droplets under various drying conditions in spray-drying systems. They used a reaction engineering approach to correlate the drying kinetics. Experimental data is required to predict the single droplet flow in the reaction engineering approach. There are two effective ways, namely a reaction engineering approach and the characteristic drying curve [25]. These were used for prediction and modeling of a drying droplet. In the reaction engineering approach, evaporation is assumed to be the activation process to overcome an energy barrier, not condensation or absorption [26].

The drying process via low-grade heat starts from approximately 200^{o}C. In an experimental test, Walton [27] showed the time required for drying of water droplets in different temperature conditions. It used a mathematical model to analyze the convection, mass transfer and heat conduction through the filament. Figure 3 shows the required time in seconds for evaporation of water droplets in free convection with an air velocity range of 0.25 to 1 m/s, and a Reynolds number from 27 to 100, based on modeling of [22]. In natural convection conditions, the evaporating droplets showed almost identical evaporative profiles. The droplet mass, viscosity and surface tension were important to implement a dimensionless correlation group, which are important in droplet oscillation. In the analysis, a possible source of error could be

attributed to droplet non-sphericity. Thus, the averaging used for calculating the diameter of a droplet becomes less accurate.

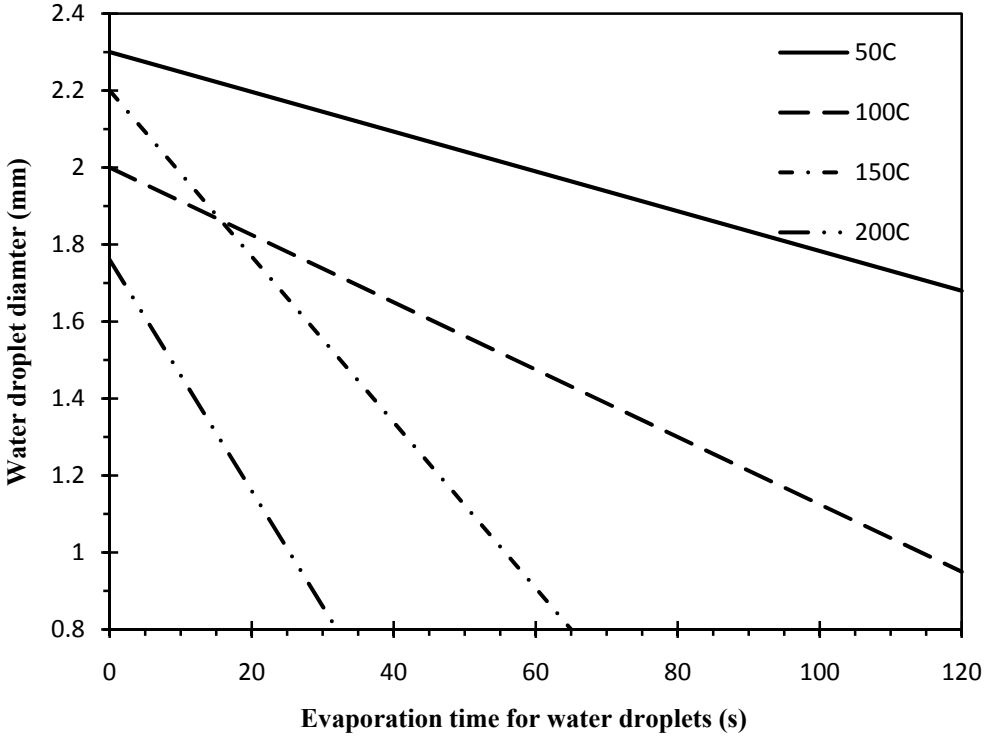

Figure 3. Evaporation of water droplet in various temperature conditions for natural convection and air velocity of 1 m/s [27].

Ranz et al. [28] observed that the variation in air velocity did not appreciably affect the droplet temperature when using dehumidified air in the experiments. Figure 4 shows the simultaneous heat and mass transfer from a droplet. The boundary of the droplet is covered by water vapour since the solid $CuCl_2$ in the droplet solution cannot evaporate at atmospheric pressure and temperature. The droplet diameter decreases nearly linearly with time, for both natural and forced convection. It is also observed that the evaporation decreased by reducing the air temperature. The kinetics of the spray-drying process is based on the moisture and temperature

history of the droplets. However, with respect to the transfer coefficient, Walton [27] suggested the transfer coefficients were independent of the droplet diameter.

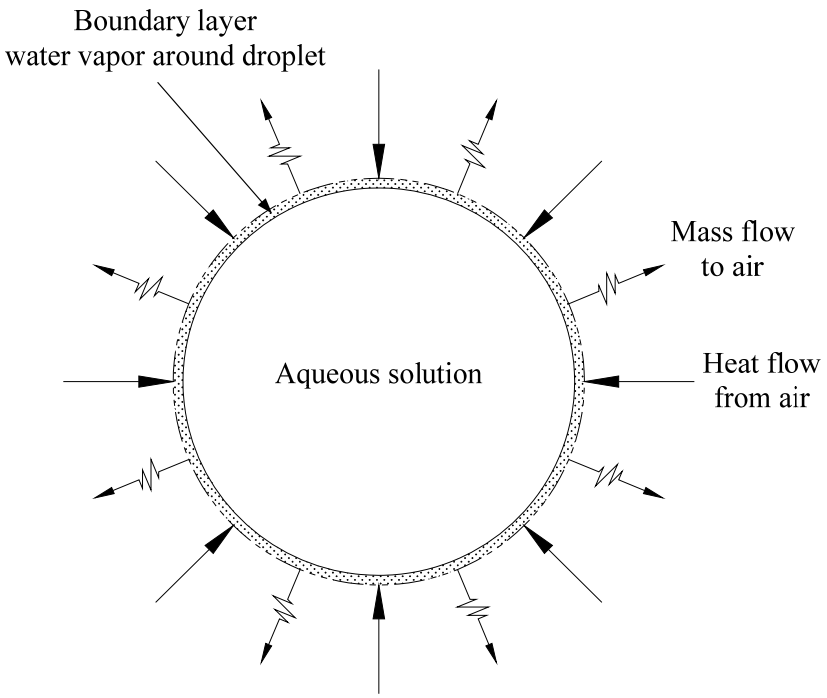

Figure 4. Aqueous solution droplet with simultaneous heat transfer into droplet, and mass transfer leaving droplet by evaporation.

Temperatures below 150^{o}C were insufficient to evaporate the entire droplet, when the effective length of the spray-drying chamber is between 1 to 2 m [27, 29]. Spray-drying of a suspended particle utilize liquid atomization to create droplets that are dried to individual particles while the particles, are moved in a hot gaseous drying medium, usually air. The advantage of this process is its one-step continuous unit processing operation. It has become one of the most important industrial drying methods [30]. The quality of dry powder is the single most important factor that is significantly affected by the operating conditions of the process. In

spray-drying, the particle size and distribution are directly related to the size of the droplets. Therefore, successful prediction of droplet size enables one to control the powder properties when dried. Iva et al. [30] shows the size distribution in spray-drying, as represented by a cumulative distribution curve or frequency.

Over 25,000 spray dryers are estimated to be in use commercially for drying products in agrochemical, biotechnology, fine and heavy chemical, dairy, dyestuffs, minerals concentrated to pharmaceuticals, and skim milk in capacities ranging from a few kg/h to over 50 tons/h of evaporation capacity [30]. In the spray-drying process, the slurry or solution is pumped to an atomization device, such as a rotary disc atomizer, pressure nozzle, pneumatic nozzle or ultrasonic nozzle. Atomizer devices are usually located in the air distributor at the top of the drying chamber. The atmospheric air passes through a filter, and it is pre-heated through a heater and supplied by a fan to the air distributor. Oil furnaces, electrical heaters, steam heaters and similar devices can be used to heat the air. Waste heat from nuclear power plants or other industrial waste heat can be used to improve the efficiency of the system. The droplets produced by the atomizer meet hot air, and evaporation accrues, thereby cooling the air.

In a spray-drying system, the dried product falls to the bottom of the chamber and enters the air, while the droplets generally do not contact the spray-drying walls. The product passes through the cyclone for separation of dried particles from the air. There may be some deposits left on the spray-drying walls. Spray-drying technology is of great industrial interest, however there are some limitations, such as high installation costs, lower thermal efficiency, product deposit on the drying chamber, possibly leading to a degraded product, or corrosive materials possibly damaging the internal wall of the spray-drying chamber. The atomizer in spray-drying is the most critical part for size distribution control of the droplets, trajectory and speed. The final

particle size depends on these factors. The drying rate and heat transfer rate can be established by the droplet size.

Aguilar et al. [31] were analyzed the velocity, drag force, and drag coefficient of droplet in cryogenic sprays. They showed that the velocity has the least influence on the cryogen droplet evolution. Muthunayagma et al. [32] studied the evaporation of water using low-grade heat under various conditions. Ocean water was injected into a low-pressure vaporizer, using fine droplets of less than 1 mm in diameter and temperatures between 26 to 32^{o}C. They showed that desalination of sea water is possible by using a low-pressure vaporization process at typical ocean surface temperatures in a small period of time, less than 1 second, and pressure of 5 to 30 mm mercury. Hence, at low temperatures, the evaporation can become possible by using a low pressure vaporization process. The method is not feasible for spray-drying or any other processes not operating at low-pressure. Therefore, depending on the application, there are many approaches to drying aqueous solutions.

Farid [33] showed a new approach for predicting the change of a single droplet mass and temperature of an aqueous solution containing dissolved or suspended solids, when exposed to hot air in a spray-drying system. Single droplets with average diameters of 200 μm to 2 mm and a velocity of 1.3 m/s, exposed to air temperatures of approximately 100^{o}C, were considered. This model took into account the temperature gradient within the droplet. The model showed that the temperature distribution within the droplet of liquid containing solid particles cannot be neglected, even for small diameter droplets of 200 μm. In this thesis, the average temperature of the droplet was calculated by integrating the measured temperature distribution in both the crust and the core regions. Based on the Biot number, which represents a dimensionless number used in transient heat transfer calculations, the temperature distribution in the droplet can be neglected

in the analysis if the Biot number is sufficiently small [34]. For Biot numbers is smaller than 0.1, the temperature gradient within the droplet becomes uniform. The Biot number in spray-drying in the copper-chlorine cycle is smaller than 0.1. Hence the temperature gradient can be assumed uniform in the spray-drying [20, 35].

Various drying techniques can be used, depending on solution conditions and rheological properties of the slurry. Other direct and indirect dryer systems include a drum, fluidized bed, thin-film contact, evaporating cooling tower and crystallizer. Mujumdar [36] reviewed the general trends in drying technologies of industrial interest. Over 400 dryer types have been cited in the technical literature. Nevertheless, only about 50 types are in various stages of development and commonly found in practice [37, 38]. Cooling towers are heat-removal devices, usually used to transfer process waste heat to the atmosphere. In addition, cooling towers can be used for evaporation of water to remove heat and cool the working fluid closer to the wet-bulb air temperature. Otherwise, they can use air to cool the working fluid closer to the dry bulb air temperature. Applications of cooling towers include oil refineries, chemical plants, power plants and building cooling. In the counter-flow cooling tower, air flow is directly opposite water flow.

Fluidized bed dryers are commonly used for drying of wet particulate. Granular materials can be fluidized. Fuidized bed dryers can also be used for slurries, pastes, and suspensions, which can be fluidized in beds of inert solids. Fluidized beds are used in various industrial processes, namely chemicals, carbohydrate, foodstuff, biomaterials, beverage products, ceramics, pharmaceuticals in powder or agglomerated form, healthcare products, pesticides and agrochemicals, dyestuffs and pigments, detergents and others. The particle sizes are between 50 to 2000 μm, which can occur with other traditional dryer types such as a rotary and tunnel [39]. The drum dryer is commonly used to dry viscous, concentrated solutions, slurries or pastes on

rotating steam- heated drums. Ramli et al. [40] examined different types of drum dryers and the principles of their operation. In drum dryers, the viscous slurry is mechanically spread by two counter-rotating drums into a thin sheet that adheres to the hotter drum in single drum dryers, or split sheets on both hot cylinders in double drum dryers. Consequently, the adhering thin sheet is dried conductively by the high heat flux of condensing steam inside the drum. In the case of very wet slurries produced into wet sheets, the drying can occur gained by blowing hot air on to the sheet surface.

2.2.4 Wet-Bulb Temperature

The wet-bulb temperature is the temperature reached by a small amount of liquid evaporating into a large amount of unsaturated vapour-gas mixture. Under properly controlled conditions, it can be used to measure humidity of the mixture. There are two types of wet-bulb temperatures: psychrometic wet-bulb temperature and thermodynamic wet-bulb temperature. In thermodynamic wet-bulb temperature, the wet-bulb temperature of heat transfer from the gas to the liquid may be equated to the product of the rate of vaporization, and the sum of the latent heat of evaporation and the sensible heat of the vapour. The adiabatic saturation temperature is the temperature at which water, by evaporating into air, can bring the air to saturation adiabatically at the same temperature. Hence, the wet-bulb temperature is the steady-state, non-equilibrium temperature reached by a small mass of liquid immersed under adiabatic conditions in a continuous stream of gas. The mass of the liquid is very small compared to the gas phase where there is a negligible change in the properties of the gas, and the effect of the process is confined to the liquid. The thermodynamic wet-bulb temperature is a temperature that can only

be approached in a limited case, and cannot be measured directly. Only the thermodynamic wet-bulb temperature is a thermodynamic property. The wet-bulb temperature can be measured with a thermometer. It is influenced by the heat and mass-transfer rates, and therefore, is not a sole function of the air state to which the thermometer is exposed. In this thesis, for the psychrometic equations and psychrometic charts where the wet-bulb temperature appears, only the thermodynamic wet-bulb temperature will be considered [41, 42].

2.3 Applications and Needs for Hydrogen

Many studies have proposed various sources of clean energy for environmental sustainability. The hydrogen and electricity economies refer to a society where these two energy carriers are the universally adopted energy carriers. In broad terms, it is estimated that by the year 2050, the world will require 17 TW of additional primary energy, with much of this energy demand coming from developing countries [43]. The notion of sustainable development has taken a prominent place in policy discussions. Energy input to society is necessary to fuel the economic development.

Hydrogen is oxidized to water, after which can be dissociated to its component elements, hydrogen and oxygen, by applying external energy. Hydrogen is today used in large scale industrial processes and rocket technology. Hydrogen has many other applications; it can be used for nearly every end-use energy need in the economy, including transportation, power generation and portable power. Currently, hydrogen is mainly employed in oil refining and ammonia and methanol production. As a fuel it is only employed in spaceship propulsion systems and ground vehicle prototypes for demonstration purposes. Hydrogen can be used in conventional power

generation technologies, while conventional technologies can offer early market entry for hydrogen as an energy carrier. Conventional technologies will continue to hold a major market advantage in terms of vehicle range [15, 44, 45]. For instance, convectional hydrogen technologies includes automobile engines, power-plant turbines, and fuel cells, which are relatively cleaner and more efficient than conventional technologies. Fuel cells have on-board application potential in both transportation and electrical power generation for individual homes and office buildings. In Canada, there is also a large demand in Alberta for hydrogen in oil sands development to upgrade bitumen to synthetic crude [21]. The opportunity for hydrogen markets is promising, since hydrogen needs are growing rapidly. Its current annual worldwide production exceeds 50 million metric tones [44]. However, hydrogen production should satisfy many criteria, i.e., no associated emissions (including CO_2), wide availability and affordability.

The primary requirements for affordable electrolysis are low capital cost and high utilization. Consequently, the electricity supply must enable high utilization, as well as being low-cost and emissions-free. Large-scale sources of electricity include nuclear technologies, which produce electricity at rates competitive with today's CO_2-emitting, fossil-fueled technologies. Energy sources for hydrogen production can be categorized into three different primary energy-supply classes, which may be used to realize the hydrogen economy, namely fossil fuels, such as petroleum, natural gas, shale oil, oil from tar sands, coal, etc. Nuclear power plants including fission reactors, CANDU reactors, breeders reactors, and the renewable energy sources are sustainable alternatives. Others include hydroelectric power systems, wind-energy systems, ocean thermal-energy conversion systems, geothermal resources, and a number of other solar-energy conversion systems such as biomass production, photovoltaic energy conversion, and solar thermal systems, among others [46].

Approximately 0.9% by weight of the earth's surface is hydrogen, which occurs in many components. For instance, it is combined with carbon and other elements in fossil fuels, and it is combined with oxygen and other minerals in water. Previous research [47] argues that the hydrogen economy is not feasible due to its lower well-to-wheel efficiencies compared to an "electron economy", which uses electricity as the main energy carrier. Nevertheless, other studies show that the efficiency of hydrogen production by thermochemical cycles or high-temperature electrolysis can be increased to more than 45% [46-48]. Hence, large-scale hydrogen production and transportation, namely by hydrogen pipelines or shipping, can significantly reduce the total net cost of production and make hydrogen economically feasible. Hydrogen has the largest energy density, as well as the highest energy content per unit weight, among any fuel. It releases higher energy on mass basis, with a low heating value of 2.4, 2.8, and 4 times higher than methane, gasoline and coal, respectively [15]. In general, there is an important advantage in moving transportation to hydrogen fuel – the greater efficiency of its conversion to energy. For instant, fuel cells burning hydrogen, although still in their infancy, already achieve over 50% efficiency. But gasoline and diesel automotive vehicles are relatively inefficient as North American cars are about 15% efficient. The European Union's 2008 goal of 140 g CO_2/km for new cars amounts to only 25% efficiency [49].

Notwithstanding its considerable diversity, more than 60% of transportation's energy use in developed economies is for personal vehicles, including cars and light trucks. However, the industrial and residential sectors achieve above 70% energy conversion efficiency [49]. The transportation sector offers more leverage in replacing carbon-based fuels than the more fuel-efficient industrial, commercial and residential sectors. The recent US Hydrogen Roadmap [45], outlined the need for rapid hydrogen deployment as an energy currency. This vision is an

opportunity for hydrogen-based technology, and also a major challenge, since, an effective contribution to the reduction of CO_2 emissions, need a low-cost sustainable supply of hydrogen.

An estimate of CO_2 emissions in the year 2000 in Canada shows that the only four sectors cover over 80% of the total emissions. The transportation sector released 30% of the CO_2 emissions, industrial 23%, power generation 21%, and fossil-fuel industries 10%, and the rest by other sectors such as waste, residential, and commercial sectors [9, 49]. Since a large proportion of fossil-fuel industries supplies transportation fuel and power generation, these two sectors actually account for over half of the total. Canadian transportation is typical of developed economies, with direct consumption of 25–30% of all energy use [49]. For instance, an estimate from the US Energy Information Administration Projects [50] showed an aspect of energy consumption by transportation in 25 years. It shows that the energy consumption by transportation from 2000 to 2025 will increase from 27% to 31%, respectively. In addition, for transportation's energy consumption in Canada [51], the share of CO_2 emissions from transportation will rise from 25.6% to 27.0% from 2000 to 2020, respectively. These percentages vary between countries. They indicate the emission growth and its growing importance, particularly for transportation. These issues show that hydrogen is becoming the reference fuel for future transportation and industrial usage. The hydrogen economy proposes to solve the adverse effects of using hydrocarbon fuels in transportation, and other end-use applications where carbon is released into the atmosphere.

2.3.1 Nuclear-Based Hydrogen Production

Nuclear power is being increasingly recognized as foremost contender to provide "carbon free" electricity for the grid. Nuclear power is not as flexible as gasoline and fossil fuel for transportation fuel, as it must be converted to other forms of energy [43]. Hydrogen has certain advantageous properties, such as the most abundant element in the universe, unlimited raw material for hydrogen production, no environmental contamination, and highest energy content per unit weight of a fuel. Aleksandrov et al. [52] described that the main solution of this global issue must be tied to the development and adoption of a large-scale nuclear- based hydrogen-production to produce hydrogen [44]. Botterud et al. [53] presented a financial model based on a real options theory of assessing the profitability of four different nuclear-based hydrogen production technologies in the evolving electricity and hydrogen markets. The research showed the significant value in the ability to switch plant output between electricity and hydrogen.

In general, there are two approaches to developing a nuclear reactor for hydrogen co-generation: an existing reactor or a new generation of advanced high-temperature reactor system. Presently, only one high-temperature nuclear reactor, the gas-cooled (helium) reactor, has the high-temperature capabilities to provide sufficient heat to drive a hydrogen-production system. Gas-cooled reactors were designed and developed for electricity production using a coated-particle fuel and high-pressure helium as a coolant [54]. Kimura et al. [55] investigated the feasibility of hydrogen production from biomass by nuclear fusion heat. Significantly better efficiency also obtained in this process than other proposed reaction processes such as electrolysis from a renewable source with a small amount of CO_2 emission. The fission reactor as a primary energy source with hydrogen as an energy carrier was suggested. Torjman et al. [56] assessed hydrogen production from nuclear energy, considering the economical and

environmental impact. It was proposed that a complete nuclear-electro-hydrogen energy system can supply the net energy requirement for a medium sized city of a population of approximately 500,000 people, including the end consumer, residential, industrial and transportation.

Light water-cooled reactors (LWRs), which are used worldwide as nuclear power reactors, use water as a coolant and metal as the in-core material. The outlet temperature of those reactors is about 300^{o}C; for instance, CANDU 6 has a 320^{o}C outlet temperature. However, high-temperature gas-cooled reactors (HTGR) are operating at a higher-temperature above 900^{o}C. They use graphite as the in-core material, and helium gas as coolant. HTGR has excellent inherent safety, as discussed by Yamawaki [57]. The first HTGR in Japan was constructed at the Oarai Research and Development Center of the Japan Atomic Energy Agency, with an outlet temperature of 950^{o}C [53]. HTGRs are suitable for electricity and hydrogen production, and they are a new generation of nuclear power plant. The European Union's countries such as France and Germany are showing a great interest in nuclear energy and hydrogen production with HTGRs.

Verfondern et al. [58] have shown the technical feasibility of HTFR, in combination with a coal gasification process. The research described German projects on a prototype nuclear process heat system. Another study was involved in the European Union in 1997, the Michelangelo Network, [59] which started research and development to bring new innovative nuclear reactor designs to the market. The Michelangelo Network was first started within the 5th European Atomic Energy Community Framework Programme, EURATOM, with the objective to elaborate a general European R&D strategy for the further development of the nuclear industry in the short, medium, and long term. To broaden the application range of nuclear power beyond dedicated electricity generation, the network proposed an orientation for future EURATOM R&D programmes including new industrial aspects of nuclear energy, such as

combined heat and power and, particularly, the production of hydrogen or other fuels as a link to CO_2-free energy sources. Michelangelo Network project ended in November 2005 [59]. Another organization in the European Union, the Hydrogen Network (introduced in 1999), focussed on the development of strategies for the introduction of a European hydrogen fuel infrastructure. Hence, the potential for high-temperature gas-cooled reactors has a promising future, with significant improvements in design, efficiency and life span of the reactors. Its high temperature outlet can be utilized in many processes including electrical, biomass hydrogen and thermochemical hydrogen production.

Onuki et al. [60] described research and development on nuclear hydrogen production using HTGR, aiming to develop technologies for safe and economical implementation, such as safety against explosion and radioactive material release, and control technology preventing thermal disturbance from hydrogen production plants to reactors. The HTGR technology was developed based on a high-temperature engineering test reactor (HTTR), constructed at Oarai by the Japan Atomic Energy Agency (JAEA). Its full operation of 30 MW began in 2001. The reactor outlet temperature of 950^{o}C was achieved in April 2004. Furthermore, JAEA has been conducting research and development on the thermochemical Sulfur-Iodine Process for hydrogen generation by water splitting. The S-I process was first described in the mid 1970s. It was achieved for the first time in the world using a bench-scaled apparatus in August 2003. Jeong et al. [16] optimized the conceptual layout of the hybrid sulphur cycle for nuclear hydrogen generation. Ways to optimize energy efficiency through configuration modifications were studied in a hybrid sulphur cycle. A cycle efficiency of 45.3% for the lower heat value (LHV) was achieved. Previous studies showed that none of the processes have yet reached the commercial stage. Indications are that 50% conversion efficiency of nuclear heat to hydrogen

(LHV) are the best that one can expect to achieve [11, 43]. S-I processes utilize multiple chemical reactions to generate hydrogen by absorbing high-temperature heat. But material problems are demanding, due to working with extremely corrosive liquids at very high temperatures. This may cause corrosion of the piping and other problems, which increase the maintenance cost of the process [11, 57].

One of the low temperature cycles is the copper-chlorine cycle, which operates at peak temperatures of less than 550^{o}C. From an engineering perspective, this has more potential due to its low temperature operation and less demanding material problems. Hori et al. [61] presented a form of nuclear based hydrogen production, with a steam reforming reaction of fossil fuels to produce hydrogen synergistically. The steam reforming process was examined using a "membrane reformer" and adopting the recirculation of reaction product in a closed loop configuration. According to Hori et al. [61], among various synergistic hydrogen-production processes, the recirculation-type membrane reformer process is believed to be the most profitable. Typical merits of this process are a nuclear heat supply at temperatures around 550°C, compact plant size, smaller membrane area for hydrogen production, efficient conversion of a feed fossil fuel, appreciable reduction of carbon dioxide emission, high purity of hydrogen without any additional process, and ease of separating carbon dioxide for future sequestration requirements.

2.3.2 Hydrogen Storage

In general, energy can be stored in different forms such as: mechanical energy (i.e., potential energy, rotational energy of a flywheel), electrical or magnetic field (capacitors and coils, respectively), chemical energy of reactants and fuels (batteries, petrol or hydrogen), and nuclear fuel (uranium or deuterium). Chemical and electrical energy can be transmitted relatively easily, as electronic coulomb interaction is involved in both cases. Chemical energy is based on energy of unpaired outer electrons (valence electrons), eager to be stabilized by electrons from other atoms. Hydrogen has the best ratio of valence electrons to protons of all elements in the periodic table. It has a very high energy gain per electron since its electron is, accompanied by only one proton [12].

Hydrogen storage can be categorized into three main techniques, namely compressed gaseous hydrogen, liquid hydrogen, and hydrides. Hydrogen is available to the market in classical high-pressure tanks usually made of steel, regularly filled up with 20 MPa pressure [12]. In most countries, however, it has been tested up to a pressure of 30 MPa. Nevertheless, the tanks cannot provide the capacity necessary for an acceptable vehicle range, which is about 483 kilometres (300 miles) [6]. Therefore, the pressure has to be increased, which in turn increases both tank weight and material costs. The primary requirements for tank materials include low density, non-reactivity with hydrogen, very high tensile strength, and low diffusivity. Properties of the tank material such as permeability, fatigue and aging are as important as the yield strength and density for material selection of hydrogen tanks.

Hydrogen absorption at a solid surface depends on the applied pressure and temperature. Due to the high permeability rate of hydrogen through many materials, which are susceptible to leaking, materials such as carbon composites with high yield stress and low density are not

suitable for hydrogen tanks. Currently, the common materials used for high-pressure hydrogen-storage tanks are steel alloys, titanium and carbon composites, for 703, 924, and 2070 MPa [12], respectively. Hydrogen can be converted to liquid at -252.75^{o}C, which is below the critical point temperature of 240.15^{o}C and 1.29 MPa [62]. Kandavel et al. [63] investigated the improvement of hydrogen-storage properties. Hydrogen-storage properties of Ti1.1CrMn AB2-type Laves phase alloys, for both low (-30^{o}C) and high (80^{o}C) temperature applications, are improved by substituting Zr at the Ti site. The increase in the Zr content leads to a decrease in the equilibrium hydrogen absorption pressure plateau and faster absorption kinetics. There is an increase in the hydrogen-storage capacity from 1.9 to 2.2wt% for Ti1.1CrMn and (Ti0.9Zr0.1)1.1CrMn alloys, respectively. Another alternative way to store hydrogen is in the liquid form.

Liquid hydrogen can be stored, which significantly increases its volumetric density at relatively low tank pressures in comparison to the gas phase. Hydrogen can be stored in compounds to make a hydride, unlike gasoline storage in vehicles where the fuel itself is contained in a closed media. Hydride storage can be categorized into two groups of metal hydrides and chemical hydrides. Metal hydrides are ionic compounds of hydrogen and metal. In chemical hydrides, hydrogen forms a covalent bond with the alloy. The metal hydrides have the potential for reversible on-board hydrogen storage and release at low temperature and pressure [64].

Chapter 3

Heat and Mass Transfer Formulation

3.1 Temperature distribution

Consider the drying of a droplet, as illustrated in Figure 5, the droplet experiences a process of shrinkage in which the temperature is approximately uniform. Based on the Biot number, which represents a dimensionless number used in unsteady-states or transient heat transfer calculations, the temperature distribution in the droplet can be neglected if the Biot number is small. The process depicting the drying stage is shown in Figure 5. In spray-drying, a droplet with a temperature lower than the wet-bulb temperature of air enters the chamber at stage 1. Fast heating occurs with a high-temperature operation of spray-drying, assuming the rate at which heat is transferred inside the droplet is substantially higher than the rate at which heat is removed from the droplet's surface. If these two rates are equal to or less than 0.1, there is no substantial temperature gradient inside the droplet, so a lumped-capacity heating method can be applied.

The evaporation occurs during stages 2 and 3, where droplets remain at a constant temperature and evaporation continues until the liquid has been removed, and random crystals of solid start to grow. After stage 3, the crystals continue to gain heat and the drying process ends with the particle deposited at the bottom of the chamber. This aspect of the droplet heating process is characterized by Biot number. The Biot number can be obtained as follows:

$$Bi = Nu(\frac{k_g}{2k_d}) \quad (1)$$

where k_g and k_d are the thermal conductivities of gas and droplet [W/mK], respectively. The Biot number of spray-drying in the copper-chlorine cycle is smaller than 0.1, so the temperature gradient will be assumed to be uniform during spray-drying [20, 34, 35, 65].

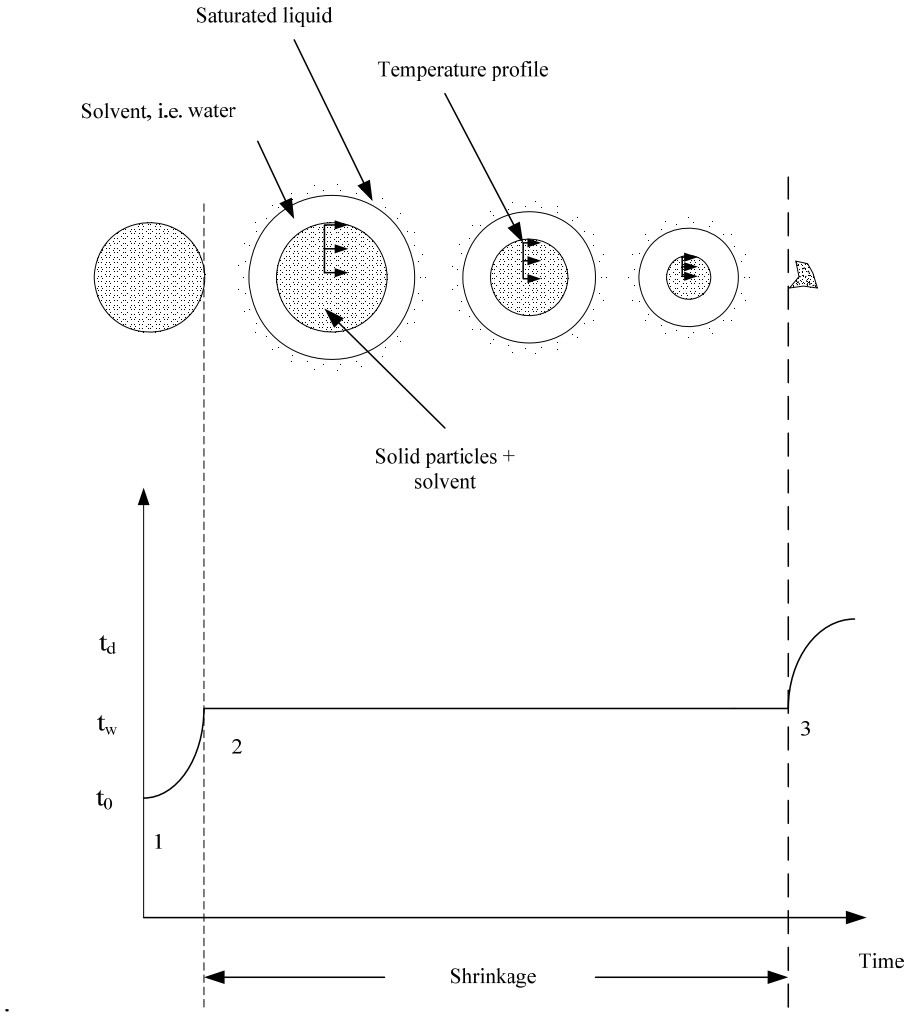

Figure 5. Evaporation process of droplet.

3.2 Mass diffusion

Mass diffusivity depends on the substance and temperature during mass transfer. Diffusion is a physical flow at a molecular scale. The nature of diffusion and the resulting flow leads to three types of processes [42]. 1) Only one component A of the mixture is transferred to from the interface, and the total flow is the same as the flow of A. Absorption of a single component from a gas into a liquid is an example of this type. This process is the primary case for study in this thesis. 2) The diffusion of component A in a mixture is balanced by an equal and opposite molar flow of component B, so there is no net molar flow. This is generally the case in distillation, and it means no net volume flow in the gas phase. However, there is generally a net volume of mass flow in the liquid phase because of the differences in molar densities. 3) Diffusion of A and B takes place in opposite directions, but the molar fluxes are unequal. This situation often occurs in diffusion of chemically reacting species to and from a catalyst surface, but the equations are not covered in this thesis.

A common mass-transfer scenario is the transfer of species A into a gas stream due to evaporation or sublimation from a liquid or solid surface, respectively. The concentration or partial pressure of species A in the gas phase at the interface may readily be determined from Raoult's law $p_A = x_A p_{A,sat}$, where p_A is the partial pressure of A in the gas phase, x_A is the mole fraction of species A in the liquid, and $p_{A,sat}$ is the saturation pressure of species A at the surface temperature. Raoult's law applies if the gas phase can be approximated as ideal, and the liquid of the solid phase has a high concentration of species A. If the liquid is a pure species A, i.e., $x_A = 1$, the above correlation can be simplified to $p_A = p_{A,sat}$. The partial pressure of the vapour at the interface corresponds to saturated conditions at the temperature of the interface, and it may be determined from standard thermodynamic tables [66].

Diffusivities can be established by experimental measurements, and where the information is available for the system of interest, it should be used directly. Often the desired values are not available, however, and they must be estimated from published correlations. A value may be available for one set of conditions of temperature and pressure; the correlations are then useful in predicting, from the known value, the desired values for other conditions.

The diffusivities in liquids are generally 4 to 5 orders of magnitude smaller than in gases at atmospheric pressure. Diffusion in liquid occurs by random motion of the molecules. The average distance traveled between collisions is less than the molecular diameter, in contrast to gases, where the mean free path has magnitudes greater than the size of the molecule.

Values of D_v in gases can be predicted with good accuracy from kinetic theory. Theoretical correlations have been modified from experimental data to give the following semiempirical equation [42, 67-69]:

$$D_v = \frac{0.01498T^{1.81}(\frac{1}{M_A}+\frac{1}{M_B})^{\frac{1}{2}}}{p(T_{cA}T_{cB})^{0.1405}(V_{cA}^{0.4}+V_{cB}^{0.4})^2} \quad (2)$$

where D_v is diffusivity [cm^2/s], T is the temperature [K], M_A and M_B are molecular masses of components A and B, respectively. T_{cA} and T_{cB} are critical temperatures of A and B, [K], V_{cA}, V_{cB} are critical molar volumes of A and B, [cm^3/g.mol], and p is the pressure [atm]. However, according to Reid et al. [69], those theoretical methods have errors of approximately 10%, so the value of diffusivity is based on experimental data [69]:

$$D_{vAB}p = 0.292\ (cm^2/s)atm \quad (3)$$

The kinematic viscosity is the ratio of the absolute viscosity to the density of the fluid, and it can be expressed as follows [42, 70]:

$$\vartheta = \frac{\mu}{\rho} \left[\frac{m^2}{s}\right] \quad (4)$$

The dimensionless combination of variables that is important in the study of viscous flow is called the Reynolds number, which is defined as follows:

$$Re = \frac{d\bar{V}}{\vartheta} \quad (5)$$

where d is the diameter of the droplet, $\bar{V}$ is the average velocity of the droplet, and ϑ is the kinematic viscosity. Since it is turbulent flow and the mass flow rate of the air is generally not equal to the solution mass-flow rate, the air mass-flow rate carries the droplet and the average velocity is assumed to be the air velocity within the chamber:

$$\bar{V} = \frac{\dot{m}}{\rho A} \quad (6)$$

where $\dot{m}$ and A are the mass-flow rate of the air [kg/h], and the area of the chamber [m^2].

3.3 Heat-Transfer and Mass-Transfer Coefficients

The convection heat transfer coefficient can be expressed as follows:

$$h_c = k\frac{Nu}{d} \quad (7)$$

where h_c is the heat transfer coefficient, and k is the thermal conductivity of the solution. In a spray-drying process, the shape of a $CuCl_2$ droplet is assumed to be spherical.

The Sherwood number (Sh) for mass transfer is a dimensionless number used in mass-transfer problem. It represents the ratio of convective to diffusive mass transport, and it is named in honour of Thomas Kilgore Sherwood, defined as follows [71]:

$$Sh = \frac{h_M L_C}{D} \tag{8}$$

where L_c is the characteristic length scale, D is mass diffusivity of the solution, and h_M is the mass transfer coefficient. For mass-transfer flow around spheres, the diffusion occurring in creeping flow around a spherical gas bubble and around a solid sphere of diameter d is considered. The Sh number is different for different Reynolds numbers (Re). Mass transfer in the continuous phase around droplets is affected by a combination of molecular diffusion and natural forced convection in the continuous phase.

For a droplet that is internally stagnant, when the continuous phase velocity is zero, the mass transfer coefficient can be found as follows [72, 73]:

$$h_M = Sh\frac{D}{L_C} = 2\frac{D}{L_C} \tag{9}$$

For other conditions such as circulating drops or oscillating drops, Sh has to be calculated by using one of various theoretical methods. For different ranges of Re, Sh for an internally circulating sphere with high Pe (thin concentration boundary-layer approximation), the continuous-phase mass transfer coefficient for creeping flow can be obtained. The following correlation can be used to obtain Sh for high Re with less than 5% error in $Sh/Pe^{1/2}$ [74]:

$$Sh = \frac{2}{\sqrt{\pi}}\left[1 - \frac{1}{Re^{1/2}}\left(2.89 + 2.15\kappa^{0.64}\right]^{\frac{1}{2}} Pe^{1/2}\right. \tag{10}$$

This applies when $\kappa \leq 2$ and Re > 70, where the Péclet number, Pe, is a dimensionless number relating the rate of advection of a flow to its rate of diffusion, often thermal diffusion. It is equivalent to the product of Re and the Prandtl number in the case of thermal diffusion, and the product of Re and Schmidt number in the case of mass dispersion. For thermal diffusion, the Pe number is defined as [75]:

$$Pe = \frac{LV}{\propto} = RePr$$
$$\propto = \frac{k}{\rho c_p} \quad (11)$$

For mass diffusion, it is defined as:

$$Pe = \frac{LV}{D} = ReSc \quad (12)$$

where V is velocity, α is thermal diffusivity, Sc is the Schmidt number, D is mass diffusivity, k is thermal conductivity, Pr is the Prandtl number, and c_p and ρ are the heat capacity and density, respectively.

The widely used parameter of Pr, a dimensionless number approximating the ratio of momentum diffusivity and thermal diffusivity, and aeronautics, is $Pr = c_p\mu/k$ [71]. The Schmidt number is a dimensionless number defined as the ratio of momentum diffusivity, velocity, and mass diffusivity. It is used to characterize fluid flows in which there are simultaneous momentum and mass diffusion processes. It physically relates the relative thickness of the hydrodynamic layer and mass-transfer boundary layer. It can be defined as follows [76]:

$$Sc = \frac{v}{D} = \frac{\mu}{\rho D} \quad (13)$$

where v is kinetic velocity and μ is the viscosity of the solution. However, by modifying the following correlation, the Sh for a Medium range of Re, 10 < Re < 100, can be achieved as follows [72]:

$$Sh = 2\left(\frac{Pe}{\pi}\right)^{1/2}\left[1 - \frac{\frac{2+3\kappa}{3(1+\kappa)}}{\left[1+\left[\frac{(2+3\kappa)Re^{0.5}}{(1+\kappa)(8.67+6.54\kappa^{0.64}}\right]^{n_1}\right]^{1/n_1}}\right]^{0.5} \quad (14)$$

where $n_1 = \frac{4}{3} + 3\kappa$

The three main transport properties are the coefficient of viscosity, thermal conductivity, and diffusion, which relate to movement or transport of momentum, heat, and mass, respectively. Each of these coefficients relates a flux or transport process to the gradient of a variable. Viscosity relates the momentum flux to a velocity gradient, thermal conductivity relates the heat flux to a temperature gradient, and the diffusion coefficient relates mass transport to concentration gradient [77].

Viscosity can be expressed as the ability of a fluid to flow freely. It is the property of a fluid which relates the applied stress to the resulting strain rate. The coefficient of viscosity, μ, is a thermodynamic property that varies with temperature and pressure. For a Newtonian fluid, the viscosity, by definition, depends only on temperature and pressure. It also depends on the chemical composition of the fluid, if the fluid is not a pure substance, not on the forces acting upon it. Furthermore, for incompressible Newtonian fluids, it is known that the stresses are linearly related to the rates of deformation. If the fluid is incompressible and viscosity is constant in the fluid, the equation governing the shear stress, in the Cartesian coordinate system, can be written as follows [78]:

$$\tau_{xy} = \tau_{yx} = \mu\left(\frac{\partial u}{\partial y} + \frac{\partial v}{\partial x}\right)$$

$$\tau_{yz} = \tau_{zy} = \mu\left(\frac{\partial v}{\partial z} + \frac{\partial w}{\partial y}\right) \quad (15)$$

$$\tau_{zx} = \tau_{xz} = \mu\left(\frac{\partial w}{\partial x} + \frac{\partial u}{\partial z}\right)$$

where u, v, and w are the velocity components of the fluid in the x, y, z directions, respectively.

The coefficient of thermal conductivity can be defined as the ability of heat to flow, due to a temperature gradient. This can be expressed as a proportionality between the heat flux and temperature gradient, called Fourier's Law:

$$q = -k\nabla T \quad (16)$$

where q is the rate of heat flow per unit area. The quantity k is the thermal conductivity.

The mass transfer coefficient is associated with the movement of mass due to molecular exchange. This process, called mass diffusion, constantly occurs in a fluid because of random molecular motion. The diffusion becomes macroscopically evident when a variable mixture of two or more species is involved. Mass diffusion occurs whenever there is a spatial gradient in the proportions of a mixture, called a concentration gradient. There are two different definitions of concentration: 1) the volume concentration $\rho_A = \frac{m_A}{Volume}$ = mass of component A per unit volume, and 2) the mass concentration, equal to ρ_A/ρ, which represents the mass of species A per unit mass of the mixture. The second definition, or mass concentration will be more useful, as it is a dimensionless fraction less than or equal to unity. The following correlation represents Fick's law of mass diffusion:

$$\frac{\dot{m}_A}{A} = -\rho_A D\nabla(\ln(\frac{\rho_A}{\rho})) \quad (17)$$

where $\dot{m}_A$ is the mass flux of species A in the direction of decreasing concentration. The quantity D is called the coefficient of diffusivity and it has dimensions of (length)^2/time.

3.4 Drying Chamber Model

Evaporative drying chambers such as cooling towers are heat removal devices used to evaporate droplets by transferring heat to the surroundings (see schematic of typical tower in Figure 6). Cooling towers may either use the evaporation of water to remove process heat and cool the working fluid to the wet-bulb air temperature, or rely solely on air to cool the working fluid closer to the dry-bulb air temperature. The main types of cooling towers are: 1) wet-cooling towers or simply cooling towers that operate on the principle of evaporation. The working fluid and the evaporated fluid (usually H_2O) are the same. 2) dry coolers, which operate by heat transfer through a surface separating the working fluid from ambient air, such as a heat exchanger, utilizing convective heat transfer. They do not use evaporation. *Fluid coolers* are hybrids that pass the working fluid through a tube bundle, upon which clean water is sprayed and a fan-induced draft is applied. The resulting heat transfer performance is much closer to that of a wet cooling tower. The advantage provided by a dry cooler is protection of the working fluid from environmental exposure. In a wet cooling tower, the warm water can be cooled to a temperature lower than the ambient air dry-bulb temperature, if the air is relatively dry. As the ambient air is drawn past a flow stream of water, evaporation occurs. Evaporation results in saturated air conditions, lowering the temperature of the water to the wet-bulb air temperature, which is lower than the ambient dry-bulb air temperature. The difference is determined based on the humidity of the ambient air. To achieve better performance, more cooling and evaporation, a

medium called “fill” can be used to increase the surface area between the air and water flows. Splash fill consists of material placed to interrupt the water flow, causing splashing. Film fill is composed of thin sheets of material, upon which the water flows. Both methods create increased surface area. Figure 6 shows a schematic of a cooling tower, with the air and water streams.

With respect to drawing air through the tower, there are three types of cooling towers: 1) natural draft, which utilizes buoyancy via a tall chimney. Warm, moist air naturally rises due to the density differential with dry, cooler outside air. It is less dense than drier air at the same pressure. This moist air buoyancy produces a current of air through the tower. 2) mechanical draft, which uses power driven fan motors to force or draw air through the tower. 3) induced draft which occurs when a mechanical draft tower with a fan at the discharge pulls air through the tower; the fan induces hot moist air out the discharge. This creates low entering and high exiting air velocities, thereby reducing the possibility of recirculation, where discharged air flows back into the air intake. This fan/fill arrangement is also known as draw-through. Forced draft occurs in a mechanical draft tower with a blower type fan at the intake, where the fan forces air into the tower, creating high entering and low exiting air velocities. The low exiting velocity is much more susceptible to recirculation. With the fan on the air intake, the fan is more susceptible to complications due to freezing conditions. Another disadvantage is that a forced draft design typically requires more motor horsepower than an equivalent induced draft design. The forced draft benefit is its ability to operate with high static pressure. The forced draft cooling tower can be installed in more confined spaces and some indoor situations. This fan/fill geometry is also known as blow-through. A fan assisted natural draft is a hybrid type that appears as a natural draft, where airflow is assisted by a fan. Hyperboloid cooling towers have become the design standard for all natural-draft cooling towers because of their structural strength and minimum use

of material. The hyperbolic form is commonly associated with nuclear power plants. However, the same kinds of cooling towers are often used at large coal-fired power plants. Not all nuclear power plants have cooling towers [79].

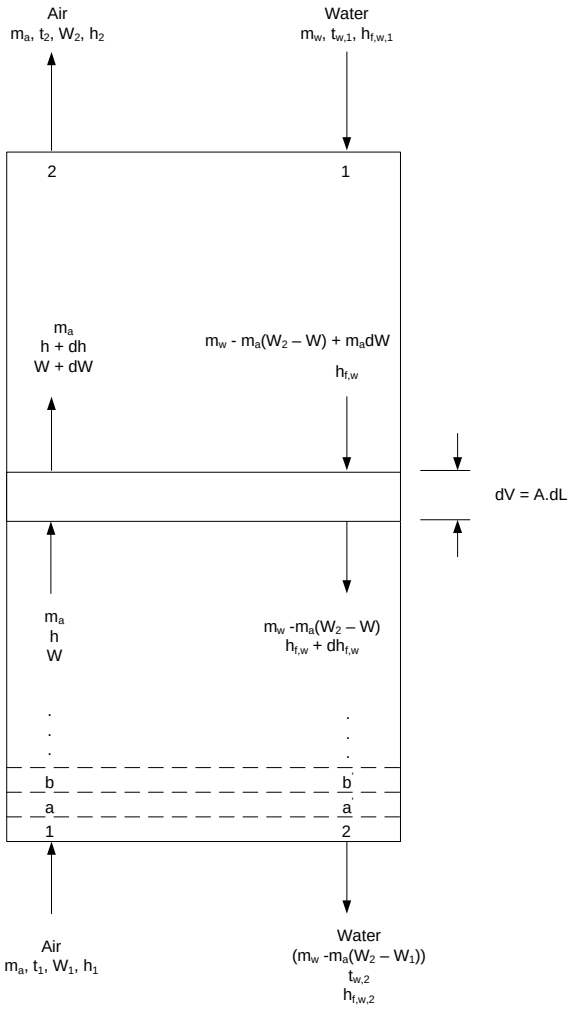

Figure 6. Schematic of counterflow cooling tower.

The earth's atmosphere is a mixture of several gases including nitrogen, oxygen, argon, carbon dioxide, water vapour, and traces of other gases. Dust particles and condensable vapours such as water vapours are usually concentrated in the atmosphere within a few thousand feet of

the earth's surface. Above an altitude of approximately 20,000 ft, the atmosphere consists essentially of dry air. Wet air composition is calculated based on the US standard dry air composition. The US standard dry air composition and molecular weight of air's components are shown in Table 2 [80].

Table 2. Composition of dry air and molar weight of air's components.

Substance	Molecular Weight kg/kmol	Mole-Fraction Composition in Dry Air %	Partial Molecular Weight in Dry Air kg/kmol
Oxygen (O_2)	31.999	0.20947	6.704
Nitrogen (N_2)	28.013	0.78086	21.878
Argon (Ar)	39.948	0.00934	0.371
Carbon Dioxide (CO_2)	44.01	0.00033	0.013
Air		1.00	28.966

The dry-bulb temperature and enthalpy reference temperature should be larger than 1°C (33.8°F) due to the limitation of the saturation steam table. The molecular weights for dry air and water vapour are 28.966 and 18.016 kg/kmol, respectively. Moist air may contain variable amounts of water vapour from zero, dry air, to saturated moist air. For a pure substance, such as water vapour or dry air, the virial equation of state can be used [41]:

$$P\bar{v} = \bar{R}T + A_2P + A_3P^2 \quad (18)$$

where $\bar{v}$ and $\bar{R}$ are molar values of the substance. The coefficients A_2 and A_3 are the second and third virial coefficients, respectively. They are functions of temperature. They account for the

force attraction or repulsion between molecules. The above equation has been predicted by theory, so experimentation is required for verifying the virial coefficients.

The formulation for specific enthalpy and specific entropy can be derived from equation 18 through appropriate relations of thermodynamics. Consequently, for moist air, statistical mechanics predicts that:

$$P\bar{v} = \bar{R}T - [x_a^2 A_{aa} + 2x_a x_w A_{aw} + x_w^2 A_{ww}]P - \quad (19)$$

$$[x_a^3 A_{aaa} + 3x_a^2 x_w A_{aaw} + x_w^3 A_{www}]P^2 - \cdots$$

where x_a and x_w are the mole-fraction of dry air and water vapour, A_{aa} is a virial coefficient for one molecule of dry air mixing with another molecule of dry air, A_{aaa} refers to three molecules of dry air, and A_{aw} is an interaction coefficient for one molecule of dry air interacting with one molecule of water vapour.

Identical relations of thermodynamics lead to the following result for specific enthalpy:

$$\bar{h} = x_a \bar{h}_a^0 + x_w \bar{h}_w^0 - [x_a^2 B_{aa} + 2x_a x_w B_{aw} + x_w^2 B_{ww}]P \quad (20)$$

$$-\frac{1}{2}[x_a^3 B_{aaa} + 3x_a^2 x_w B_{aww} + x_w^3 B_{www}]P^2 - \cdots$$

where $\bar{h}_a^0$ and $\bar{h}_w^0$ are specific enthalpies at a reference temperature for dry air and water vapour, respectively. For convenience in the calculations, the enthalpy, h, is based upon a unit weight of dry air. Eq. (20) reduces to the perfect-gas law for very low pressures. At regular atmospheric pressures, $P\bar{v} = \bar{R}T$ is an excellent approximation to Eq. (19). The enthalpy is calculated as a real gas, it is assumed as an ideal gas, thus, Eq. (20) can be rewritten as follows:

$$\bar{h} = x_a \bar{h}_a^0 + x_w \bar{h}_w^0 \quad (21)$$

To convert the moist air enthalpy to units of kg per kJ, the above equation is divided by $28.966x_a$, where x_a is the mole-fraction of dry air (moles of dry air per mole of moist air). Thus:

$$h = h_a^0 + W h_w^0 \quad (22)$$

where W is the absolute humidity of moist air (kg of water per kg of dry air). The specific enthalpies h_a^0 and h_w^0 are functions of temperature only. Also, the reference temperature is 0^oC, so

$$h_a^0 = 1.004t \quad (23)$$

The specific heat of air as a perfect gas at the reference point is C_p = 1.005 kJ/kgK, so:

$$h_w^0 = h_g = C_{pw}t + h_g^0 = 1.004t + 2501 \quad (24)$$

where h_g^0 is the enthalpy of saturated water vapour at the reference temperature.

Thus:

$$h = C_p t + W h_g^0 \quad (25)$$

and:

$$C_{pa} = 0.24 + 1.004W \quad (26)$$

The following correlation is obtained by substituting the values for enthalpy and specific heat capacity of air into the above equation, thereby yielding:

$$h = C_{pa}t + 1061W = (0.24 + 1.004W)t + 2501W \quad (27)$$

3.4.1 Direct Contact between Moist Air and Water

3.4.1.1 Mass Transfer to Air

The mass flow rate of water and air can be written as follows [79]:

$$\frac{\dot{m}_a}{A_{cs}} = m_a \quad (28)$$

And:

$$\frac{\dot{m}_w}{A_{cs}} = m_w \left[\frac{kg}{sm^2}\right], \dot{m}_w = \left[\frac{kg}{s}\right] \quad (29)$$

$$m_w = Wm_a \quad (30)$$

where m_a and m_w are the mass flow rate of air, [kg/s], and mass flow rate of liquid, [kg/h]. Also, A_{cs} is the cross-sectional area of mass transfer, [m^2]. Thus the equations for the process that occurs over a differential length, dl, can be written as follows:

$$-dm_w = m_a dW$$

$$m_a dW = h_M a_M (W_i - W) A dl \quad (31)$$

where h_M is the mass transfer coefficient [kg/s.m^2], a_M is the dimensionless surface area per unit volume or water air interface [m^2/m^3], A is the tower cross-sectional area, and subscripts i and Mrefer to the initial value and mass transfer quantity (i.e. $a_M = 0.02\ \frac{m^2}{m^3}$).

3.4.1.2 Heat Transfer to Air

The conservation of energy for an adiabatic control volume yields:

$$m_a \Delta h = C_{pa} d(t m_w) = C_{pa}[m_w dt + t dm_w] \quad (32)$$

The second term of Eq. (32) can be neglected [81], since it contributes only about 2% of the energy balance. But in steady-flow conditions, it includes the evaporation rate, so it is included and Eq. (32) becomes [41]:

$$m_a dh = -[m_w - m_a(W_2 - W)]dh_{f,w} + h_{f,w} dm_w \quad (33)$$

where $-dm_w = m_a dW$ and heat transfer through the walls in the process has been neglected. Also, the subscripts f and w refer to saturated liquid water, evaluated at the water temperature. The heat transfer to the water can be written as follows:

$$\pm m_w c_w dt_w = h_w a_H (t_w - t_i) A dl \quad (34)$$

Therefore the heat transfer rate is:

$$m_a dh = -m_w dh_{f,w} + m_a dW h_{f,w} \quad (35)$$

3.4.1.3 Total Energy Transfer to Air

The total energy transfer to the air, which includes the heat transfer and mass transfer in the process, can be written as follows:

$$m_w \Delta h_{f,w} = m_a \left(C_{pa} dt_a + h_{fg0} dW\right) = \quad (36)$$

$$[h_D a_M (W_i - W) h_{fg,w} + h_a a_H (t_i - t_a)] A dl$$

where the subscripts fg, w and $fg, 0$ are the latent heat of vaporization for water at the water temperature, and the latent heat of vaporization for water at the reference temperature of 0°C (i.e. $h_{fg,w} = h_{g,w} - h_{f,w}$). The difference between the surface area of water droplets for heat transfer, a_H, and the surface area of water droplets for mass transfer, a_M, are negligible, so it can be assumed that $a_M = a_H = A_V$.

Eq. (36) can also be rewritten with respect to the differential volume as follows:

$$-m_w dh_{f,w} = h_c A_V dV (t_w - t) + h_D A_V dV (W_2 - W) h_{fg,w} \quad (37)$$

The dimensionless term $\frac{h_c}{h_M C_{p,a}}$ is called the Lewis number (Le). Kusuda [82] reviewed the available correlations for calculating Le. Its magnitude expresses the relative rates of propagation of energy and mass within a system. It is relatively insensitive to a temperature variation. For air and water vapour mixtures, the ratio is (0.60/0.71) or 0.845. At low diffusion rates, where the heat-mass transfer analogy is valid, the Le number for air and water vapour mixtures can be expressed as follows [79]:

$$Le = \frac{h_c}{h_M C_{p,a}} \approx 1 \quad (38)$$

By substituting Eq. (38) into Eq. (37), the following correlation can be obtained:

$$-m_w dh_{f,w} = h_D A_V dV \left[Le C_{p,a} (t_w - t) + (W_2 - W) h_{fg,w} \right] \quad (39)$$

Therefore, from eqns. (31), (35), and (39), the following correlation is obtained:

$$\frac{dh}{dW} = Le C_{p,a} \frac{t_w - t}{W_{s,w} - W} + h_{g,w} \quad (40)$$

Substituting Eq. (25) and using an approximation of $C_{p,a}$ in Eq. (40), the differential enthalpy can be written as follows:

$$h_{s,w} - h = C_{p,a}(t_w - t) + h_g^o(W_{s,w} - W) \quad (41)$$

where the subscript s,w stands for the enthalpy of saturated moist air evaluated at the water temperature and h_g^o is the specific enthalpy of saturated water vapour at the reference temperature (i.e. superscript ^{o} is stands for reference temperature). Hence, Eq. (41) can be written as:

$$\frac{dh}{dW} = Le\frac{h_{s,w} - h}{W_{s,w} - W} + (h_g + h_g^o Le) \quad (42)$$

Therefore, for water, Eq. (42) can be rewritten as:

$$\frac{dh}{dW} = Le\frac{h_{s,w} - h}{W_{s,w} - W} + (h_g + 2501Le) \quad (43)$$

By assuming the water temperatures at $t_{w,\ 1}$ and $t_{w,2}$, represent the inlet and outlet water temperature at states 1 and 2, respectively, the water-flow rate m_w, the air-flow rate m_a, and the entering air state are known.

With this information, we may solve Eq. (43) for the direction of dh/dW of the condition line at State (1) as shown in Figure 7, and the schematic of a cooling tower in Figure 6. In the psychrometric chart with a chart protractor, a line segment with this direction can be drawn though State (1). A short distance from State (1) on this line, to an arbitrary location of State (a), next point, can be defined. Therefore Eq. (35) can be rewritten as follows [41]:

$$-\Delta T_w = \frac{m_a}{m_w c_w}(\Delta h - \Delta W h_{f,w}) \quad (44)$$

With Eq. (44), the water temperature can be calculated for state (a). Then Eq. (39) can be solved and the procedure is continued until the complete condition line is drawn and the final air state is determined. The accuracy of this method depends upon the extent of the assumed incremental changes of air state. Therefore, finding the water temperature corresponding to the new state, (a'), the enthalpy of the water state (a) can be calculated by the following correlations:

$$m_a dh = -m_w dh_{f,w} + m_a dW h_{f,w}$$
$$m_a(h_1 - h_2) = -m_w(h_{f,w,1} - h_{f,w2}) + m_a(W_1 - W_2)h_{f,w} \quad (45)$$

By rearranging the above equation, the new enthalpy can be defined.

There are many ways to find the enthalpy within the tower. Muangnoi et al. [83] used a differential length instead, and consequently the other properties were defined by increasing the height of the tower. However, the method adopted in this thesis will use the psychrometric chart to find the properties of water and air inside the cooling tower, then find the corresponding properties by using commercial software, such as Engineering Equation Solver, EES. The inlet temperature, mass flow and other properties of air and water are given. The outlet temperature and mass flow rate of the outlet water have also been given, depending on the application and requirement of the outlet temperature.

The accuracy of the methods depends upon the extent of the assumed incremental changes of air state and other parameters such as the height of the tower [72, 73, 79, 84]. The slope on the chart protractor can be determined as follows:

$$\left(\frac{dh}{dW}\right)_{point\ 1} = Le\frac{h_{s,w,2} - h_1}{W_{s,w,2} - W_1} + (h_{g,w,2} + 2501Le) \quad (46)$$

where $h_{s,w,2}$, and $W_{s,w,2}$ are the enthalpy of saturated moist air, evaluated at the water temperature, and humidity ratio of saturated moist air, evaluated at the water temperature, respectively. Consequently, h_1 and W_1 are the enthalpy of moist air and humidity ratio of moist air at a given location. For instance, 1 is the inlet location of the air, and 2 is the outlet location for the water according to Figure 6, both at the same elevation. Also $h_{g,w,2}$ is the enthalpy of saturated water vapour evaluated at its elevation. For example, $h_{g,w,2}$ is the enthalpy of saturated water with a quantity of $x = 1$ at the exit water temperature.

By having inlet properties of air and outlet properties of water, the first term of the previous equation can be determined from the psychrometric protractor chart, thus:

$$\frac{h_{s,w,2} - h_1}{W_{s,w,2} - W_1} \rightarrow arbitrary\ location \tag{47}$$

Therefore, $h_{s,w,2}$ is the enthalpy of moist air at the inlet temperature of water and the same for $W_{s,w,2}$. Also, h_1 and W_1 are the enthalpy and humidity ratios of moist air, evaluated at the inlet air temperature. Eq. (46) is represented by the slope in the chart protractor. It can be solved by substituting Eq. (47) into Eq. (46):

$$\left(\frac{dh}{dW}\right)_{point\ 1} \rightarrow\ slope\ at\ chart\ protractor \tag{48}$$

Using the slope and initial point for the enthalpy of moist air, a parallel line in the direction of the slope can be drawn from the enthalpy point. The accuracy of this method is dependent upon the length line. In other words, smaller increments can lead to more accurate results. By following the line in the direction of the slope, the next enthalpy of water can be predicted. In real cases, it is not a linear line, so a shorter distance between each increment would give better results. From that location the new properties of moist air can be obtained. By having the

arbitrary location of the next state (State (a)), the new water temperature can be determined from Eq. (47), yielding:

$$-\Delta T = t_{w,a'} - t_{w,2} = \frac{m_a}{m_w c_w}\left[(h_a - h_1) - (W_a - W_1)h_{f,w,2}\right] \quad (49)$$

In this thesis, the 1, a, b, c, ... represent the arbitrary location of the new state for moist air, and 2, a', b', c', ... represent the arbitrary locations of water as presented in Figure 6.

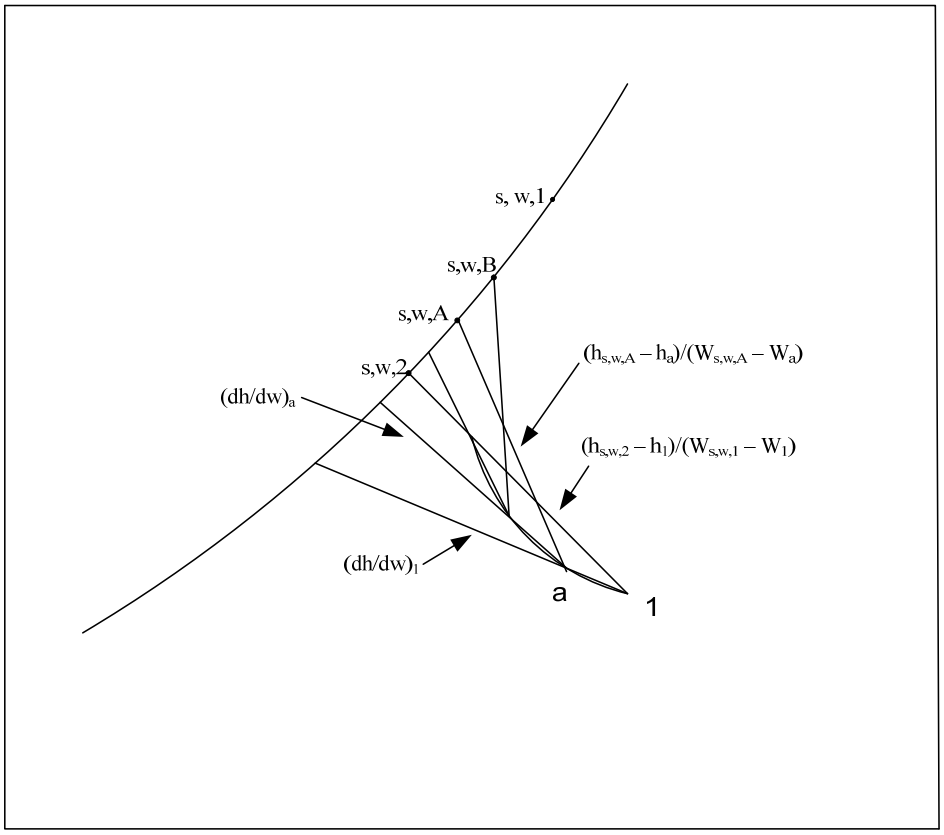

Figure 7: Graphical solution of Eq. (48) on psychrometric chart.

By having both the water temperature and the enthalpy of moist air from the psychrometric chart at the new state, the procedure can be repeated in order to obtain the properties for new states,

and calculated the other properties of water and moist air at the corresponding states. In order to automate this process the method has been modified to find the properties without using the psychrometic chart protractor. Using the inlet properties of liquid, and moist air, and the outlet temperature of the liquid, (dh/dW) can be calculated from Eq. (48). Substituting the result from Eq. (48) into Eq. (49), the new slope of (dh/dW) can then be found. Hence, by choosing an enthalpy close to the moist air enthalpy as the next selection for moist enthalpy, smaller increments lead to more accurate results and Eq. (49) can be rearranged and solved for W_a for the new State (a). Therefore:

$$\frac{h_{s,w,2} - h_1}{W_{s,w,2} - W_1} \rightarrow slope \tag{50}$$

Thus:

$$\frac{h_a - h_1}{W_a - W_1} = \left(\frac{dh}{dW}\right)_1 \tag{51}$$

The humidity ratio of moist air at State (a), the next state, can be obtained by rearranging Eq. (50) and using Eq. (51) to calculate $(dh/dW)_1$:

$$W_a = W_1 + \frac{h_a - h_1}{(dh/dW)_1} \tag{52}$$

Consequently, using the humidity ratio and enthalpy of State (a), the other properties can be calculated. For this method, the EES program was used to calculate the properties of moist air and water, then comparing it to the graphical method using the chart protractor and psychrometric chart. Therefore, the temperature of moist air can be calculated based on the humidity ratio and enthalpy of moist air at atmospheric pressure.

3.4.2 Direct Contact of Moist Air and $CuCl_2$ Solution

In the $CuCl_2$ aqueous solution drying process, air is assumed to be a perfect gas. Therefore the enthalpy of the process can be written as follows:

$$\bar{h} = x_a \bar{h}_a^0 + x_w \bar{h}_w^0 \quad (53)$$

To convert the moist air enthalpy to units of kg per kJ, the above equation is divided by $28.966x_a$, where x_a is the mole-fraction of dry air (moles of dry air per mole of moist air). Thus:

$$h = h_a^0 + W h_w^0 \quad (54)$$

where W is the absolute humidity of moist air (kg water per kg dry air). The specific enthalpies h_a^0 and h_w^0 are functions of temperature only. Also, the reference temperature of 0^oC is used, so:

$$h_a^0 = 1.004t \quad (55)$$

The specific heat of air as a perfect gas is C_p = 1.004 kJ/kgK at the reference temperature of 0^oC. The specific enthalpy of saturated water vapour at the reference temperature is $h_g^0 = 2501 kJ/kg$ therefore:

$$h_w^0 = h_g = C_{pw}t + h_g^0 = 1.004t + 2501 \quad (56)$$

The solubility of $CuCl_2$ in an aqueous solution has been determined experimentally [85], and shown in Table 3. It shows the solubility of $CuCl_2$ at different temperatures for 100 grams of pure water. In this thesis, a 30% concentration of solid $CuCl_2$ is assumed to be dissolved in the water.

Table 3. The amount of $CuCl_2$ powders that are soluble in 100 g of water at temperature indicated, and percentage of anhydrous $CuCl_2$ soluble in 100 g of solution [85].

Temperature ^oC	Grams of Solid $CuCl_2$ in the Solution g	Weight of Solute per Weight of Solution %
0	70.70	41.42
10	73.76	42.45
20	77.00	43.50
30	80.34	44.55
40	83.80	45.59
50	87.44	46.65
60	91.20	47.70
70	-	-
80	99.20	49.80
90	-	-
100	107.9	51.90

Since there is no experimental enthalpy data available for the cupric chloride solution at different temperatures and concentrations, the enthalpy is therefore estimated by using the summation of weight percentage of solute and solvent, multiplied by the enthalpy of the solute and solvent, respectively. Table 4 presents the enthalpy at the reference temperature of 0^oC for 30% $CuCl_2$ concentration in the solution.

Table 4. Enthalpy of $CuCl_2$ and solution at reference temperature [86].

Substance	Specific Enthalpy kJ/kg
$CuCl_2$	1398.52
Water	2501.00
Solution	2170.26

Thus, Eq. (56) can be rewritten as follows for the $CuCl_2$ solution:

$$h_w^0 = h_g^0 = C_{pw,solution}t + (2170.26) \quad (57)$$

The enthalpy can be determined as follows:

$$C_p t + Wh_g^0 = 0.24t + Wh_g^o \quad (58)$$

$$h = C_{pa}t + 2170.26W = \left(1.004 + c_{pw\,solution}W\right)t + 2170.26W \quad (59)$$

$$C_{pa} = 1.004 + C_{pw\,solution}W \quad (60)$$

where C_p = 1.004 kJ/kgK. The enthalpy of air as an ideal gas at the reference point is:

$$h_w^0 = h_g = C_{pw}t + h_g^0 = 1.004t + 2024 \quad (61)$$

where h_g^0 is the enthalpy of saturated water solution at the reference temperature. Therefore:

$$h = C_p t + Wh_g = 0.24t + Wh_g \quad (62)$$

thus:

$$h = C_{pa}t + 2024W = (0.24 + 0.45W)t + 2024W \quad (63)$$

By following the same procedure for water and moist air heat transfer, mass transfer, and total energy, the following correlation can be obtained for the enthalpy difference in the water:

$$-m_w dh_{f,w} = h_D A_V dV\left[LeC_{p,a}(t_w - t) + (W_{s,w} - W)h_{fg,w}\right] \quad (64)$$

Therefore, the enthalpy difference in the drying chamber can be written as follows:

$$m_a dh = -m_w dh_{f,w} + m_a dW h_{f,w} \quad (65)$$

The water temperature gradient can be written as follows:

$$\Delta t_w = \frac{m_a}{m_w C_w}(\Delta h - \Delta W h_{fw}) \quad (66)$$

In Eq. (64), using the water temperature, t_w, humidity ratio of dry air and humidity ratio of saturated moist air evaluated at the water temperature, $W_{s,w}$, and other parameters, the enthalpy change in the increment of volume, dV, can be calculated.

The enthalpy difference in moist air can be obtained with Eq. (65) from the enthalpy change in water and mass flow rate of gas and liquid. The water temperature difference in the small increment can be calculated from Eq. (66). Integrating the heat transfer coefficient over the surface yields the total heat transfer from the object. This total heat transfer can be written as the average heat transfer coefficient, $\bar{h}$, multiplied by the temperature difference, T_s - T_{∞}, where:

$$\bar{h} = \frac{1}{A_V}\int_{A_V} h dA_V \quad (67)$$

In a similar way to heat transfer, an analogous set of equations and coefficients can be obtained for mass transfer arising from species concentration differences in the flow field [71].

The evaporation heat transfer inside a cooling tower is often much greater than the convective heat transfer rate [87]. The heat transfer rates inside the cooling tower due to convection and evaporation can be expressed as follows, respectively:

$$\dot{Q}_{conv} = h_c A_V (t_w - t_{db}) \quad (68)$$

$$\dot{Q}_{evap} = h_M A_V (W_{s,w} - W_a) h_{fg,w} \quad (69)$$

A computer program was developed based on these equations to determine the heat transfer rates within the drying chamber.

3.5 Spray-drying process

In spray-drying, many properties of the product, including critical moisture content, structure and morphology, depend on the drying rate. The critical moisture content is different for slow drying processes carried out in band or tumble dryers, vs. very fast processes, such as spray dryers [88]. Figure 10 shows a schematic diagram to be used in this analysis, including an electric heater to preheat the ambient air and air filter for the moist air at the end of the product before releasing it into the environment. If an insoluble dry gas is brought into contact with sufficient liquid, the liquid will evaporate into the gas until ultimately, at equilibrium, the partial pressure of liquid in the vapour-gas mixture reaches its saturation value. As long as the gas can be considered insoluble in the liquid, the partial pressure of vapour in the saturated mixture is independent of the nature of the gas and total pressure. It is dependent only upon the temperature and type of liquid. However, the saturated molal absolute humidity is dependent upon the total pressure. The saturated absolute humidity depends on the type of gas.

Both saturated humidities become infinite at the boiling point of the liquid at the prevailing total pressure [89]. In the experimental spray-drying test, the inlet and outlet temperatures, mass flow rate of water/air and humidity ratio were specified to generate solid product. The exiting gas-vapour mixture is saturated. In the experimental test, the outlet and inlet temperatures can be decreased until the product becomes slurry or contains a significant amount of water. In the analysis, the inlet and outlet temperatures and humidity ratio of the inlet air are kept constant, and the required time, volume flow rate, and evaporation of solution with different concentrations are examined for each inlet and outlet temperature.

It will be assumed that the rate at which make-up water is added to the system is negligible compared to the rate of water flow though the nozzles. Also, heat transfer through the walls of the chamber from the ambient surroundings may be neglect and the small addition of energy to the water by the pump has a negligible effect on the water temperature. Thus, transfer processes in the chamber involve evaporation of droplets and convection heat transfer from the air to the water. For steady-flow conditions, in a differential volume dV, the mass balance equation can be expressed as follows:

$$dm_w = m_a(W_2 - W_1) \tag{70}$$

The internal energy U of a substance is the total energy residing in the substance owing to the motion and relative position of the constituent atoms and molecules. The absolute values of internal energy are not known, but numerical values relative to some standard state for the substance can be computed. The sum of the internal energy and the product of pressure and volume of the substance, when both quantities are expressed in the same units, is defined as the enthalpy of the substance:

$$H = u + pv \tag{71}$$

In a batch process at constant pressure, where work is done only by expansion against pressure, the heat absorbed by the system is the gain in enthalpy, i.e.,

$$Q = \Delta H = \Delta(u + pv) \tag{72}$$

In a steady-state continuous-flow process, the net transfer of energy to the system as heat and work will be the sum of its gains in enthalpy and potential and kinetic energies. The change in enthalpy can be calculated by use of an average heat capacity, therefore:

$$h_1 - h_2 = C_{avg}(t_1 - t_2) \tag{73}$$

where C_{avg} is the average heat capacity.

The dew point is the temperature at which a vapour-gas mixture becomes saturated when cooled at constant total pressure, out of contact with a liquid. Therefore, when a mixture is cooled at constant pressure, out of contact with liquid, the mixture becomes more nearly saturated as the temperature is lowered, and fully saturated at t_{dp}, dew point temperature. All mixtures of absolute humidity w_s have the same dew point. If the temperature is reduced by only an infinitesimal amount below t_{dp}, vapour will condense as liquid dew. Therefore, the ratio of mass of vapour / mass of gas is the molal absolute humidity $w_{s,}$, which can be defined as follows [89]:

$$w'_s = \frac{w_w}{w_a} = \frac{P_w}{P_a} = \frac{P_w}{P_t - P_w} \frac{moles\ of\ vapour}{moles\ of\ air} \tag{74}$$

where vapour is designated as substance w, and the gas is designated as substance a, which is a relatively highly superheated gas. Thus, the absolute humidity can be rewritten as follows:

$$w_s = w'_s \frac{M_w}{M_a} = \frac{P_w}{P_a} = \frac{P_w}{P_t - P_w} \frac{M_w}{M_a} \frac{mass\ of\ vapour}{mass\ of\ gas} \quad (75)$$

where M is the molar mass.

The humidity volume, v_H, of a vapour-gas mixture is the volume of a unit mass of dry gas and its accompanying vapour at the prevailing temperature and pressure. For a mixture, the ideal-gas law humidity volume can be written as follows

$$v_H = \left(\frac{1}{M_a} + \frac{w\prime}{M_w}\right) 22.41 \frac{t_a + 273}{273} \frac{1.013 \times 10^5}{p_t} = 8315 \left(\frac{1}{M_a} + \frac{w\prime}{M_w}\right) \frac{t_a + 273}{p_t} \quad (76)$$

where v_H is in unit of m^3/kg, t_a in Celsius and p_t is the total pressure in N/m^2. The humidity volume of a dry gas is zero. For partially saturated mixtures, v_H can be interpolated between values for 0 and 100% saturation, at the same temperature according to the percentage saturation.

The heat required to raise the temperature of a unit mass of gas and its accompanying vapour by one degree at constant pressure is called humidity heat, C_s. Hence, for a mixture of absolute humidity, w'_s, the humidity heat can be defined as follows:

$$C_s = C_a + w' C_w \quad (77)$$

If neither vaporization nor condensation occurs, the heat required to raise the temperature of a mass of W_a dry gas and its accompanying vapour and amount Δt will be

$$Q = w_a C_S \Delta t \quad (78)$$

The enthalpy of a vapour-gas mixture is the sum of enthalpies of the gas and vapour. If the mixture is unsaturated, the vapour has a superheated state, therefore the enthalpy can be calculated relative to the reference states of gas and saturated liquid at t_0. The enthalpy of the gas

alone is $C_a(t_a - t_0)$. Therefore, the enthalpy per unit mass of vapour will be written as follows below, where t_{dp} is the dew point of the mixture and h_{fg} is the latent heat of vaporization of the vapour at that temperature:

$$C_a(t_{db} - t_{dp}) + h_{fg} + C_w(t_{dp} - t_0) \quad (79)$$

where:

$$t_{db} - t_w = h_M \frac{h_{fg}(w'_w - w')}{h_a} \quad (80)$$

and:

$$\frac{h_c}{h_M C_S} = \left(\frac{Sc}{\Pr}\right)^{0.567} \quad (81)$$

Then the total enthalpy of the mixture per unit mass of dry gas can be written as follows,

$$h = C_a(t_a - t_0) + w'[C_w(t_a - t_{dp}) + h_{fg}^0 + C_w(t_{dp} - t_0)] \quad (82)$$

Therefore, the total enthalpy can be rewritten as follows:

$$h = C_a(t_a - t_0) + [C_w(t_a - t_0) + h_{fg}^0]w' \quad (83)$$

By substitution of the absolute humidity with the appropriate humidity heat, the enthalpy of saturated mixtures can be computed. When the inlet and outlet humidity ratios are known, then the evaporation rate can be calculated for different temperatures at the inlet and outlet.

Chapter 4

Results and Discussion

This chapter deals with the main findings and numerical results of models developed in the previous chapter, including validation results for water and $CuCl_2$. Several sensitivity studies will be performed to determine the effects of different variables. The effects of inlet and outlet temperature, mass flow rate and the rate of evaporation are investigated. Model validations are performed for both the cooling tower and spray-drying problems, to ensure the model is an accurate simulation of real-world processes. In the analysis, the heat and mass transfer coefficients and heat capacity of the gas and liquid were assumed to be constant.

4.1 Model Validation

Models developed in the previous chapter will be validated by comparing the results with previous data for pure water in a cooling tower and experimental results for $CuCl_2$ in spray-drying.

4.1.1 Cooling Tower Validation

Consider a cooling tower problem depicted in Figure 6. The problem parameters are shown in Table 6. An experiment with pure water was performed to compare the predicted results with previous study [41]. Then the model was applied to aqueous $CuCl_2$ solution to compute the evaporation rate within the cooling tower.

Figures 8 and 9 represent a comparison of results between experimental and theoretical results in the cooling tower. The results show there is a close agreement, within 1%. Table 5 shows the temperatures for air, water, and the reference temperature that was used in the cooling tower simulation.

Table 5. Temperatures of air and water in cooling tower.

Water Inlet Temperature °C	Water Outlet Temperature °C	Air Dry-Bulb Inlet Temperature °C	Air Dry-Bulb Outlet Temperature °C	Air Wet-Bulb Inlet Temperature °C	Reference Temperature °C
29.4	37.8 °C	34.4 °C	37.8°C	23.9 °C	0 °C

The value for the mass and heat transfer coefficient, Lewis number, and other parameters are shown in Table 6.

Table 6. Problem parameters for cooling tower.

Lewis Number	$h_D A_V$ kg/m^{3}s	Tower Area m^2	m_w/m_a kg_{moist}/kg_{air}	Pressure Pa
0.895	3.025	1.025	1.00	101.3

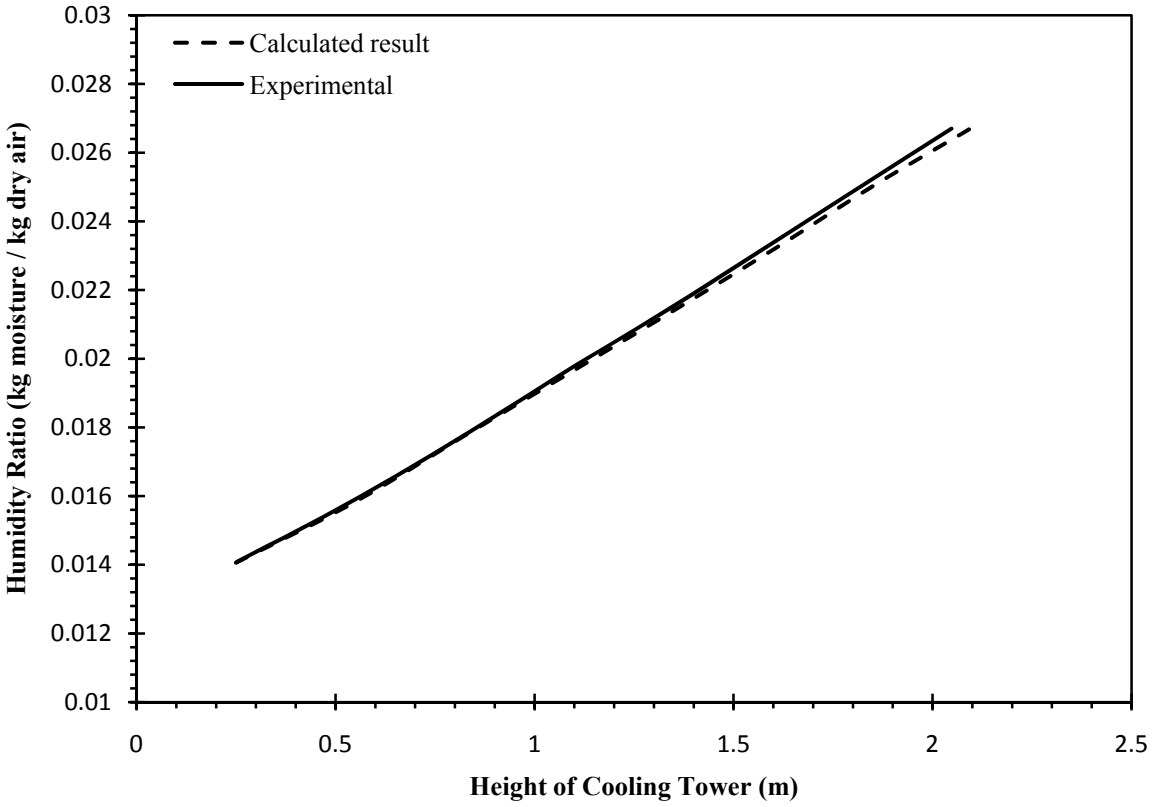

Figure 8. Comparison of humidity ratios within the cooling tower with experimental data [41].

Figure 8 shows that the humidity of air increases with height along the cooling tower. Since the air stream travels from the bottom to the top of the cooling tower, as shown in Figure 6, the humidity of air increases as it approaches the top of the cooling tower. Therefore, by increasing the height of the cooling tower, more evaporation occurs. The water temperature profile, plotted against the height of the tower, is shown in Figure 9. It shows the water temperature within the cooling tower against the height of the tower.

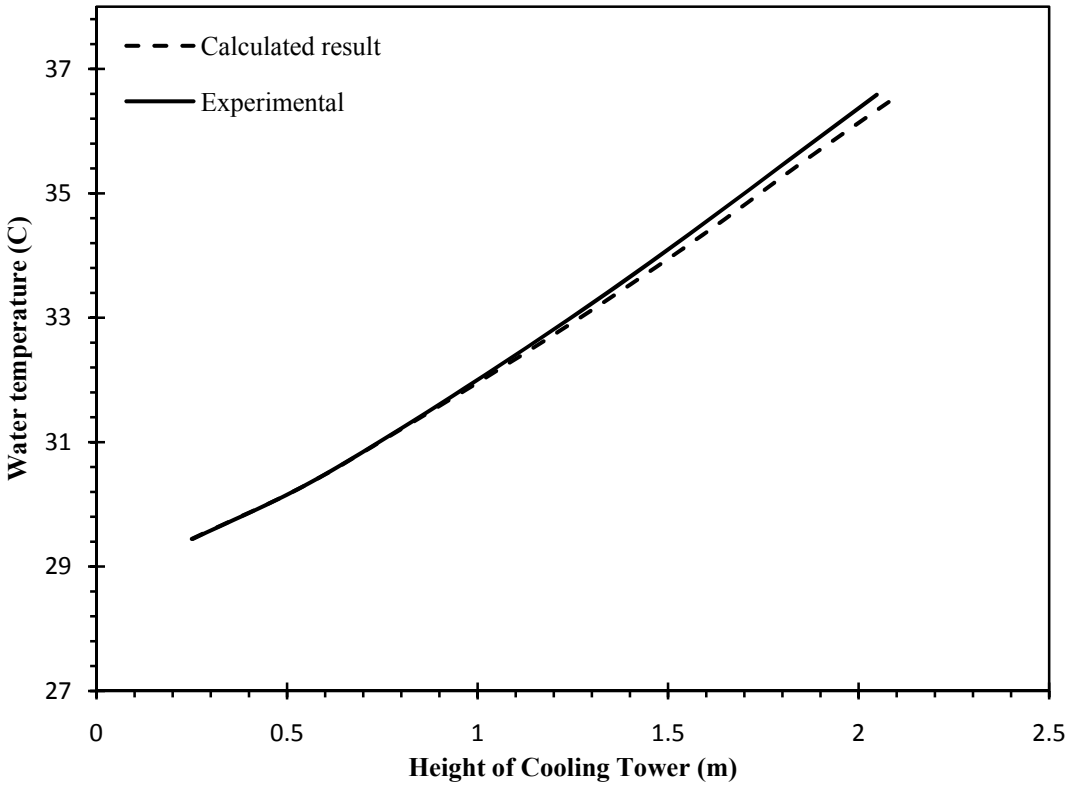

Figure 9. Comparison of the water temperature within the cooling tower to past data of Threlkeld et al. [90].

4.1.2 Comparisons with Experimental Data

An experimental test for a $CuCl_2$ solution was performed with a Niro Mobile Minor Spray-Dryer to obtain solid powder of $CuCl_2$. The color of cupric chloride at the beginning of the test was light green, indicating the cupric chloride was in dehydrate form. The atomization method was a Schlick two-fluid nozzle in the top spray configuration with a size 0.8 mm nozzle tip. Each test performed two different feed rates. Multiple runs were also performed for each individual mass flow rate to confirm the experimental results. In total, 8 experimental values were obtained for two different flow rates. From the manufacturer, the measurement uncertainty due to the two-

fluid nozzle atomization air flow rate is at most 5%. In the first case, the air was preheated from an ambient temperature to 200^{o}C, when it entered the spray dryer. The average outlet temperature was 110^{o}C. Table 7 shows the experimental values and results. The experiments were performed three times with the same parameters. The spray dryer was 31 inches in diameter, with a 24 inch cylindrical height and a 60^{o} conical bottom. The two-fluid nozzle was attached to the ceiling of the spray dryer. The drying gas in the experiment was ambient air, heated by an electric heater. The heated air entered the chamber through the ceiling and exited through the base of the chamber along with the dry powder. In the drying process, the hot gas and droplets do not contact the chamber's wall. The air and powder travel through a cyclone, where powder is collected and air moves to a cartridge filter. The purpose of the cartridge filter was to remove very fine material before air can be safely released into the environment. As an extra precaution to ensure the outlet air is clean, the air was released into a water container. The experiments were performed with two different runs, each with settings selected to test the range of cupric chloride's sensitivity to spray-drying. In the first and second run, air was used for the drying gas. In first run, 0.45 kg/s of feed material was sprayed. The inlet temperature was 200^{o}C, and the outlet temperature was 110^{o}C. Figure 10 shows a schematic of the spray dryer. The inlet solution of $CuCl_s(2H_2O)$ enters the atomizer at an ambient temperature of 25^{o}C for all of the experimental tests.

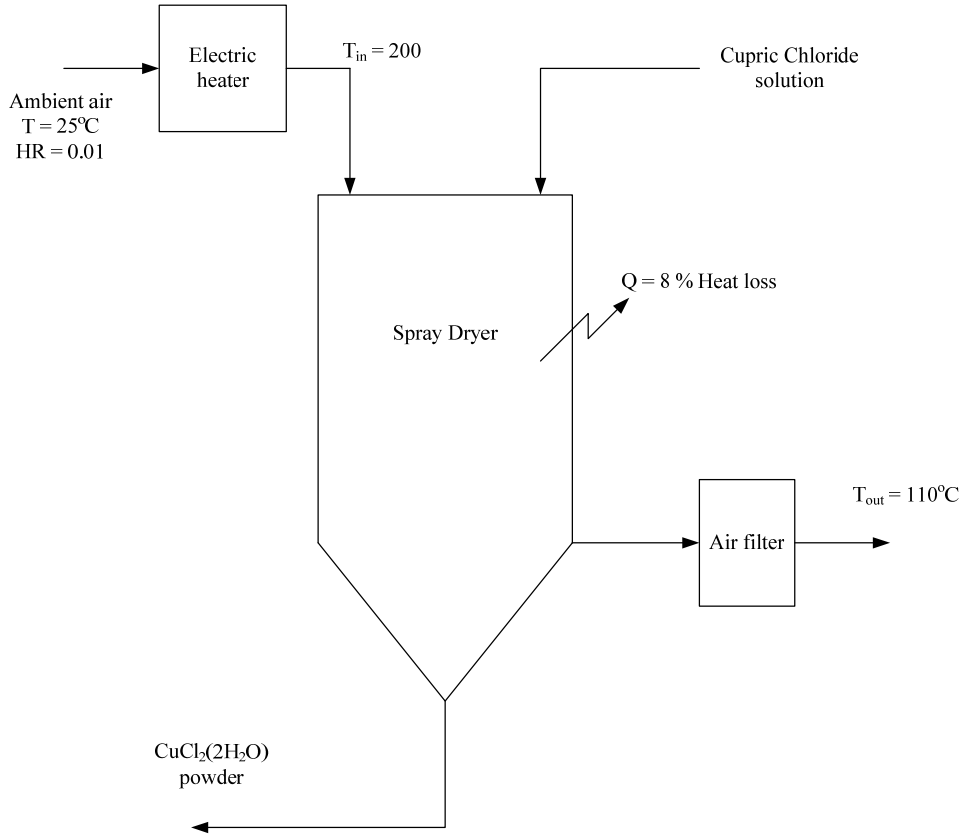

Figure 10. Schematic of spray dryer with components such as electric heater and air filter.

The color of cupric chloride before it was mixed with water was green, indicating the powder was dihydrate. Product collection from the cyclone appeared normal with a brown color, indicating the product was anhydrous and it contained a small amount of moisture. From weight measurements, 331 grams of brown powder was recovered for a recovery rate of 88.6%. In the first experiment, the inlet air flow rate was 82 kg/h.

Table 7. Experimental results from Niro-Spray Dryer, using hot air at 200°C as the drying gas and an outlet average temperature of 110°C.

Inlet Temperature °C	Outlet Temperature °C	Atomizing Gas Pressure bar	Inlet Gas Pressure Mbar	Chamber Pressure Mbar	Solution Feed Rate ml/h	Solution Density g/cc	Solid Product kg	Product Rate kg/h	Mass Transfer Rate kg/h	Feed Solids %
200	112	2.0	30	13	780	1.46	0.183	0.361	0.77	44.8
200	110	2.0	31	19	780	1.46	0.183	0.361	0.77	44.8
200	110	2.0	32	20	780	1.46	0.183	0.361	0.77	44.8

Figure 11 shows the experimental and analysis results. In the analysis, an 8% heat loss was assumed (heat loss though atomizer nozzle and chamber wall prediction). Figure 11 shows a 2% difference from the actual value. In the experimental results, an outlet average temperature of 110°C and 100°C were obtained.

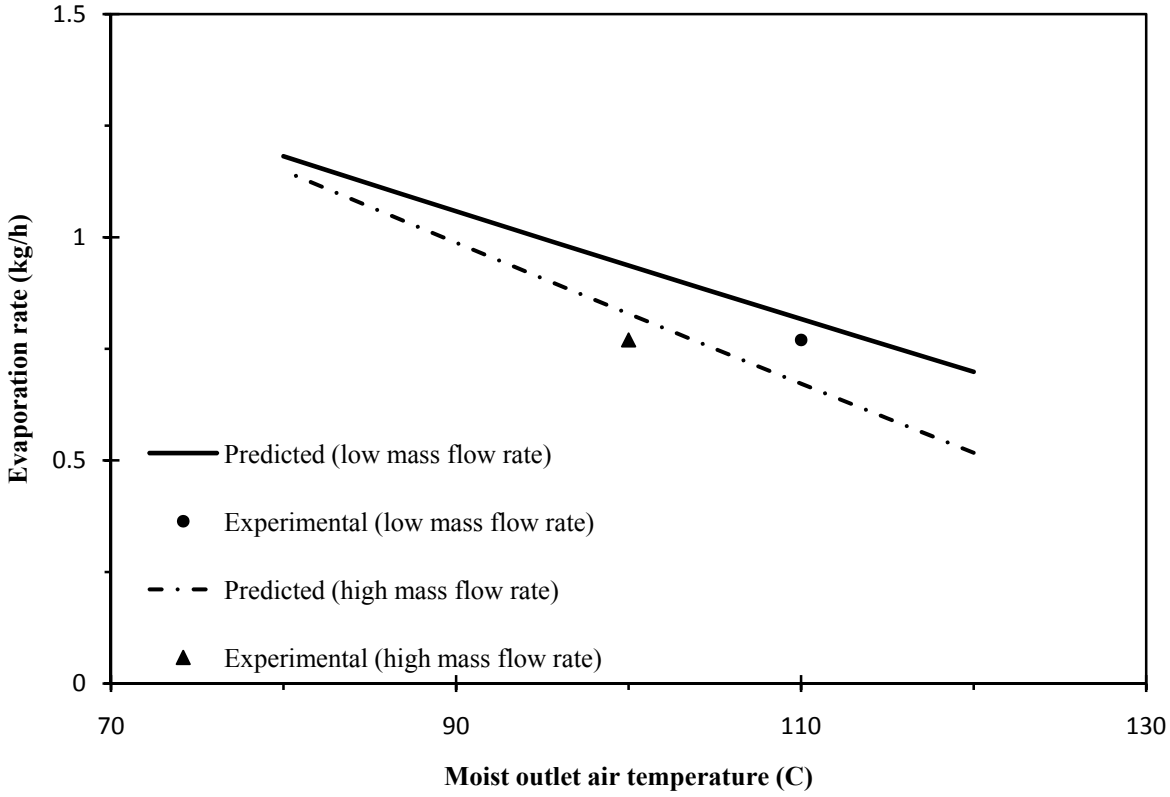

Figure 11. Experimental and predicted results for $CuCl_2$ solution (Inlet and outlet temperature of 200^{o}C and 110^{o}C, and inlet and outlet air temperature of 170^{o}C and 100^{o}C).

The second test was performed with the same conditions. Air was used for the drying gas and 0.87 kg/s of feed material was sprayed. To assess sensitivity of cupric chloride in spray-drying, a different inlet and outlet temperature of 170^{o}C and 100^{o}C, for drying gas was assumed, respectively. The product collection from the cyclone appeared to be normal with a brown color. At the end of the process, 331 grams of brown powder was recovered for a recovery rate of 80.08%. The inlet air flow rate was set as 82 kg/h. Table 8 shows data values for the second experimental test for different inlet and outlet drying gas temperatures.

Table 8. Experimental results for Niro-Spray dryer, using hot air at lower temperature of 170°C as drying gas, and outlet average temperature of 100°C.

Inlet Temperature °C	Outlet Temperature °C	Atomizing Gas Pressure bar	Inlet Gas Pressure Mbar	Chamber Pressure Mbar	Solution Feed Rate ml/h	Solution Density g/cc	Solid Product kg	Product Rate kg/h	Mass Transfer Rate kg/h	Feed Solids %
170	99.0	1.5	22	6	950	1.27	0.3313	0.41	0.79	31.6
170	100	1.5	22	8	950	1.27	0.3313	0.41	0.79	31.6
170	101	1.5	22	8	950	1.27	0.3313	0.41	0.79	31.6
170	100	1.5	22	7	950	1.27	0.3313	0.41	0.79	31.6
170	101	1.5	22	8	950	1.27	0.3313	0.41	0.79	31.6

The comparison results of the second run and theoretical results are also shown in Figure 11. A 2% error can be observed from the graphs which again can be attributed to the heat loss within the wall of the dryer. In the theoretical calculation only, 8% loss due to the heat loss was considered, nevertheless this heat loss can vary and can be more than 8%. Therefore, the error is a reasonable value and consequently the theoretical calculation can be validated. The photographic results for products of both runs are shown in Figure 12. It can be observed from the photos that the particle sizes vary between 20 to 40 μm.

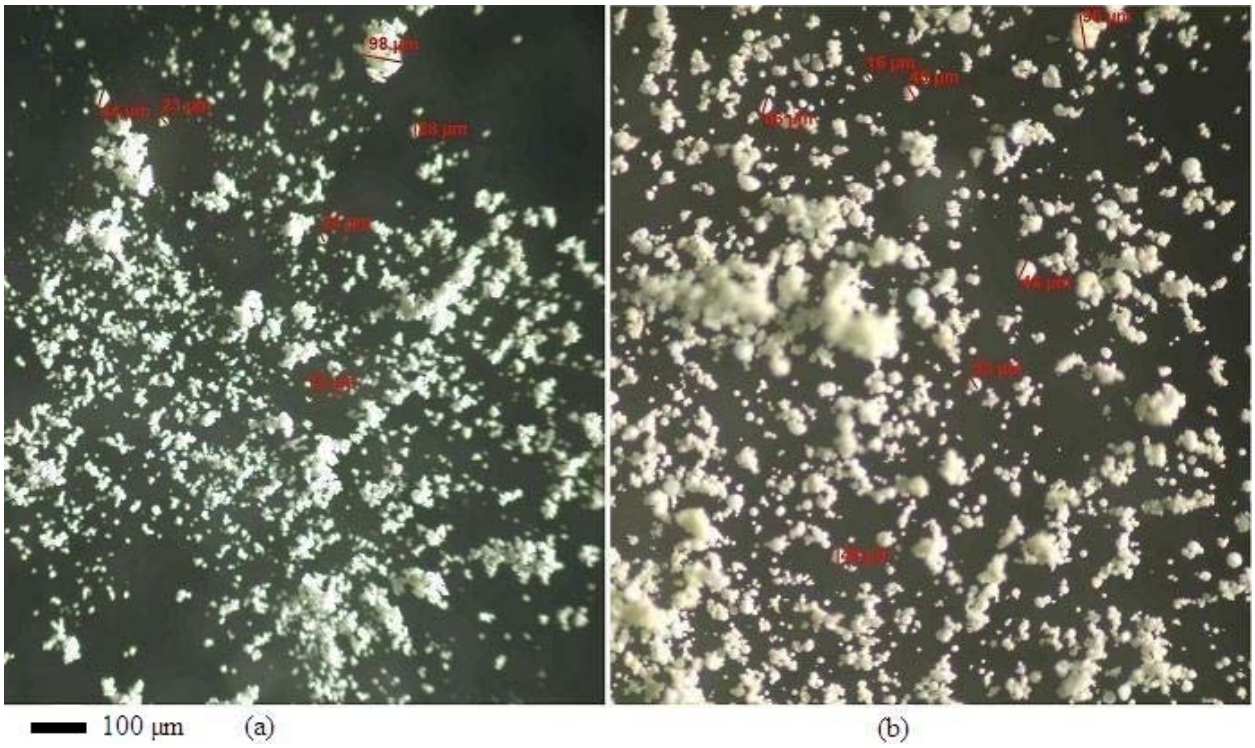

Figure 12. a) Particles of first run with 70% air to liquid content in atomizer, b) powder size for second run with 54% atomizing gas flow.

In the process, it is possible to control the particle size by changing the atomizing gas flow percentage. The results show that a lower atomizer gas flow, with an air to solution percentage of 54%, can produce a larger powder size as the product.

4.2 Cooling Tower Prediction

The cupric chloride solution is assumed to enter the tower from the top, with air blowing from the bottom to the top. In this section, a solution of cupric chloride with 20% solid in the solution will be studied to determine the temperature gradient of water, air dry-bulb, air wet-bulb and evaporation rate within the tower. $CuCl_2$ has a different solubility with respect to the water

temperature. The density of the solution varies with temperature. The solid concentration in the solution is presented in Figure 13.

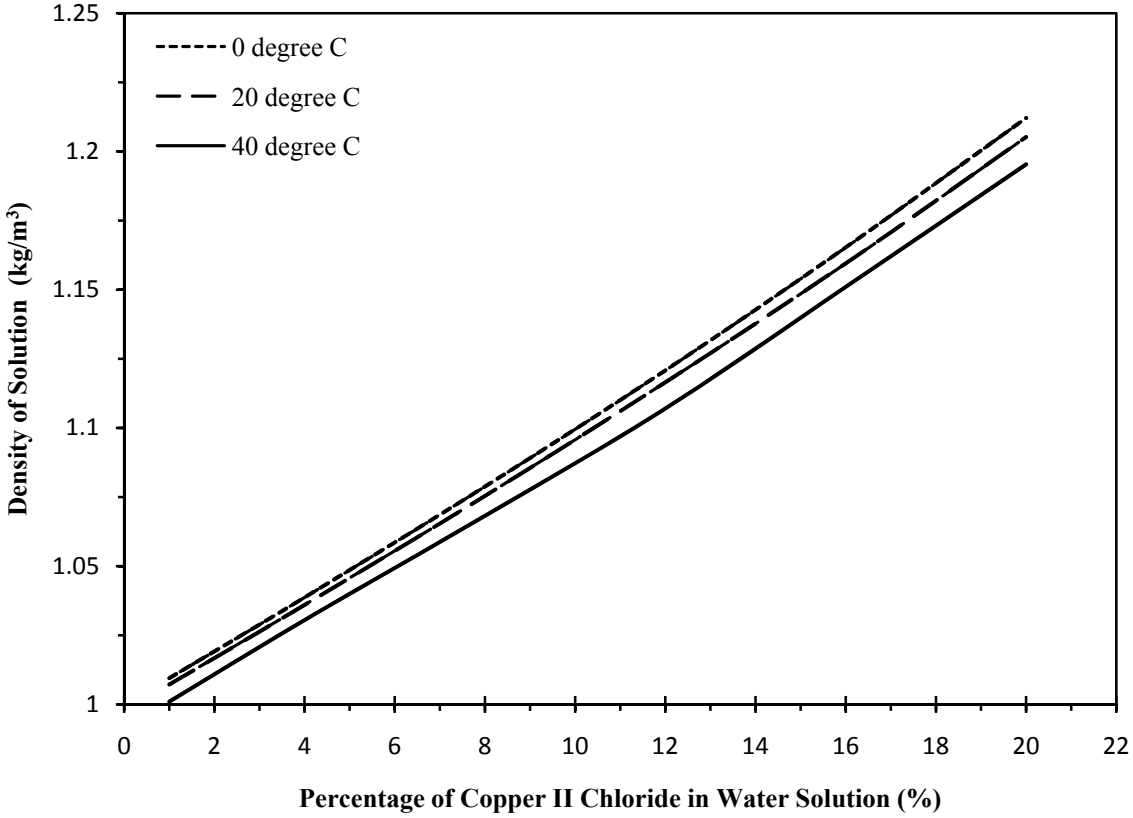

Figure 13. Density of solution of $CuCl_2$ in water at different temperatures and concentrations.

The solubility of $CuCl_2$ in an aqueous solution has been determined by experimental studies that are summarized in Table 3. It presents the solubility of $CuCl_2$ at different temperatures for 100 grams of pure water. In this section, a 25% concentration of solid $CuCl_2$ is assumed to be dissolved in the water. At ambient temperatures, the $CuCl_2$ has a weight content of 44% in water, with the solution at its saturation. Figure 14 shows the viscosity of $CuCl_2$ in a water solution at different temperatures and Copper II Chloride concentrations. Therefore, at a temperature of 308.15 K and 25% concentration by weight of $CuCl_2$, the viscosity can be determined as

$0.80x10^{-3}$ [Pa.S] [70]. The kinematic viscosity is the ratio of the absolute viscosity to the density of a fluid and it can be expressed as follows [42, 70]:

$$\vartheta = \frac{\eta}{\rho}\ [\frac{m^2}{Sec}]$$

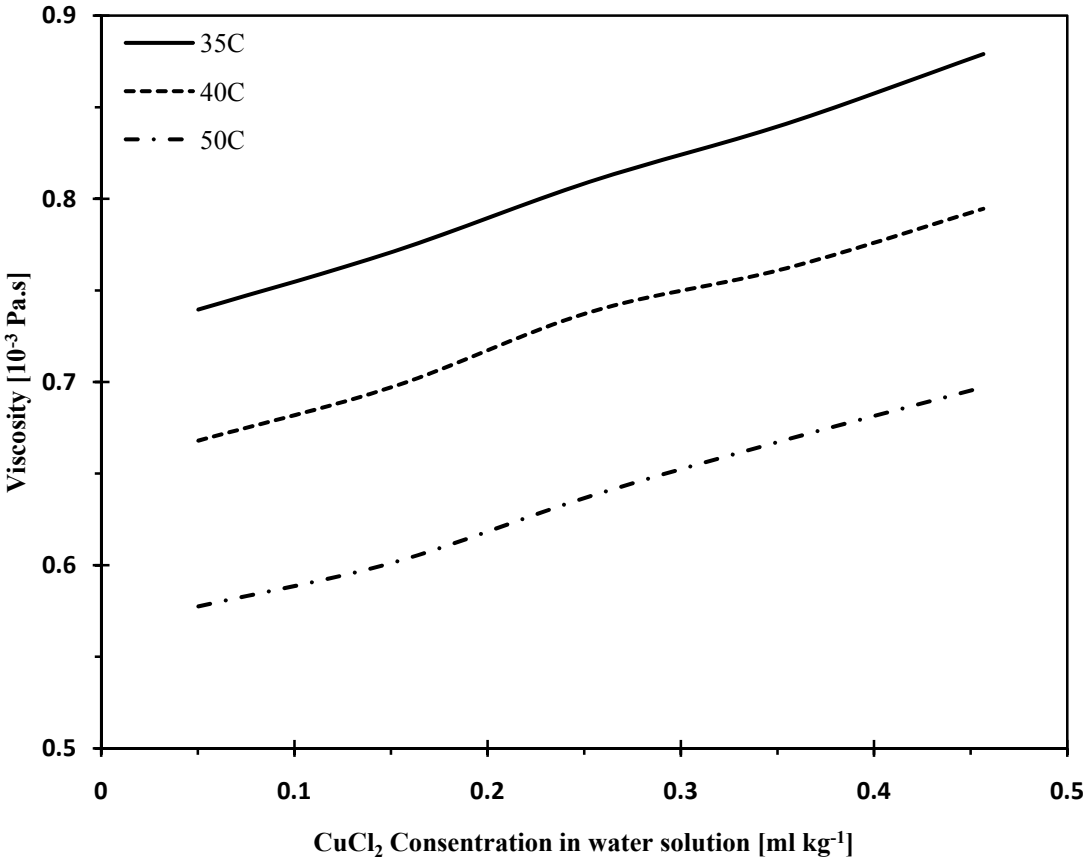

Figure 14. Viscosity of copper II chloride in water solution at different temperature conditions.

Also, the density of the solution at 25% concentration is approximated according to Figure 13, $\rho = 1255\ kg/m^3$. Also, the kinematic viscosity can be calculated as $\vartheta = \frac{\eta}{\rho}\ [\frac{m^2}{Sec}]$.

Substituting the values of diffusivity and viscosity into the dimensionless Schmidt number, $Sc = \frac{v}{D} = \frac{\mu}{\rho D}$

Numerical calculations were performed for two different mass flow ratios of air and liquid. In this thesis, the mass of water per mass of gas were considered 1 and 1.5 kg of water per kg of moist air. Table 9 shows the parameters that were obtained and used in the numerical calculations.

Table 9. Dimensionless parameters for cooling tower.

Density, ρ kg/m^3	Kinematic Viscosity, υ 10^{-6} m^2/s	Schmidt Number, Sc	Reynolds Number, Re	Prandtl Number, Pr	Biot Number, Bi
1255	0.637	0.0218	25.1	0.0177	0.00241

In the cooling tower, water and air are the working fluids in operation. In a counterflow cooling tower, water flows downwards, while air flows upwards. It is assumed that the conditions of water and air vary only with vertical position in the tower. The differential section of the tower height and boundary conditions are given in Figure 6. The important assumptions of the model are given as follows. Heat transfer from the tower fan to air and water, and through the tower wall to the environment is assumed to be negligible. Heat and mass transfer coefficients throughout the entire tower are constant. Also, heat and mass transfer occurs in a direction normal to the flow. Water loss by drift is negligible. Temperatures of air and water at any cross-section are uniform. Table 10 shows the tower characteristics and outlet / inlet air temperatures.

Table 10. Problem parameters for cooling tower.

Cross-Sectional Area m^2	Inlet water Mass Flow Rate kg/s	Percent Solid %	Average Velocity m/s	Inlet Dry-Bulb Temperature ^oC	Inlet Wet-Bulb Temperature ^oC	Outlet Water Temperature ^oC
1.22	1.2	25	0.8	30	21	24.2

Figure 15 shows the temperature profile of the water and air within the cooling tower. From the temperature graph, it can be observed that wet-bulb and dry-bulb temperatures remained almost constant. However, water temperature associated with a higher air mass flow rate significantly increases in comparison to the lower air flow rate.

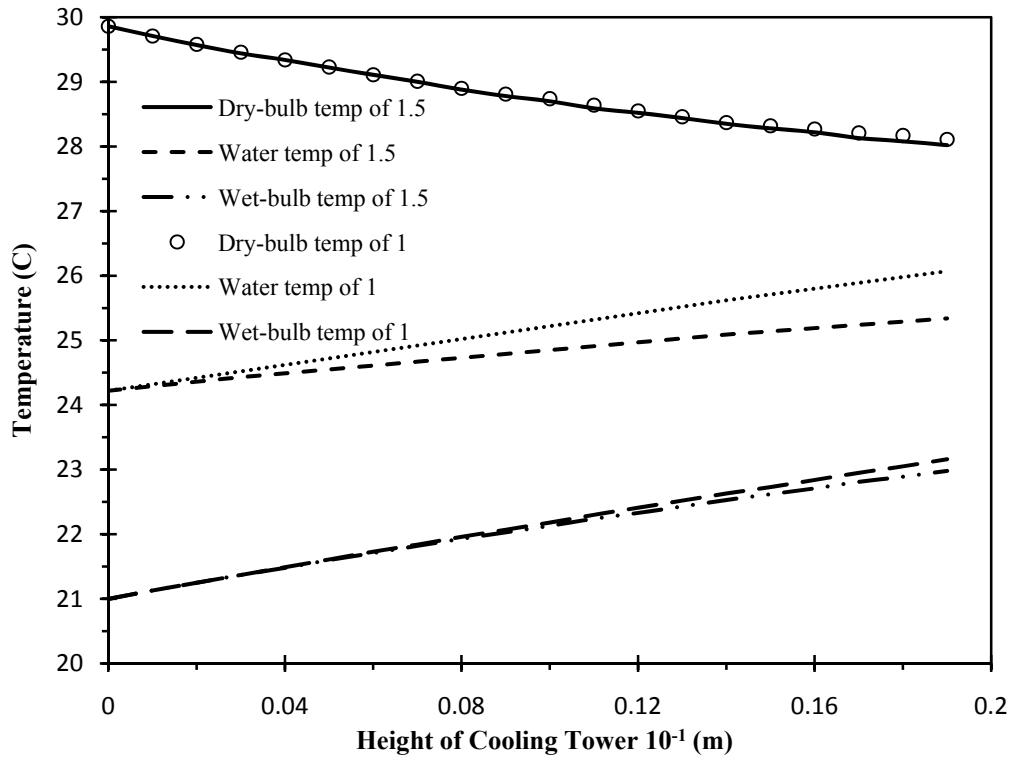

Figure 15. Temperature profile in cooling tower for different mass flow ratios of 1 and 1.5 kg of water per kg of moist air.

A higher water temperature can increase the potential evaporation and convection rate in the tower. The web-bulb temperature of the air in the cooling tower increases continuously from the bottom to the top. It is less than the water temperature. Therefore, heat can still flow from water to air, and as a result, the heat transfer mode in the cooling tower is dominated by evaporation. The driving potentials for evaporation heat transfer ($w_s - w_a$) and convective heat transfer ($t_w - t_{db}$) versus tower volume are presented in Figure 18 for m_w/m_a ratio varying from 1 to .5 kg/s. It can be observed in Figure 16 that the humidity ratio of saturated moist air, W_{sw}, decreases with tower height measured from the top because the water temperature decreases as it moves down. The humidity ratio of moist air, W_a, increases with tower volume measured from the bottom, because the air absorbs moisture as it moves upwards.

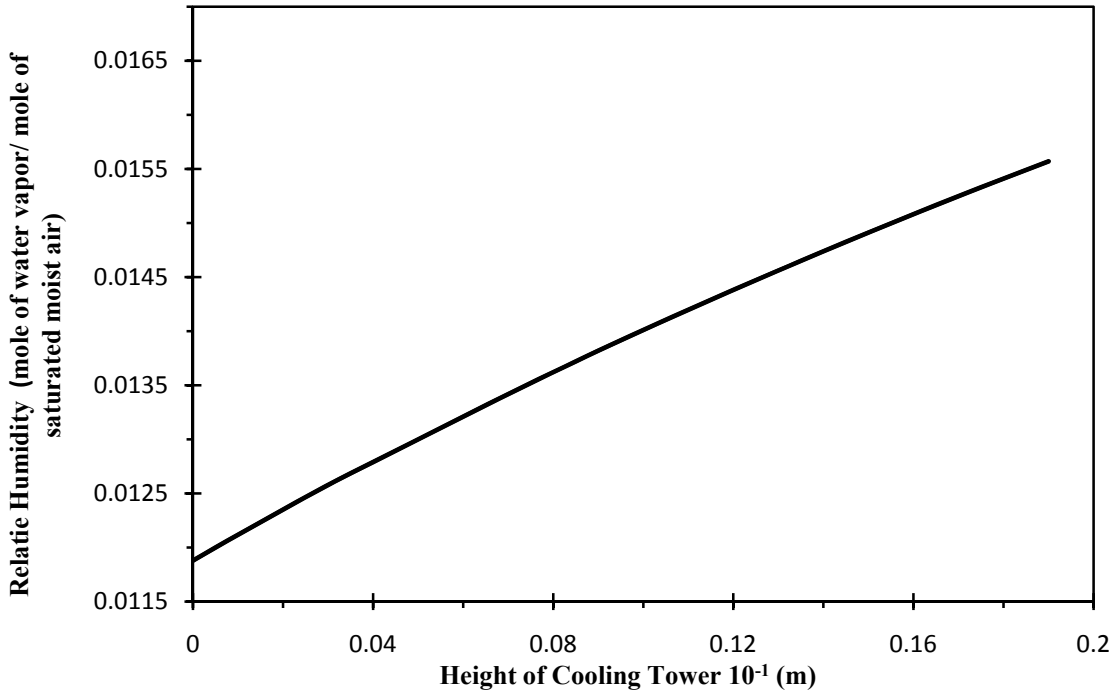

Figure 16. Relative humidity ratio profile within cooling tower.

The driving potential for convection heat transfer decreases with tower volume, and it becomes negative after reaching some height up the tower. It results in a negative convection heat transfer in the tower (from water to air). The negative convection in the tower occurs when the water temperature is lower than the air dry-bulb temperature. The potential of evaporation increases continuously and it is dependent upon the air temperature, length of the cooling tower and air mass flow rate. A higher water mass flow rate causes higher potential evaporation due to the increase of contact cross-sectional area.

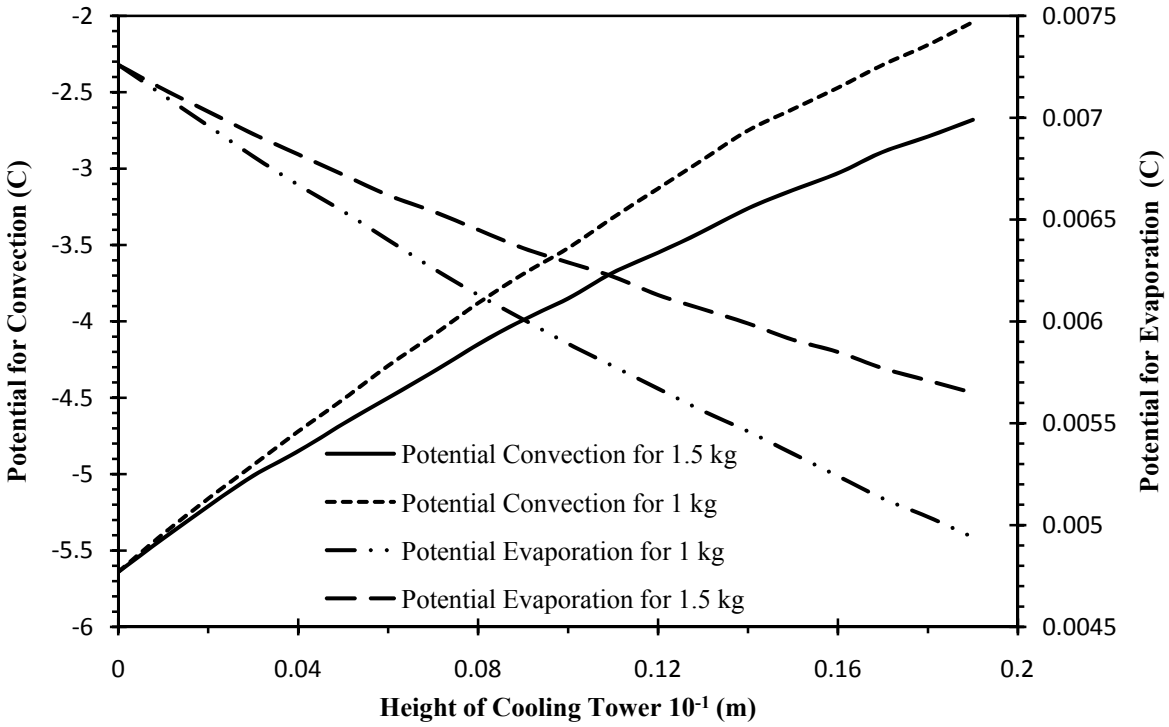

Figure 17. Variation of driving potential for convection and evaporation heat transfer with height of tower, for different mass flow ratios of 1 to 1.5 kg of water per kg of moist air.

The potential evaporation can be decreased by raising the inlet air temperature or increasing the air mass flow rate. Potential evaporation or potential evapotranspiration is defined as the amount of evaporation that would occur if a sufficient water source were available. Figure 18 shows the

evaporation rate and convection rate versus height of the tower. As a result, evaporation increases along the tower and is dependent on the air temperature. The effect of the mass flow ratio, m_w/m_a, is investigated by varying the mass flow rate of water, m_w, while keeping the air flow rate, m_a, constant. The results are shown in Figure 15 to 17. As a result, with an increase of water mass flow rate, the dry-bulb temperature of the air decreases over a relatively small height of the tower, and the temperature drop of water is less with the increase of mass flow rate of water, m_w. With an increase in mass flow rate ratio, more water is cooled for a given tower volume. Therefore, one would expect that the surface area required for both convection and evaporation will be reduced, resulting in higher water outlet temperatures and reduced heat transfer rates.

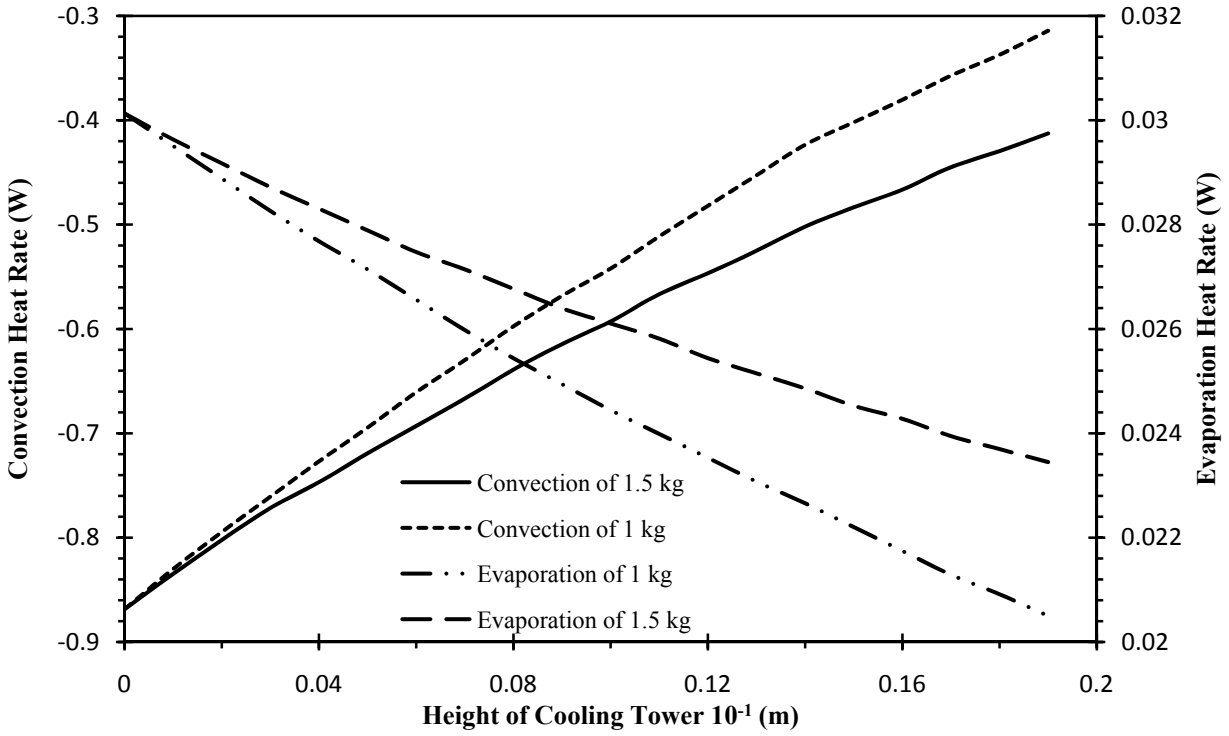

Figure 18. Variation of heat flow rates with height of tower for 1 to 1.5 kg of water per kg of moist air.

All figures are plotted as a function of tower height, measured from the bottom to the top of the tower. These figures show that the heat transfer rates are high in the top portions of the tower and then decrease as the water moves from the top to the bottom of the tower. It can also be concluded that evaporation is mainly controlling the total heat flow in a cooling tower.

4.3 Spray-drying Prediction

Drying processes occur in a number of industrial applications. The main principle of spray-drying is the atomization of the liquid phase into droplets and their dispersion in a hot gas stream. Because the atomization of the liquid increases the surface area for heat and mass transfer, the interfacial surface per volume of all droplets, and the increased surface area causes a shorter drying period. The main greatest advantage of spray-drying is the short residence time, approximately 20 to 40 seconds, which depends on the inlet and outlet gas temperatures and the mass flow rate of liquid and hot gas [91].

In the spray-drying model, hot gas and liquid enter the spray-drying system from the top of the spray dryer and the solid particles exit at the bottom of the dryer as a product. The spray dryer configuration in this analysis is a Niro Mobile Minor Spray Dryer with a 30" diameter, 24" cylindrical height, and a 60^{o} conical bottom. The two-fluid nozzle was attached to the ceiling of the spray dryer. The solution enters at the ambient temperature of $25^{o}C$ and air is used as the drying gas. In the numerical calculations, three different inlet gases at $200^{o}C$, $170^{o}C$, and $120^{o}C$ were studied. For each inlet hot gas, different outlet gas temperatures were considered. For instance, for inlet air at $200^{o}C$, the outlet air was varied from $130^{o}C$ to $50^{o}C$. Hence, for each

inlet and outlet temperature, the other variables, such as evaporation rate, residence time and feed rate of air and solution, were calculated. Also, for each specific inlet and outlet temperature, three different solid concentrations in the solution were considered to find the optimum feed rate and drying time. Different solid concentrations of 20%, 30%, and 50% cupric chloride in the water were assumed. In addition to the above parameters, two different air mass flow rates of 50 kg/h and 60 kg/h were used in the analysis. An 8% heat loss in the calculation was attributed to the heat loss from the wall of the chamber. In the spray-drying process, the solution droplet temperature suddenly increased due to the high inlet air temperature. The droplet temperature continuously increased until it reached its saturation point. After saturation, the temperature remained constant until the end of evaporation.

4.3.1 High Air Mass Flow Rate

In this section, a higher mass flow rate of air (60 kg/h) is considered. Table 11 shows the inlet and outlet temperatures of hot air.

Table 11. Values for temperatures, solid concentrations, and heat loss in spray-drying problem.

Inlet Temperature ^{o}C	Outlet Temperature ^{o}C	Solution inlet Temperature ^{o}C	Solid Concentration in the Feed %	Heat Loss
200	130 to 50	25	20, 30, and 50	8
170	130 to 50	25	20, 30, and 50	8
130	90 to 40	25	20, 30, and 50	8

Figure 19 to 21 show the evaporation rate plotted against the solution feed rate, with different solid concentrations in the feed solution. It can be observed from each plot that the higher feed mass flow results in a higher evaporation rate.

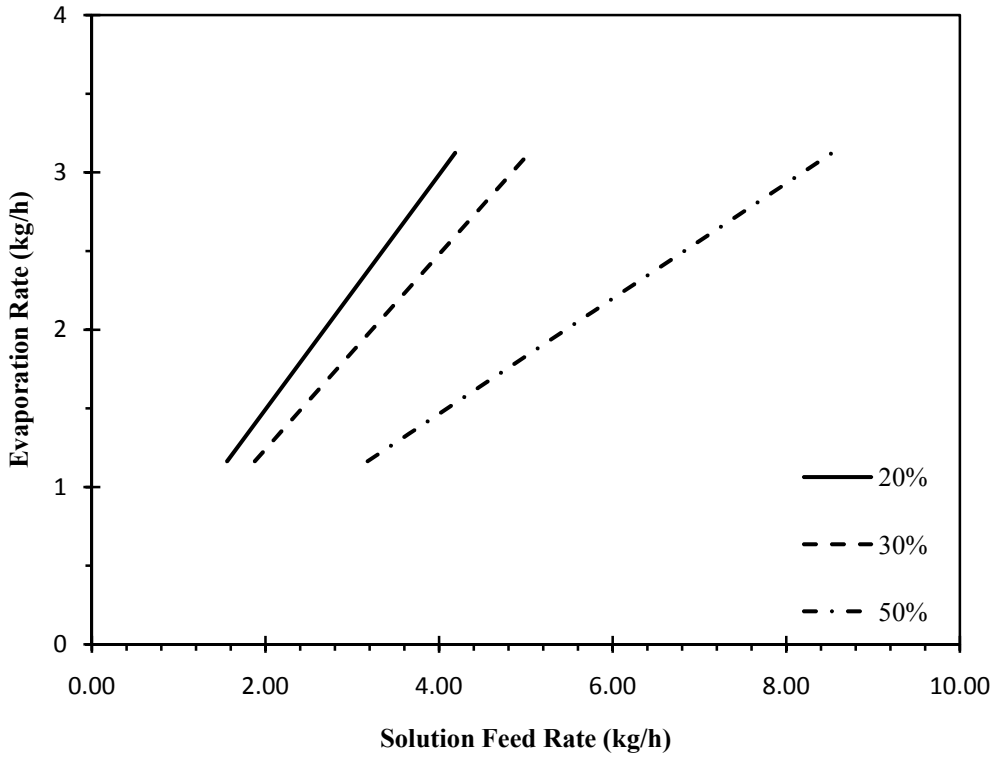

Figure 19. Evaporation rates for different solution feed rates at mass flow rate of 60 kg/h and 200^{o}C with different air outlet temperatures.

The evaporation rate will rise by increasing the mass flow rate, due to the residence time for drying. A higher feed mass flow rate requires a longer residence time for drying, as shown in Figure 22. For lower air inlet temperatures, the residence time is significantly increased, which indicates there is more energy required to transfer heat from the air to solution.

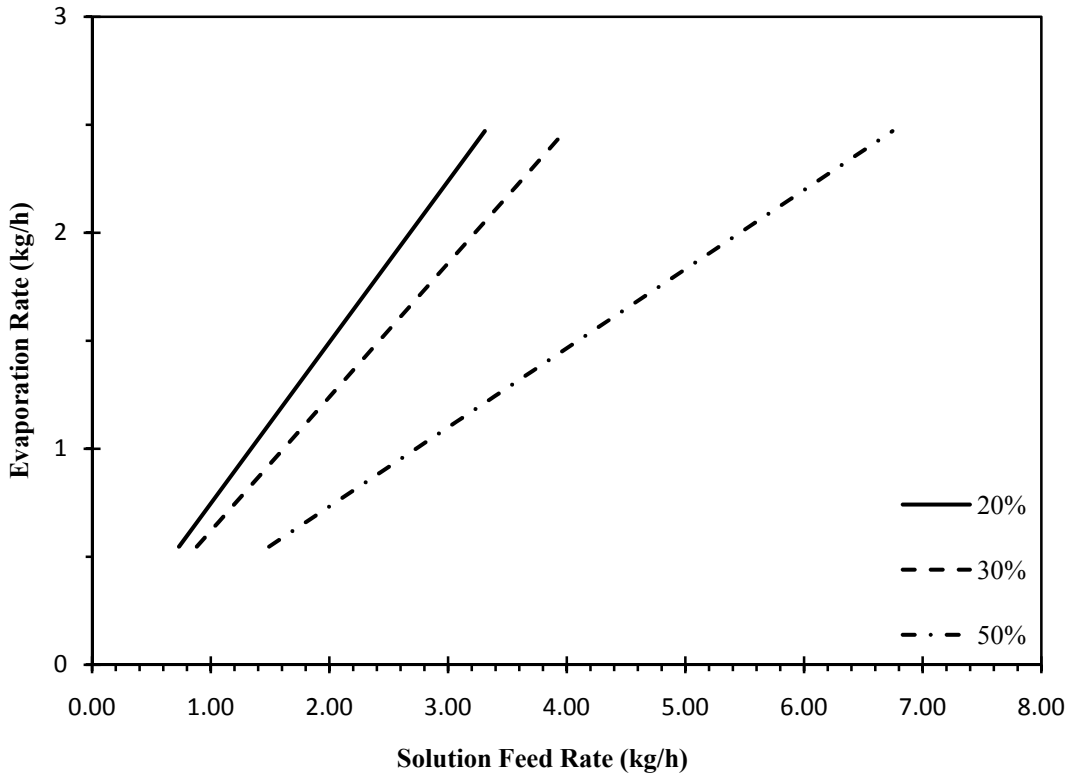

Figure 20. Evaporation rates for different solution feed rates at high mass flow rate of 60 kg/h and 170^{o}C with different air outlet temperatures.

In comparison to the plots of evaporation against solution feed rate, it can be observed that there is a significant increase in the evaporation rate at high inlet temperatures and shorter residence times. The inlet temperature is a key factor for fast evaporation processes such as spray dryer to increase the evaporation rate in a short residence time. This can be explained as follow, after a droplet reach to its saturation point the evaporation occurs during this stage, where the droplets remain at a constant temperature until the liquid has been removed from the droplet and a random crystal of solid start to grow. Because the evaporation occurs after a droplet reaches its saturation, a higher inlet temperature cause the droplet to reach its saturation in shorter time and a faster evaporation rate.

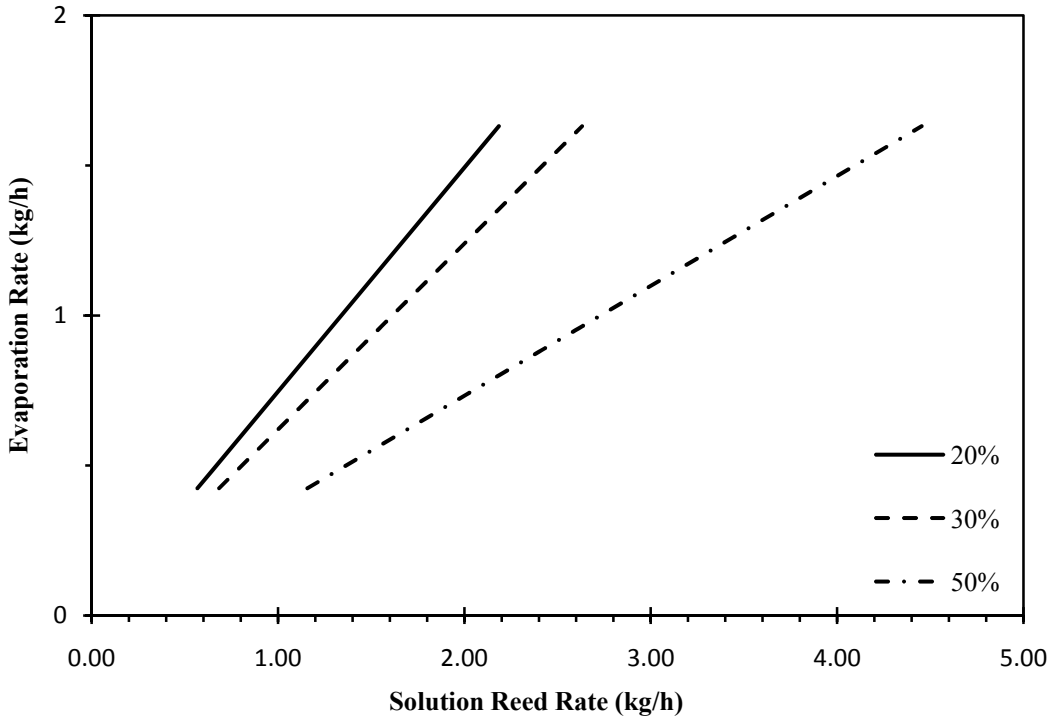

Figure 21. Evaporation rates for different solution feed rates for a high mass flow rate of 60 kg/h and 120^{o}C with different air outlet temperatures.

The results shown that the high inlet temperature of 200^{o}C has almost twice the 120^{o}C evaporation rate under the same conditions. Also, the residence time can be decreased by 10 to 15 seconds using a higher inlet air temperature.

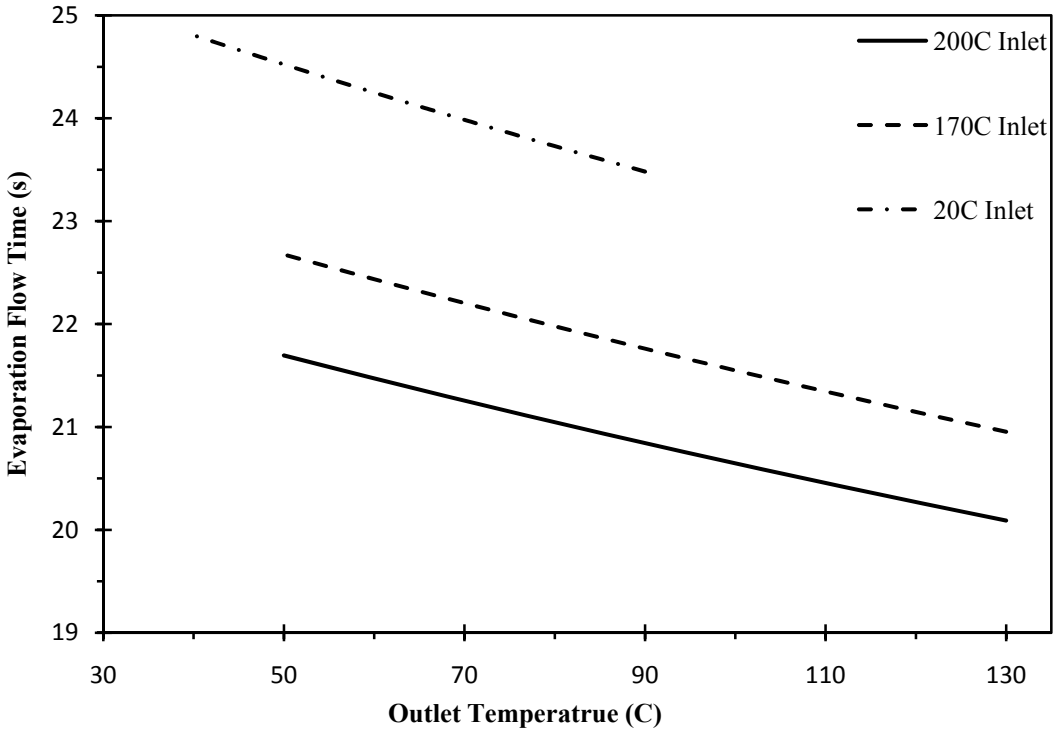

Figure 22. Residence time for evaporation at different inlet gas temperatures of 200, 170, and 120^{o}C.

Figure 22 presents the evaporation rate against the outlet air temperature. Lower temperatures require more residence time. As a result, it may not be practical for some spray dryers, since the required time to dry the solution is more than the required time for the droplet to reach the bottom of the spray dryer.

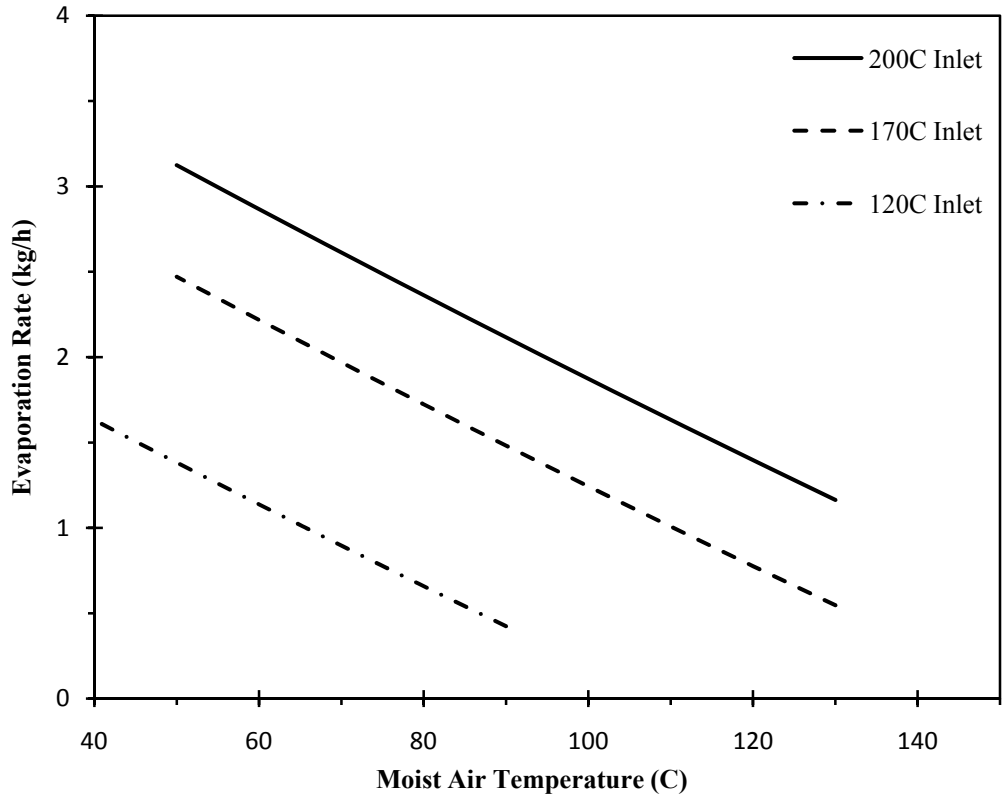

Figure 23. Evaporation rate for different inlet gas temperatures vs. outlet moist air temperatures.

On the other hand, there are some limitations to the inlet and outlet temperatures of the hot gas. According to Parti et al. [91], the residence time in spray dryer varies from 30 to 40 seconds. There are many parameters that influence the required time for droplets, before they reach the bottom of the spray dryer, such as the type of atomizer, properties of the solution, pressure, inlet and outlet temperatures, humidity ratio, spray dryer's volume and other factors. Figure 23. shows that higher temperatures have a higher evaporation rate and higher humidity ratio at the exit.

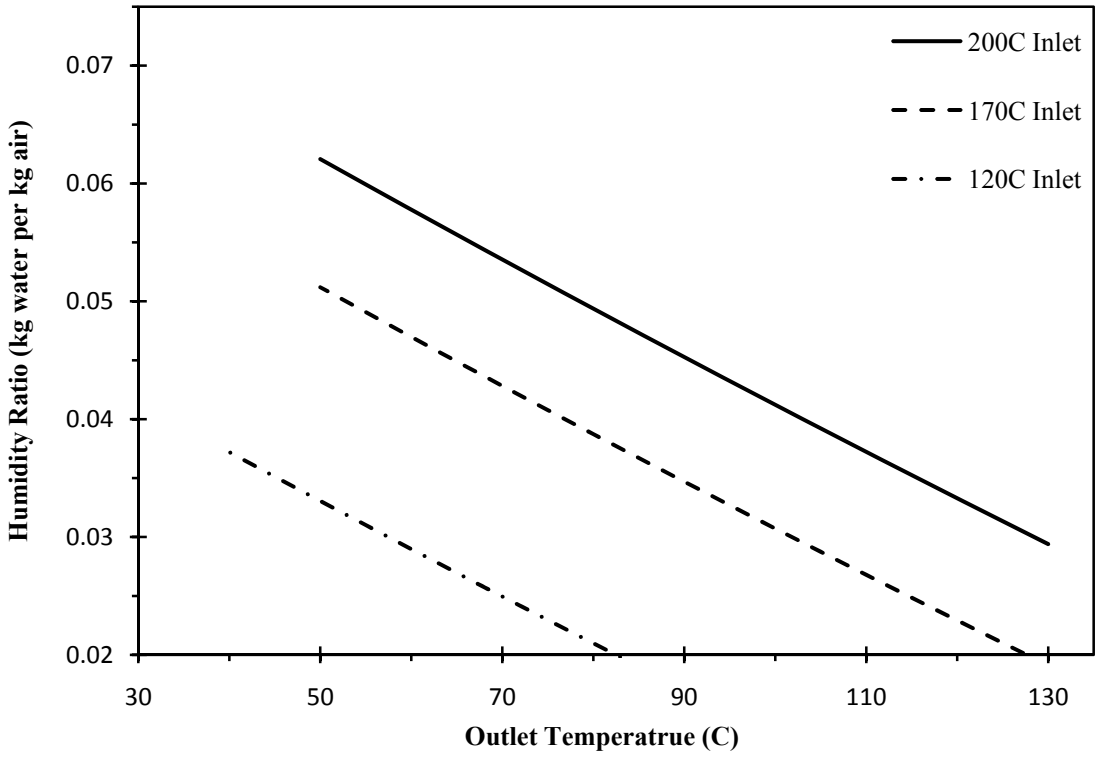

Figure 24. Humidity ratio for three different inlet air temperatures, against outlet temperatures of moist air.

4.3.1 Low Air Mass Flow Rate

In this section, a lower mass flow rate of air (50 kg/h) was considered. The same conditions were applied as a high flow rate of air. The temperatures at the inlet and outlet are given in Table 11. The purpose of this section is to compare the effects of different mass flow rates of air on drying of the solution, at the same conditions, using three different solid concentrations in the solution. Different solid concentrations and outlet air temperatures are used to study the effects on the drying processes. In this section, the hot air stream and solution enter at the top of the spray dryer and the solid product is discharged from the bottom of the dryer. Using the formulations developed in the previous chapter, the evaporation rate against solution

feed rate with different solid concentrations of 20%, 30%, and 50% were plotted. The evaporations against solution feed rate were calculated for three different inlet temperatures. For each inlet temperature, the outlet temperature varies over a range of 50°C, depending on the inlet conditions. Figures 25 - 27 show the effect of solid concentration in the solution on the drying processes, and consequently on the evaporation rates.

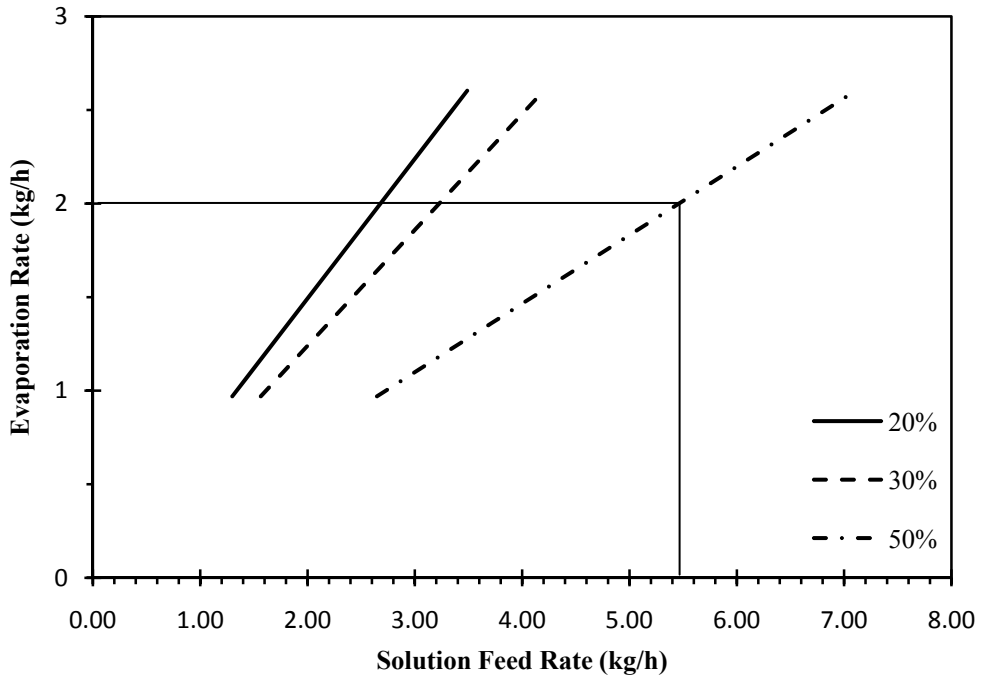

Figure 25. Evaporation rates for three different solid concentrations of 20%, 30%, and 50% $CuCl_2$ against solution feed rates, for a mass flow rate of 50 kg/h and inlet temperature of 200°C.

The effect of density on the solution feed rate in drying processes can be observed from the graphs. A higher density requires a higher mass flow rate, and consequently, by knowing the evaporation rate, the outlet temperature can be obtained, as shown in Figure 28. For instance, in Figure 25, at high temperatures, the evaporation at a solution feed rate of 5.50 kg/h is equal to 2 kg/h. It can be observed from Figure 28 that the outlet temperature for an evaporation rate of 2

kg/h and a different concentration has a minimum of 78°C. By knowing the outlet temperature, the residence time and humidity ratio of the air at the outlet can be found. This is shown in Figure 28 and 29. Therefore, higher evaporation requires higher inlet and outlet temperatures. The graphs show that the evaporation can increase by increasing the inlet temperature. A higher solution feed rate causes a higher evaporation rate. The residence time will also increase as a result. It can be explained that a solution with a lower solid concentration of 20% has more liquid content for evaporation, so more evaporation occurs during the process.

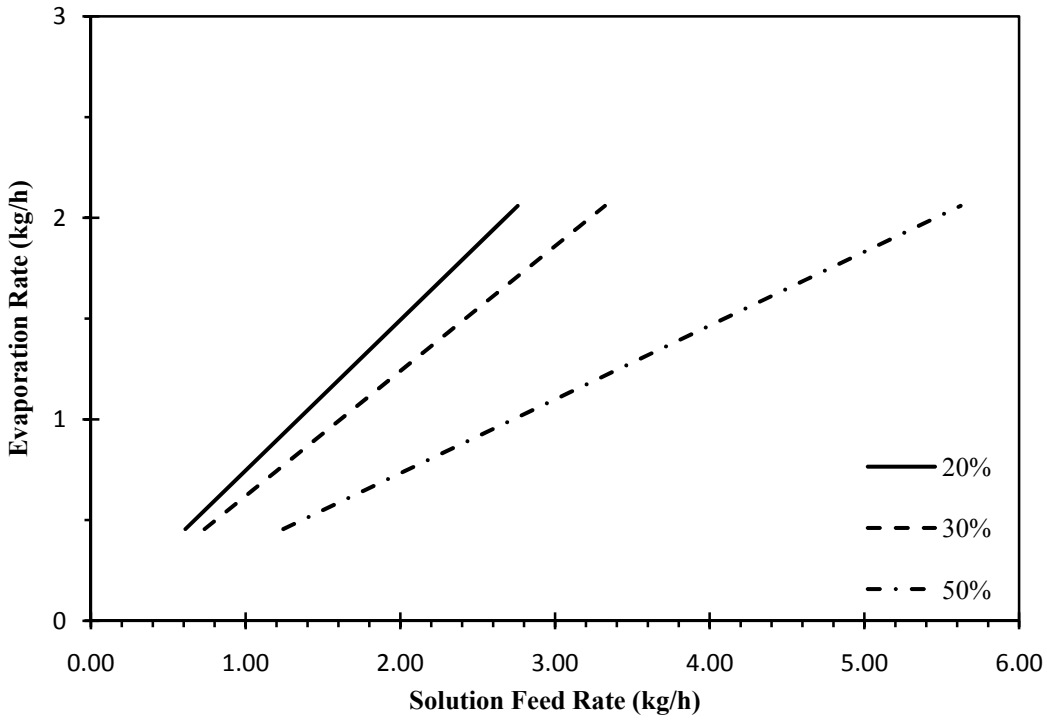

Figure 26. Evaporation rates for three different solid concentrations of 20%, 30%, and 50% $CuCl_2$ against solution feed rate for mass-flow rate of 50 kg/h and inlet temperature of 170°C.

At a lower inlet temperature of 170°C or 120°C, the evaporation rate significantly drops by a magnitude of almost 0.5. However, as discussed by Walton [27, 29], temperatures below 150°C are insufficient to evaporate the entire droplet if the effective height of the spray-drying chamber

is between 1 to 2 m. Therefore, for temperatures lower than 150^{o}C, the product may contain a significant amount of water.

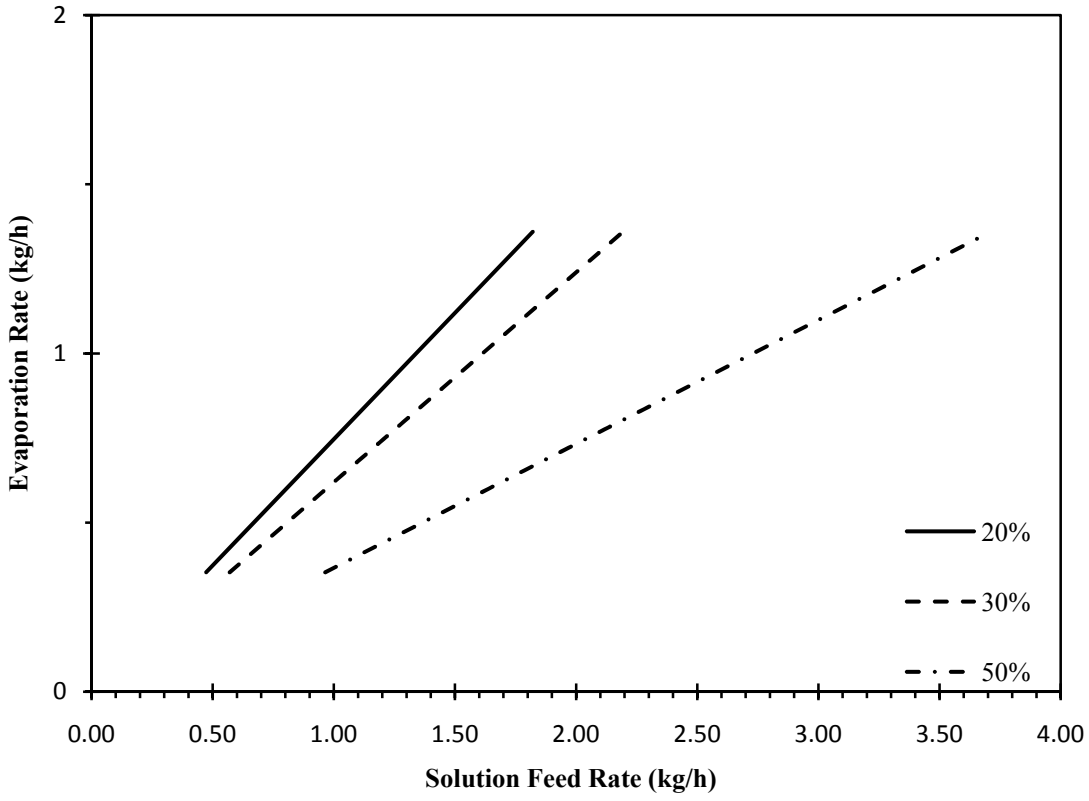

Figure 27. Evaporation rates for three different solid concentrations of 20%, 30%, and 50% $CuCl_2$ against solution feed rate for mass-flow rate of 50 kg/h and inlet temperature of 120^{o}C.

The evaporation depends on the solution feed rate and inlet and outlet temperatures. The fastest drying may be achieved by a higher inlet temperature, which can instantly increase the droplet temperature to the saturation point, and the temperature of the droplets will remain constant until evaporation occurs. In other words, the temperature of a droplet remains constant during evaporation.

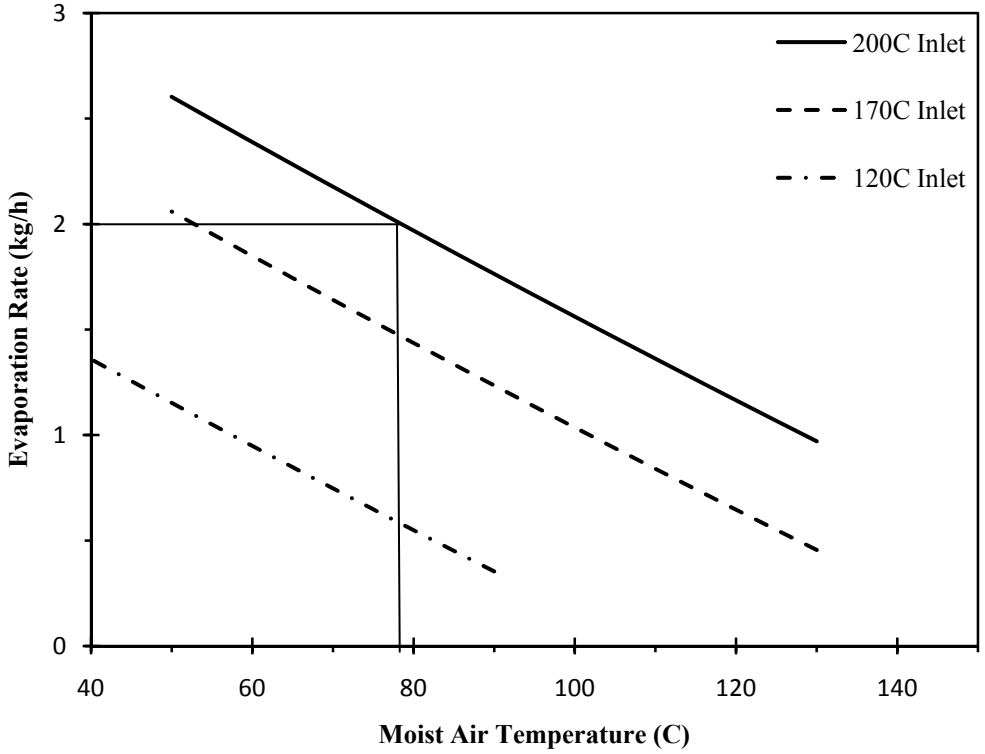

Figure 28. Evaporation rates for different inlet temperatures against outlet air temperatures.

Figure 28 shows the outlet temperature with respect to the evaporation rate and solution feed rate. Higher evaporation requires more energy to absorb heat from the hot air. For lower temperatures of outlet air, the feasibility of the system needs to be experimentally examined. There could be a considerable amount of water in the solution, which can only be observed by an experimental test at a particular outlet temperature. Figure 29 presents the residence time for drying processes for a given inlet and outlet temperature. There are three inlet temperatures that are constant during the entire process. The outlet temperatures were calculated based on the inlet temperature and feed rate of the solution.

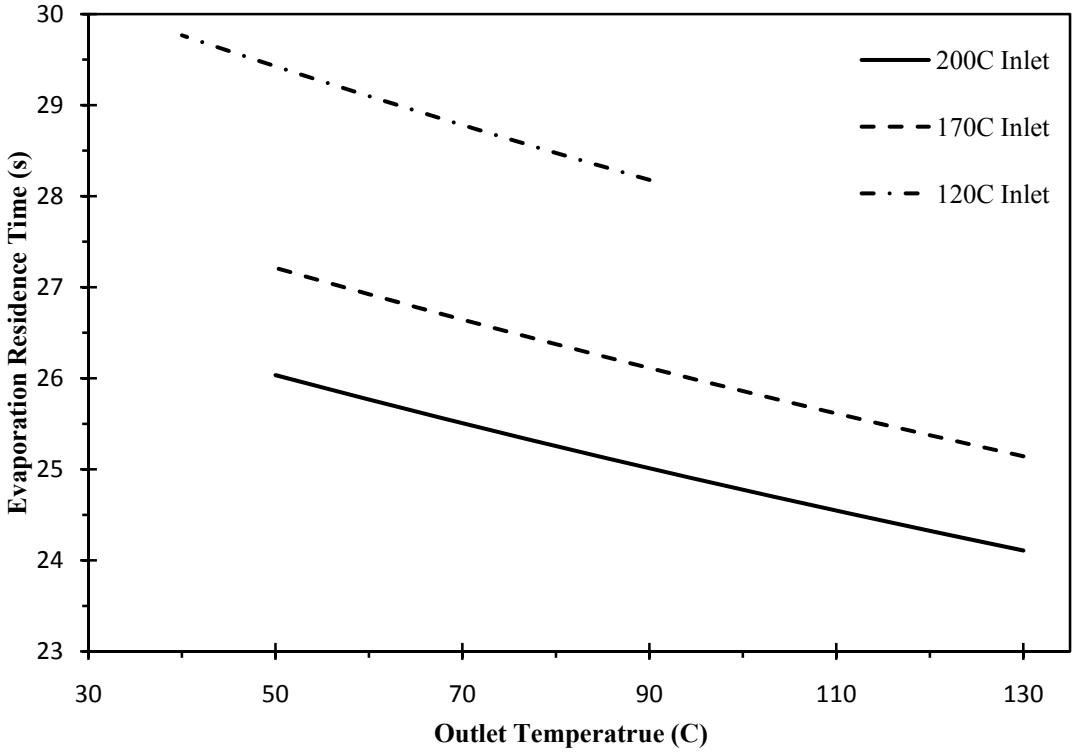

Figure 29. Residence times for evaporation against outlet air temperatures for three different drying inlet gases at 200^{o}C, 170^{o}C, and 120^{o}C.

Hence, the lower inlet and outlet temperatures required a higher residence time. The residence time can vary from 20 to 40 seconds, depending on the condition of drying processes [91].

In the drying processes with the spray-drying system, high temperature inlet gas is the most important factor for drying the solution, which can increase the residence time and decrease the evaporation by decreasing the inlet temperature. Also, the density of the solution can affect the solution feed rate, which is an important factor in calculating the amount of materials charged / discharged in the process.

Chapter 5

Conclusions and Recommendations for Future Research

This thesis has examined the drying process within a Cu-Cl cycle of hydrogen production. Cupric chloride is present as an aqueous solution that leaves the electrochemical cell, enters a spray dryer in aqueous form, and later moves into the hydrolysis reactor as a solid. The presence of cupric chloride in the Cu-Cl cycle occurs from electrolytic separation of CuCl into solid copper and aqueous $CuCl_2$, subsequent drying and then recycling of the particulate. A spray-drying process and a cooling tower are used to examine water removed from the aqueous solution.

This thesis presented an analytical solution for drying of the cupric chloride solution. Sensitivity studies were then performed to examine the effects of different solution concentrations and inlet temperatures on the drying process. This thesis showed a potential for drying a $CuCl_2$ solution in a co-current or counter-current drying process. The $CuCl_2$ slurry, with different solid concentrations, was used to predict the residence time and enthalpy change in the system. The processes of drying and solidification of cupric chloride solution were performed in experimental tests and numerical analysis. In the experimental tests, the color of the feed material before it was mixed with water was light green, indicating the powder contained some water. After drying, the product's color was brown, indicating dryness of the product powder.

In the numerical analysis for the cooling tower, the temperature gradient, enthalpy, and evaporation rates were obtained. The analysis showed that waste heat from nuclear power plants can be used for the drying process for $CuCl_2$, however, the cooling tower or other drying processes require more than one step to dry the solution. The waste heat temperature from nuclear power plants would be an abundant source of energy that can be used to heat the air for the drying process. In spray-drying, it was shown that the required heat for the drying process is much higher than the cooling tower. But the advantage of the process is a one-step fast drying process. As observed from the experimental results, the powder's size is controllable by changing the percentage of air to solution flow in the atomizer. A higher atomizer gas flow percentage yields a lower product.

Spray dryers are operated at high temperatures, and the waste heat from nuclear power plants can be used to preheat the air to a certain temperature. The remaining energy needed can be supplied by an electric heater. Therefore, in both cases, the waste heat from nuclear power plants can be used for the drying process, depending on the applications and conditions. In spray-drying, results have shown that a higher temperature carries more and faster evaporation, with a lower residence time.

It was shown that a lower temperature can be used for drying. However, using an inlet gas temperature of 150^oC may cause the product to contain water, and this increases the residence time of the process. In spray-drying, many properties of a product, such as the critical moisture content and the inlet air temperature, depend on the drying rate. The droplet experiences a process of shrinkage in which the temperature is approximately uniform. Based on the Biot number, the temperature distribution in the droplet was neglected in the analysis, since the Biot number is much smaller than 0.1.

In the drying process, evaporation occurs after the droplet reaches the saturation point. During this stage, the droplet remains at a constant temperature and evaporation continues until the liquid has been removed and random crystals of solid start to grow. After evaporation, the crystals continue to gain heat and the drying process ends, with the particle deposited at the bottom of the chamber. Therefore, for a lower outlet temperature in the spray-drying process, it is necessary to run an experimental test in order to examine the dryness of the product. The results in this thesis have shown both fast and slow drying of a $CuCl_2$ slurry solution**.** Using waste heat from nuclear power plants as a source of heat to preheat the drying gas can decrease the environmental impact by preventing the power plant emissions into the environment. The powder produced by spray-drying is injected into a fluidized bed to later produce hydrogen in a closed system.

Future research is recommended to perform additional experimental studies, in order to better understand whether the $CuCl_2$ solid matrix during spray-drying will contain entrapped internal pockets of liquid. Future information on the internal microscopic characteristics of solidified $CuCl_2$ is needed. Also, alternative techniques that might reduce the inlet gas temperature would be beneficial, to utilize lower grade waste for the drying process. Other alternative techniques should be employed to find heat and mass transfer in the droplet using higher Biot numbers. For instance, using a higher Biot number, the heat transferred inside the droplet is almost equal or has a smaller difference than the rate at which heat is removed from the droplet's surface.

References

[1] Nel, W.P., Cooper, C. J., "Implications of Fossil Fuel Constraints on Economic Growth and Global Warming", *Energy Policy*, vol. 37, pp. 166-180, 2009.

[2] Klass, D.L., "A Critical Assessment of Renewable Energy Usage in The USA", *Energy Policy*, vol. 31, pp. 353-367, 2003.

[3] Naterer, G.F., Fowler, M., Cotton, J., Gabriel, K., "Synergistic Roles of Off-peak Electrolysis and Thermochemical Production of Hydrogen from Nuclear Energy in Canada", *International Journal of Hydrogen Energy*, vol. 33, no. 23, pp. 6849-6857, 2008.

[4] Hamilton, T., Naterer, G. F., "Hydrogen's Role in a Nuclear Renaissance", *TorontoStar*, Toronto, Canada: TorontoStar, October 22, 2007.

[5] Hu, B., Chen, S., "Biological Hydrogen Production Using Chloroform-Treated Methanogenic Granules", *Applied Biochemistry and Biotechnology,*, vol. 148, no. 1-3, pp. 83-95, 2008.

[6] Cumalioglu, I., Ertas, E., Ma, Y., Maxwell, T., "Hydrogen Storage", *Journal of Fuel Cell Science and Technology*, vol. 5, no. 3, pp. 1-10, 2008.

[7] Lodhi, M.A.K., "Helio-Hydro and Helio-Thermal Production of Hydrogen", *International Journal of Hydrogen Energy*, vol. 29, pp. 1099-1113, 2003.

[8] "Greenhouse Gases, Climate Change & Energy", Washington, D.C.: Energy Information Administration, pp. 1-2, May 2008.

[9] Jaques, A., Neitzert, F., White, R., "Greenhouse Gas Sources and Sinks in Canada", *National Inventory Report, Greenhouse Gas Division*, vol., pp. 60-70, May 2008.

[10] Sherif, S.A., Barbir, F., Veziroglu, T. N., "Wind Energy and the Hydrogen Economy - Review of the Technology", *Solar Energy*, vol. 78, pp. 647-660, 2005.

[11] Brown, L.C., Besenbruch, G. E., Lentsch, R. D., Schultz, K. R., Funk, J. F., Pickard, P. S., Marshall, A. C., Showalter, S. K., "High Efficiency Generation of Hydrogen Fuels Using Nuclear Power": Nuclear Energy Research Initiative (NERI) Program, June 2003.

[12] Schlapbach, L., Züttle, A., "Hydrogen-Storage Materials for Mobile Applications", *Nature*, vol. 414, no. 6861, pp. 353-358, 2001.

[13] Fishtik, I., Datta, R, "Systematic Generation of Thermochemical Cycles for Water Splitting", *Computers and Chemical Engineering*, vol. 32, pp. 1625-1634, 2008.

[14] Sadhankar, R.R., Li, J., Li, H., Ryland, D. K., Suppiah, S., "Future Hydrogen Production Using Nuclear Reactors", *Engineering Institute of Canada - Climate Change Technology Conference*, May 2006.

[15] Marban, G., Valdes-Solis, T., "Towards the Hydrogen Economy?", *International Journal of Hydrogen Energy*, vol. 32, pp. 1625-1637, 2007.

[16] Jeong, Y.H., Kazimi, M. S., "Optimization of the Hybrid Sulfur Cycle for Nuclear Hydrogen Generation", *Nuclear Technology*, vol. 159, no. 2, pp. 147-157, 2007.

[17] Rosen, M.A., "Thermodynacim Investigaion of Hydtofen Production by Steam-Methane Reforming", *International Journal of Hydrogen Energy*, vol. 16, no. 3, pp. 207-217, 1992.

[18] Yildiz, B., Kazimi, M. S., "Efficiency of Hydrogen Production Systems Using Alternative Nuclear Energy Technologies", *Hydrogen Energy*, vol. 31, pp. 77-92, 2006.

[19] Chow, C.K., Khartabil, H. F., "Fuel channel Designs for CANDU-SCWR", *International conference on Nuclear Engineering*, Shanghai, China: Atomic Energy of Canada, Limited, pp. 1-9, 2007.

[20] Naterer, G.F., Daggupati, V. N., Marin, G., Gabriel, K. S., Wang, Z. L., "Thermochemical Hydrogen Productin with a Copper-Chlorine Cycle, II: Flashing and Drying of Aqueous Cupric Chloride", *International Journal of Hydrogen Energy*, vol. 33, pp. 5451-5459, 2008.

[21] Rosen, M.A., Naterer, G. F., Sadhankar, R., Suppiah, S., "Nuclear-Based Hydrogen Production With Thermochemical Copper-Chlorine Cycle and supercritical Water Reactor", *Canadian Hydrogen Association Workshop*, Quebec, Canada: Atomic Energy of Canada, pp. 1-8, 2006.

[22] "Spray Drying": Wikipedia, Dec 1st, 2008.

[23] Li, X., Zbicinski, I., "A Sensitivity Study on CFD Modelling of Cocurrent Spray-Drying Process", *Drying Technolosy*, vol. 23, pp. 1681-1691, 2005.

[24] Zbicinski, I., Delag, A., Strumillo, C., Adamiec, J., "Advanced experimental analysis of drying kinetics in spray drying", *Chemical Engineering Journal*, vol. 86, pp. 207-216, 2002.

[25] Lin, S.X.Q., Chen, X. D., "A Model for Drying of an Aqueous Lactose Droplet Using the Reaction Engineering Approach", *An International Journal Drying Technology*, vol. 24, no. 11, pp. 1329-1334, 2006.

[26] Chen, X.D., Xie, G. Z., "Fingerprints of the Drying Behavior of Particulate or Thin Layer Food Materials Established Using a Reaction Engineering Model", *Chemical Engineering*, vol. 75, pp. 213-222, 1997.

[27] Walton, D.E., "The Evaporation of Water Droplets. A Single Droplet Drying Experiment", *An International Journal Drying Technology*, vol. 22, no. 3, pp. 431-456, 2004.

[28] Ranz, W.E., Marshall, W. R., "Evaporation from Drops", *Chemical Engineering Progress*, vol. 48, no. 3, pp. 141-146, 1952.

[29] "Niro Mobile Minor Spray Dryer Specification Sheet", Columbia, MD: GEA Process Engineering Inc., pp. 1-19, 2008.

[30] Iva, F., Li, X. H., Mujumdar, A. S., *Handbook of Industrial Drying - Industrial Spray Drying Systems*, Boca Rotan, FL: Taylor & Francis.

[31] Aguilar, G., Majaron, B., Verkruysse, W., Zhou, Y., Nelson, J. S., Lavernia, E. L., "Theoretical and Experimental Analysis of Droplet Diameter, Temperature, and Evaporation Rate Evalution in Cryogenic Sprays", *International Journal of Heat and Mass Transfer*, vol. 44, pp. 3201-3211, 2001.

[32] Muthunayagam, A.E., Ramamurthi, K., Robert Paden, J., "Modelling and Experiments on Vaporization of Saline Water at Low Temperature and Reduced Pressures", *Applied Thermal Engineering*, vol. 25, pp. 941-952, 2005.

[33] Farid, M., "A New Approach to Modelling of Single Droplet Drying", *Chemical Engineering Science*, vol. 58, pp. 2985-2993, 2003.

[34] Feng, C.G., Scott, S. K., "Surface Temperature Gradients and Rates of Internal Heat Evolution at Criticality for Generalized Heat Transfer", *Journal of Chemical Society*, vol. 79, no. 2, pp. 1629-1163, 1983.

[35] Mills, A.F., *Heat Transfer*, 2nd ed., New Jersey: Prentice Hall.

[36] Mujumdar, A.S., "Drying Technologies of the Future", *Drying Technology*, vol. 9, no. 2, pp. 325-347, 1991.

[37] Zeljko, B.G., Zorana, L. A., Radmila, V. G. G., "Drying of Slurries in Fluidized Bed of Inert Particles", *Drying Technology*, vol. 22, no. 8, pp. 1793-1812, 2004.

[38] Mujumdar, A.S., *Handbook of Industrial Drying - Indirect Dryers*: Taylor and Francis Group LLC.

[39] Mujumdar, A.S., *Handbook of Industrial Drying*, 3rd ed., Boca Raton, FL: CRC/Taylor & Francis.

[40] Ramli, W., Daud, W., *Handbook of Industrial Drying - Drum Dryers*, 2nd ed., Boca Raton, FL: CRC/Taylor & Francis.

[41] Threlkeld, J.L., *Thermal Environmental Engineering*, 2nd ed., Englewood Cliffs, N.J.: Prentice-Hall.

[42] McCabe, W.L., Smith, J. C., Harriott, P., *Unit Operations of Chemical Engineering*, 6th ed., Boston: McGraw Hill.

[43] Lewis, D., "Hydrogen and Its Relationship with Nuclear Energy", *Progress in Nuclear Energy*, vol. 50, pp. 394-401, 2008.

[44] Ponomareve-Stepnoi, N.N., "Nuclear-Hydrogen Power", *Atomic Energy*, vol. 96, no. 6, pp. 375-385, 2004.

[45] Serfass, J., Davis, M., Balog, F., Nemanich, G., Katsaros, A., Ogden, J., Niedzwiecki, A., "National Hydrogen Energy Roadmap", Washington, DC, pp. 1-50, 2002.

[46] Penner, S.S., "Steps Toward the Hydrogen Economy", *Energy*, vol. 31, pp. 33-43, 2006.

[47] Bossel, U., "Does Hydrogen Economy Make Sense", *Proceedings of the EEEE*, vol. 94, no. 10, pp. 1826-1837, 2006.

[48] Taljan, G., Fowler, M., Canizares, C., Verbic, G., "Hydrogen Storage for Mixed Wind-Nuclear Power Plants in the Context of a Hydrogen Economy", *International Journal of Hydrogen Energy*, vol. 33, pp. 4463-4475, 2008.

[49] Miller, A.I., Duffey, R. B., "Sustainable and Economic Hydrogen Cogeneration from Nuclear Energy in Competitive Power Markets", *Energy*, vol. 30, pp. 2690-2702, 2005.

[50] "Annual Energy Outlook 2003", Washington, DC: Energy Information Administration, pp. 1-267, 2006.

[51] "Canada's Emissions Outlook 2003: an Update": National Resources Canada, 1999.

[52] Aleksandrov, A.P., Pnomarev-Stepnoj, N. N., "Atomic Power Generation and Future Technical Progress", *Indian Journal of Power and River Valley Development*, vol. 25, no. 7, pp. 209-212, 1975.

[53] Botterud, A., Yildiz, B., Conzelmann, G., Petri, M. C., "Nuclear Hydrogen: An Assesment of Product Flexibility and Market Viability", *Energy Policy*, vol. 36, pp. 3961-3973, 2008.

[54] Forsberg, C.W., "Hydrogen, Nuclear energy, and the Advanced High-Temperature Reactor", *International Journal of Hydrogen Energy*, vol. 28, pp. 1073-1081, 2003.

[55] Kimura, H., Tekeuchi, Y., Yamamoto, Y., Konishi, S., "Hydrogen Production from Biomass using Nuclear Fusion Energy", *Symposium on Fusion Engineering*, Japan, pp. 1-4, 2007.

[56] Torjman, M., Shaaban, H., "Nuclear Energy as a Primary Source for a Clean Hydrogen Energy System", *Energy Conver. Mgmt*, vol. 39, no. 1/2, pp. 27-32, 1998.

[57] Yamawaki, M., Nishihara, T., Inagaki, Y., Minato, K., Oigawa, H., Onuki, K., Hino, R., Ogawa, M., "Application of Nuclear Energy for Environmentally Friendly Hydrogen Generation", *International Journal of Hydrogen Energy*, vol. 32, pp. 2719-2725, 2007.

[58] Verfondern, K., Von Lens, W., "Past and Present Research in Europe on the Production of Nuclear Hydrogen with HTGR", *Progress in Nuclear Energy*, vol. 47, no. 1-4, pp. 472-483, 2005.

[59] Verfondern, K., Von Lens, W., "Michelangelo Network recommendations on nuclear hydrogen production", *International Journal of Nuclear Hydrogen Production and Applications*, vol. 1, no. 1, pp. 68-78, 2006.

[60] Onuki, K., Inagaki, Y., Hino, R., Tachibana, Y., "Research and Development on Nuclear Hydrogen Production Using HTGR at JAERI", *Progress in Nuclear Energy*, vol. 47, no. 1/4, pp. 496-503, 2005.

[61] Hori, M., Matsui, K., Tashimo, M., Yasuda, I., "Synergistic Hydrogen Production by Nuclear-Heated Steam Reforming of Fossil Fuels", *Progress in Nuclear Energy*, vol. 47, no. 1-4, pp. 519-526, 2005.

[62] Lide, D.R., Baysinger, G., Berger, L. I., Goldberg, R. N., Kehiaian, H. V., Kuchitsu, K., Rosenblatt, G., Roth, D. L., Zwillinger, D., "CRC handbook of chemistry and physics", Boca Raton, Fl.: CRC Press, pp. v., 2003.

[63] Kandavel, M., Bhat, V. V., Rougier, A., Aymard, L., Nazri, G. A., Tarascon, J. M., "Improvement of hydrogen storage properties of the AB2 Laves phase alloys for automotive application", *International Journal of Hydrogen Energy*, vol. 33, pp. 3754-3761, 2008.

[64] Damle, A., Ordaz, G., Alkire, J., "Development of Regenerable High Capacity Boron Nitrogen Hydrides as Hydrogen Storage Materials", Washington DC: U.S. Department of Energy, pp. 460-463, 2007.

[65] Kadja, M., Bergeles, G., "Modelling of Slurry Droplet Drying", *Applied Thermal Engineering*, vol. 23, pp. 829-844, 2003.

[66] Incropera, F.P., D.P. DeWitt, *Fundamentals of Heat and Mass Transfer*, 5th ed., New York: Wiley.

[67] Bird, R.B., Lightfoot, E. N., Stewart, W. E., *Transport Phenomena*, 2nd ed., New York; Toronto: J. Wiley.

[68] Present, R.D., *Kinetic Theory of Gases*, New York: McGraw-Hill.

[69] Reid, R.C., Prausnitz, J. M., Poling, B. E., *The Properties of Gases and Liquids*, 4th ed., New York: McGraw-Hill.

[70] Afroz, S., Motin, M. A., Biswas, T. K., Huque, E. M., "Volumetric and Viscometric Studies on Some Inorganic Electrolytes in Water and in Water-SDS Solution Systems", *Physics and Chemistry of Liquids*, vol. 41, pp. 249-262, 2003.

[71] Naterer, G.F., *Heat Transfer in Single and Multiphase Systems*, Boca Raton, Fla.; London: CRC Press.

[72] Kumar, A., Hartland, S., "Correlations for Prediction of Mass Transfer Coefficients in Single Drop Systems and Liquid-Liquid Extraction Columns", *Chemical Engineering Research and Design*, vol. 77, no. 5, pp. 372-384, 1999.

[73] Langmuir, I., "The Evaporation of Small Spheres", *Physical Review*, vol. 12, no. 5, pp. 368-370, 1918.

[74] Webber, M.E., "Mass Transfer from Spherical Drops at High Reynolds Numbers", *Industrial and Engineering Chemistry Fundamentals*, vol. 14, no. 4, pp. 365-366, 1975.

[75] Patankar, S.V., *Numerical Heat Transfer and Fluid Flow*, Washington, New York: Hemisphere Pub. Corp. ;McGraw-Hill.

[76] O'Gorman, P.A., Pullin, D. I., "Effect of Schmidt Number on the Velocity-Scalar Cospectrum in Isotropic Turbulence with a Mean Scalar Gradient", *Journal of Fluid Mechanics*, vol. 532, pp. 111-140, 2005.

[77] White, F.M., *Viscous Fluid Flow*, 3rd ed., New York, NY: McGraw-Hill Higher Education.

[78] Young, D.F., Munson, B. R., T.H. Okiishi, *A Brief Introduction to Fluid Mechanics*, 2nd ed., New York: Wiley.

[79] American Society of Heating Refrigerating and Air-Conditioning Engineers., *2005 ASHRAE handbook : fundamentals*, SI ed ed., Atlanta: ASHRAE.

[80] Babcock & Wilcox Company., *Steam : Its Generation and Use*, 41st ed., Ohio: Babcock & Wilcox.

[81] Osterle, F., "On the Analysis of Counter-Flow Cooling Towers", *International Journal of Heat and Mass Transfer*, vol. 34, pp. 1316-1318, 1991.

[82] Kusuda, T., "Calculation of the Temperature of a Flat-plate Wet Surface under Adiabatic Conditions with Respect to the Lewis Relation", *Humidity and Moisture, Volume One: Principles and Methods of Measuring Humidity in Gases*, vol., pp. 16-32, 1965.

[83] Kanoglu, M., Bolatturk, A., "Performance and parametric investigation of a binary geothermal power plant by exergy", *Renewable Energy*, vol. 33, pp. 2366-2374, 2008.

[84] Muangnoi, T., Asvapoositkul, W., Wongwises, S., "An Exergy Analysis on the Performance of a Counterflow Wet Cooling Tower", *Applied Thermal Engineering*, vol. 27, no. 5-6, pp. 910-917, 2007.

[85] Perry, R.H., D.W. Green, *Perry's Chemical Engineers' Handbook*, 8th ed., New York: McGraw-Hill.

[86] Mathias, P.M., "Modelling of the Copper Chloride Thermoc", Argonne, Illinois: Argonne National Laboratory Report, Dec 06, 2006.

[87] Khan, J., Yaqub, M., Zubair, S. M., "Performance Characteristics of Counter Flow Wet Cooling Towers", *Energy Conversion and Management*, vol. 44, pp. 29073-22091, 2003.

[88] Zbicinski, I., Pitkowski, M., Prajs, W., "Determination of Spray-Drying Kinetics in a Small Scale", *Drying Technology*, vol. 23, pp. 1751-1759, 2005.

[89] Treybal, R.E., *Mass-transfer operations*, 3d ed., New York: McGraw-Hill.

[90] Badescu, V., "Economic Aspects of Using Ground Thermal Energy for Passive House Heating", *renewable Energy*, vol. 32, pp. 895-903, 2007.

[91] Parti, M., Palancz. B., "Mathematical Model For Spray Drying", *Chemical Engineering Science*, vol. 29, pp. 355-362, 1974.